



**Politecnico
di Torino**

Politecnico di Torino

Master's Degree in Automotive Engineering
Class LM-33 (DM270)

**TRANSMISSION DESIGN FOR A FORMULA
STUDENT ELECTRIC RACE CAR:
Geartrain evolution for transition from 13" to
10" rims**



Supervisor:

Prof. Andrea Tonoli

Candidate:

Stefano Orlando

Academic Year 2022/2023

TABLE OF CONTENTS

ABSTRACT	5
1. INTRODUCTION	7
1.1. Formula Student competition.....	7
1.2. Squadra Corse.....	10
1.2.1. History of Squadra Corse	10
1.2.2. SC22 EVO	12
1.3. Benchmarking.....	13
1.4. Future SC cars and target setting.....	16
2. PRELIMINARY CALCULATIONS	17
2.1. Motor layout evaluation	17
2.1.1. Single in-board motor	17
2.1.2. Twin in-board motors	18
2.1.3. Four in-board motors	19
2.1.4. Two out-board motors.....	20
2.1.5. Four out-board motors	21
2.1.6. Conclusions	21
2.2. AMK electric motors	22
2.3. 10" wheels	23
2.4. Laptime simulation and target transmission ratio.....	26
2.5. Gearbox layout evaluation.....	29
2.5.1. Two gear pairs in series	30
2.5.2. Simple planetary system in series to a gear pair.....	31
2.5.3. Simple planetary system.....	32
2.5.4. Two planetary systems in series	33
2.5.5. Compound planetary system	34

2.5.6. Conclusions	35
2.6. Design constraints	35
2.7. Preliminary sizing.....	37
2.8. Load spectrum and service life.....	39
3. KISSOFT TRANSMISSION MODEL	42
3.1. Introduction to KISSsoft and KISSsys	42
3.2. KISSsys transmission model	42
3.2.1. Model setup	43
3.2.2. Kinematics	47
3.3. KISSsoft calculation modules	48
3.3.1. Coaxial shafts calculation module.....	49
3.3.2. Gear pair calculation module.....	49
3.4. Gear pair calculation.....	50
3.4.1. Basic data.....	50
3.4.2. Reference profile	51
3.4.3. Manufacturing	52
3.4.4. Tolerances	52
3.4.5. Modifications.....	53
3.4.6. Rating	53
3.4.7. Factors	53
3.5. Spur gears load capacity	54
3.5.1. ISO 6336:2019 standard.....	54
3.5.2. Pitting	55
3.5.3. Tooth root breakage	56
3.6. Material choice	58
3.7. Macrogeometry dimensioning.....	62

3.8. Microgeometry dimensioning	66
3.9. Gear life calculation: peak load	71
3.10. Gear life calculation: load spectrum.....	77
3.11. Efficiency.....	79
3.11.1. Power losses.....	79
3.11.2. Efficiency model.....	80
4. GEARTRAIN COMPONENTS DESIGN.....	83
4.1. Sun gear	83
4.1.1. Motor interface	84
4.1.2. FEM analysis	87
4.2. Planet gears assembly.....	89
4.2.1. P3G connection	90
4.2.2. First and second stage planet gears.....	92
4.2.3. Pin shaft.....	97
4.2.4. Bearings.....	100
4.3. Ring gear	103
4.3.1. Upright interface.....	104
4.3.2. FEM analysis	104
5. WHEEL BEARINGS AND LUBRICATION	107
5.1. Wheel bearings	107
5.1.1. Layout selection.....	107
5.1.2. Model selection	109
5.1.3. Life calculation.....	110
5.1.4. Preload.....	112
5.2. Lubrication	113
5.2.1. Lubricant oil	114

5.2.2. Lubricant grease	118
5.3. Seals.....	119
5.3.1. Radial shaft seal.....	119
5.3.2. O-rings.....	122
6. PLANETARY CARRIER AND WHEEL HUB	125
6.1. Mechanical design.....	125
6.2. Material selection	127
6.3. Loading conditions	128
6.4. Topology optimization.....	130
6.5. FEM analysis	136
6.6. Fatigue analysis	140
6.7. Wheel nut.....	145
7. CONCLUSIONS AND FUTURE PERSPECTIVES	147
7.1. Results obtained.....	147
7.1.1. Weight reduction.....	149
7.1.2. Volume reduction.....	150
7.1.3. General improvements.....	151
7.2. Future perspectives	151
7.3. Conclusions	152
APPENDICES	154
Appendix A. AMK motor datasheet	154
Appendix B. Ferrium C61 datasheet	157
Appendix C. Lubricant datasheet	159
REFERENCES	163
LIST OF FIGURES	165
LIST OF TABLES	171

ABSTRACT

This thesis work is the conclusion of my journey with Squadra Corse and Formula Student competition. Formula Student is an international engineering competition, which challenges student teams from all over the world to design, engineer, produce and race a single seater formula-style race vehicle. Squadra Corse is the team from Politecnico, and almost each season since 2005 it realizes a new vehicle, the last one being SC22 EVO, a 4WD electric race car powered by 4 independent motors mounted out-board.

Motivated by the emerging trend of reducing wheel size from 13" to 10" rims to enhance overall vehicle performance, which will be soon followed by Squadra Corse, this thesis delves into the task of redesigning the car's transmission system to accommodate this transition. The primary objectives are to achieve weight reduction, volume reduction, and increased durability, all while maintaining the high-performance standards set by Formula Student.

After a brief overview of the framework of Formula Student competition and of some of the teams involved, the design work commences with a comprehensive preliminary analysis and calculations phase. It includes assessing the advantages of 10" wheels over 13" ones, lap time simulations to determine the optimal transmission ratio, exploring various gearbox layouts, and performing preliminary sizing, all while considering loading scenarios from track testing data. This phase sets the stage for the subsequent design and engineering process.

The design of the transmission system is done with KISSsoft software, a powerful engineering tool for machine design and sizing. The compound epicyclic system transmits power from the electric motor to the wheel. The transmission ratio, crucial for performance, is achieved with precision, with profile modifications enhancing efficiency. Extensive calculations confirm the system's robustness under various loading conditions.

The thesis further delves into the detailed design and engineering of mechanical components, such as gears, planetary carrier, wheel hub and bearings. The materials, interfaces, and construction methods are carefully chosen to optimize performance, reduce weight, and enhance overall system durability. The software used have been Catia

V5 for the creation of 3D models and Altair suite for finite element analysis, including topology optimizations, FEM and fatigue analysis.

In conclusion, the thesis showcases the successful design of a transmission assembly that accommodates the transition from 13" to 10" rims. This results in a reduction in assembly mass and axial size, without compromising component strength or safety factors. The new design also extends the service life, even under more demanding loading conditions.

1. INTRODUCTION

1.1. Formula Student competition

Formula Student, or Formula SAE depending on the specific event, is an international engineering competition born in 1981 thanks to the Society of Automotive Engineers. Formula Student provides the opportunity to exploit the “learning by doing” methodology, challenging student teams from all over the world to design, engineer, produce and race a single seater formula-style race vehicle for each season.



Figure 1. SC22 at Formula ATA

Formula Student cars are classified into three different categories:

- Combustion (CV), for vehicles equipped with an internal combustion engine;
- Electric (EV), for vehicles powered by one or more electric motors using the energy stored in a battery pack;

- Driverless (DV), both for combustion and electric vehicles equipped with hardware and software capable of substituting the driver in all driving scenarios.

Following the current trends that are shaping the automotive industry of the future, combustion vehicles are reducing in number and won't be admitted to some events starting from the next season, while electric vehicles are becoming more and more popular, with event organizers pushing to stimulate the transition to electric and autonomous cars as a single category.

Formula Student competitions take place every year during the summer period with races organized in different countries around the world. During the events the effort of the teams is evaluated in static and dynamic disciplines, considering not only the raw performance of the vehicle, but also other aspects, such as the use of innovative solutions and the cost-effectiveness of the project. These disciplines are:

- Static events:
 - Engineering Design event, during which teams present the engineering design and the technical choices to a panel of judges, who evaluate the design innovation, feasibility and the knowledge of general engineering principles that led to a particular design choice;
 - Cost and Manufacturing, during which teams present detailed documents regarding the costs of materials and of manufacturing and assembly processes used in the production of the vehicle. Judges scrutinize the team's ability to manage a budget and make cost-effective decisions without compromising performances;
 - Business Plan Presentation, that is structured as a pitch meeting with potential investors, during which teams present their vehicles as marketable products, focusing on financial feasibility and marketing strategies.
- Dynamic events:
 - Acceleration, a 75 meters straight drag race starting from standstill, assessing the car's acceleration performance and traction capabilities;
 - Skidpad, in which the vehicle has to travel a figure-eight course with constant radii turns in both directions. The average time between the two

circles is measured, reflecting the car's cornering performance and lateral stability;

- Autocross, a fast lap in which the car must complete a course with various twists, turns, and slaloms in the shortest time possible. This event showcases the overall dynamic performance of the vehicles, as well as the drivers' abilities;
- Endurance, a 22km long race on a track with similar characteristics to the autocross one, with a stop for driver change at halfway. This event is the ultimate test for the vehicle's durability and reliability;
- Efficiency, evaluating the net energy consumption of the vehicle during the endurance event. The efficiency scoring is based on a combination of track pace and energy consumption, also considering as a negative contribution the regenerated energy.

The total amount of achievable points is 1000, of which around 1/3 is attributed to static events and 2/3 to dynamic ones, highlighting how each aspect of the project must be dealt with care to reach higher positions in the competition ranking.

Static Events	
Business Plan Presentation	75
Cost and Manufacturing	100
Engineering Design	150
Dynamic Events	
Skidpad	75
Acceleration	75
Autocross	100
Endurance	325
Efficiency	100
Overall	1000

Table 1. Events scoring

Formula Student vehicles must be designed and built following a devoted rulebook, published and updated every year, containing mainly indications regarding the safety of

all people working with the car. The compliance to the rules is checked before the car can participate to dynamic events during technical inspections and during specific tests, such as the brake test, the rain test and the tilt test. The latter one is the most critical for the transmission assembly, since it is devoted to check if there are fluid leakages and in particular lubricant leakages from the transmission.

1.2. Squadra Corse

1.2.1. History of Squadra Corse

Squadra Corse is the Formula Student team of Politecnico di Torino, established in 2004 as the first student team of Politecnico. The first car was produced for the 2005 racing season and was powered by an internal combustion engine. Since then, the team designed and produced a new vehicle almost every year.

In 2012 Squadra Corse was the first Italian team to switch to a full electric powertrain, with the production of the SC12e. It was a RWD vehicle, powered by two 3-phase Magneti Marelli synchronous motors, one for each rear wheel, with a power limited to 42,5 kW each. The motors were mounted transversally inside the vehicle body and transferred torque to the wheels via a chain transmission with reduction ratio of 6.



Figure 2. SC12e and its transmission

In 2013, SCR was the first Squadra Corse's car equipped with a gear transmission. The vehicle was RWD and powered by two 3-phase Magneti Marelli synchronous motors, one for each rear wheel, mounted longitudinally inside the vehicle's monocoque. The torque was transmitted to the ground with a two-stage gear transmission, with a bevel and a spur gear pair in series, achieving a reduction ratio of 9.



Figure 3. SCR and its transmission

SCXV, built in 2015, was the first four-wheel drive vehicle engineered by Squadra Corse. The car was powered by four electric motors, one for each wheel, mounted out-board. The transmission consisted in a dual stage planetary gearbox, with gears having a normal modulus of 1,25mm, reaching a transmission ratio of 16. This powertrain and transmission layout was a great improvement with respect to the previous solutions and has been adopted since then on the following SC vehicles, optimizing every year the existing components, adapting to the needs and targets of the season.

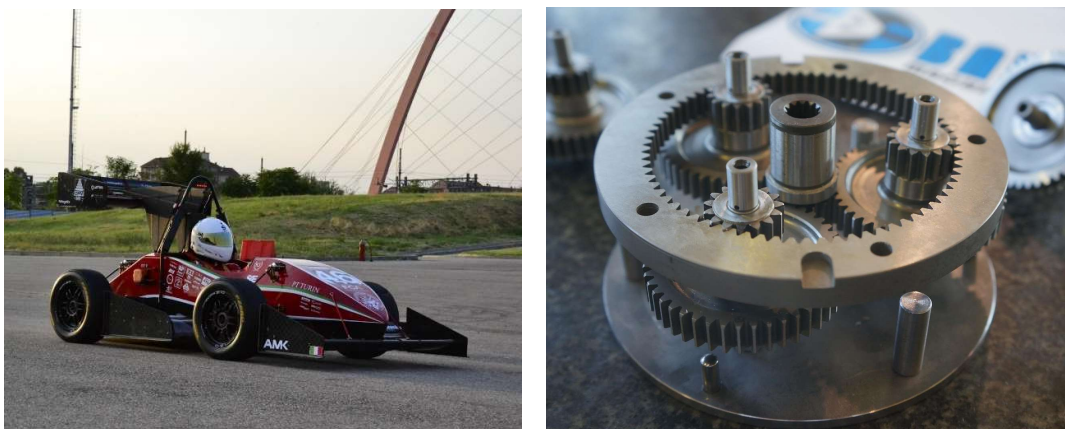


Figure 4. SCXV and its transmission

1.2.2. SC22 EVO

The 2023 vehicle, called SC22 EVO, is the last and most advanced prototype presented by Squadra Corse at the time of writing. Unfortunately, due to financial difficulties occurred during the 2023 season, it is not a brand-new vehicle but an update of the SC22, built for the 2022 season, to solve the problems of electric reliability faced during last seasons. SC22 participated to three competitions, including the most prestigious one Formula Student Germany, achieving some good results. The main characteristics of the vehicle are listed below:

- Mass without driver 211 kg
- Wheelbase 1525 mm
- Track width 1200 mm
- Carbon fibre monocoque
- 4WD with outboard AMK electric motors controlled independently
- 7,7 kWh Li-ion battery at 600V
- 185/40 R13 slick tires on 13" OZ Racing magnesium alloy rims
- Double stage epicyclic geartrain integrated into the upright, with reduction ratio of 14,69 and normal modulus 0,8 mm
- Carbon fibre aerodynamic package with $C_L * A$ of 4,8 and efficiency 3,1
- Maximum power 80 kW, limited by rules
- Maximum speed 120 km/h
- 0-100 km/h in 2,6 s



Figure 5. SC22 EVO and its wheel assembly

1.3. Benchmarking

Benchmarking is a crucial activity in Formula Student as it is in every other competitive environment. Analysing the design solutions adopted by other teams, in particular the ones at the top of the leaderboard, allows to get to know innovative solutions; comparing your own work with that of others achieving better performances is crucial for continuous improvements and examining a diverse range of approaches can serve as an inspiration and starting point for future vehicles.

Amongst the top teams the powertrain layout adopted is the one consisting of four independent motors mounted outboard with the transmission mounted in series. The geartrain used are different, but the most common is the double stage epicyclic gearbox with different characteristics. Moreover, it is present a trend towards smaller wheel size, with many of the teams adopting 10" rims, often custom designed in carbon fibre. Custom designed rims offer a great advantage regarding the packaging of the wheel assembly and consequently of the transmission. Below the solutions adopted by some top teams are presented.

GreenTeam is the team from the Stuttgart University in Germany. In 2022 they led the world ranking, and they achieved the world record for the fastest accelerating electric car. Their vehicle is equipped with custom designed electric motors, allowing more freedom

in the design of the sun gear. The transmission is planetary with two stages, transmitting torque through the rotating ring gear to 10” custom carbon fibre rims.

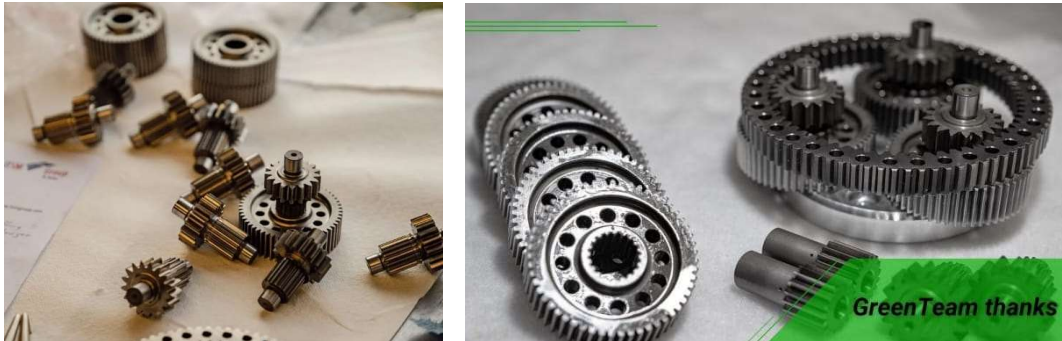


Figure 6. GreenTeam transmission

TuFast is a German team from the University of Munich known for the extreme design solutions adopted in their vehicles. The powertrain layout consists of four outboard motors mounted with a radial offset with respect to the wheel centre, to lower the centre of gravity. The transmission is composed by two stages, the first being a simple spur gear couple and the second being an epicyclic gearset. The vehicle uses 10” custom carbon fibre rims.

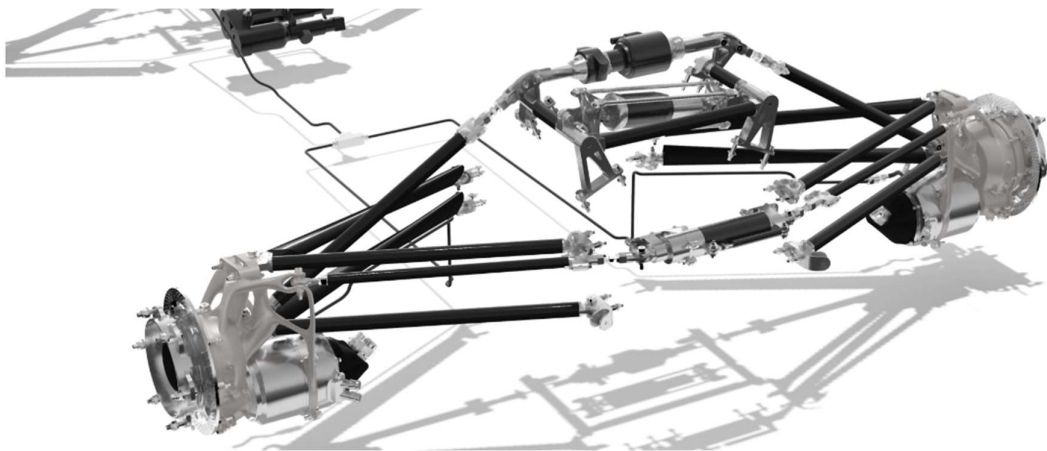


Figure 7. TuFast unsprung masses

Formula Student Team Delft is a Dutch team from Delft, the only one currently running with 8” rims, the smallest size allowed by the rules. This extreme choice requires them to design not only custom carbon fibre rims but also custom tires, since there are no suppliers for this tire size. The vehicle is powered by four outboard electric motors and the transmission is a planetary gearbox. This transmission layout is possible due to the lower reduction ratio needed with the smaller wheels.



Figure 8. Formula Student Team Delft wheel assembly

DHBW Engineering Stuttgart is a German team from Stuttgart. The vehicle is equipped with four outboard electric motors with a double stage epicyclic geartrain. The interesting aspect about this transmission is the fact that the two stages are inverted in space, having a long sun gear passing through the ring gear, for a better packaging. The custom rims are 10” and manufactured in carbon fibre.



Figure 9. DHBW transmission

1.4. Future SC cars and target setting

Following the current trend of the reduction of wheel size, whose benefit will be analysed in detailed in following sections, Squadra Corse will transition to 10” rims in the near future. This great change will provide advantages in terms of performances but will cause the need to redesign many of the components of the wheel assembly. The transmission is one of the assemblies to be modified, and its design will be covered in depth in this thesis. Being this a research project about a future vehicle, some characteristics of the vehicle and its components will be approximated to maintain overall performances aligned to SC22 EVO.

The smaller rims will complicate the packaging inside the wheel assembly, for this reason one of the targets for the transmission design was to reduce the overall volume of the assembly. Regarding the radial dimension, the target was to remain inside an overall diameter of 100 mm, the outer dimension of wheel bearings. The axial length should be reduced, improving the integration of the assembly inside the wheel, leaving more design freedom for the suspension arms and reducing the impact of in-wheel motors on aerodynamics. Along with the volume reduction, also the weight reduction is always an important target for a racing vehicle. Moreover, since the transmission is integrated into the upright, a weight reduction would also reduce the unsprung masses, with benefit on performances. Finally, due to the wish of performing more tests during the season to increase the car reliability, the durability of the gearbox should be increased to guarantee a full year of races and tests or even two racing seasons.

2. PRELIMINARY CALCULATIONS

2.1. Motor layout evaluation

The powertrain layout composed by four independent electric motors, one for each wheel, mounted in out-board position is the most adopted by top teams and has been used by Squadra Corse since 2015. It offers many advantages but is not the only possibility regarding the possible layouts of electric motors inside a Formula Student race car. In this section different powertrain architectures with different traction characteristics will be evaluated, analysing pros and cons of each possibility, to understand which is the most suitable for this application. The possible powertrain layouts considered for this analysis are:

- Single in-board motor
- Twin in-board motors
- Four in-board motors
- Two out-board motors
- Four out-board motors

2.1.1. Single in-board motor

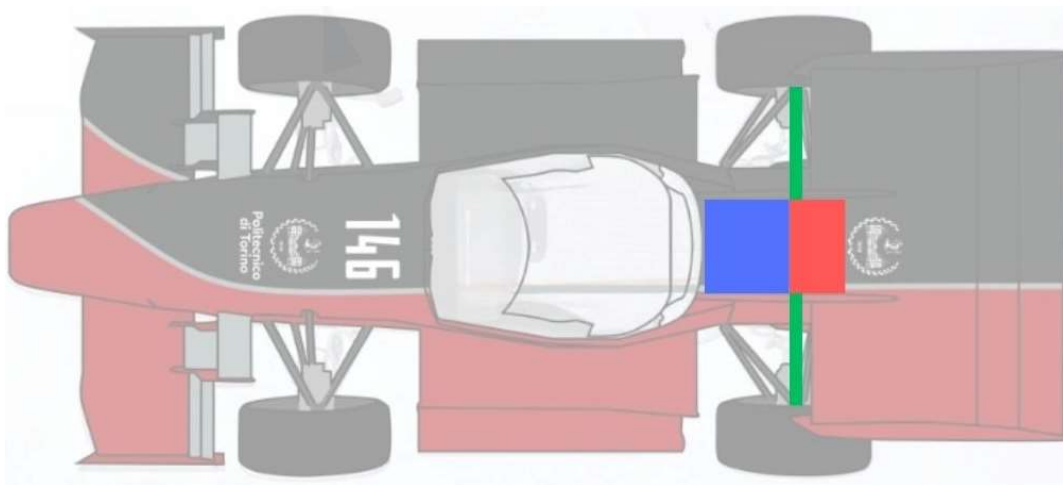


Figure 10. Single in-board motor scheme

The configuration with a single in-board motor consists of a single electric motor mounted inside the vehicle chassis and powering the two rear wheels, making a rear wheel drive vehicle. From the electric and electronics point of view this configuration is the simplest one, needing only one inverter and relative controls. Also, the amount of high voltage cables and cooling hoses is minimized since there is only one motor and one inverter to connect and to cool. On the other hand, to provide the torque necessary to power the vehicle, the single motor is heavy and bulky, representing a problem for the packaging inside the monocoque and for the weight distribution. The torque coming from the motor is split through a differential, very complex from the design and control point of view, between the two rear wheels only, providing less than optimal traction and regenerative braking. Moreover, with a single motor it is not possible to exploit torque vectoring.

2.1.2. Twin in-board motors

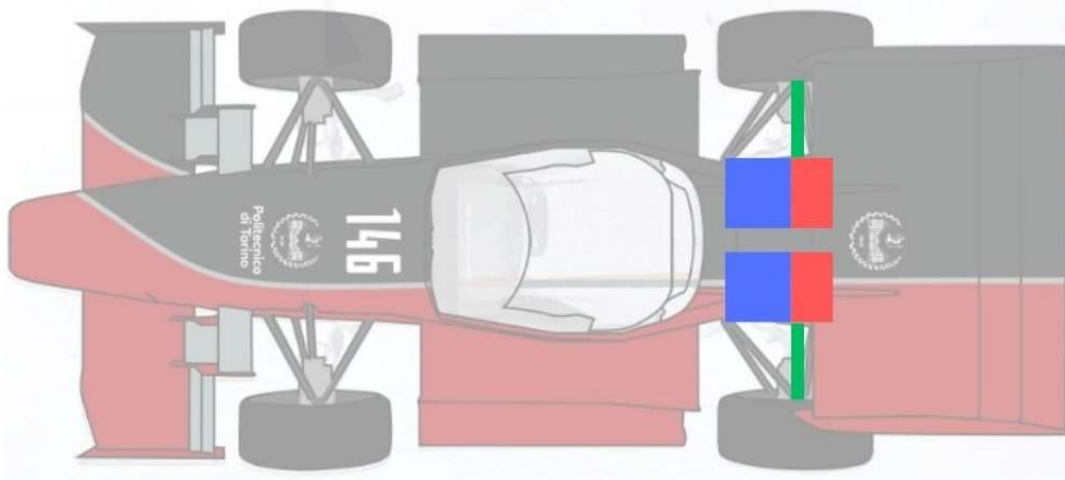


Figure 11. Twin in-board motors scheme

The layout with twin in-board motors consists of two electric motors mounted longitudinally or transversally inside the vehicle body: each motor powers independently one rear wheel, for a rear wheel drive traction. It was the layout used in Squadra Corse's first electric vehicles, since it is quite simple but able at the same time to deliver decent performances. The advantages of this solution are the relative simplicity of the power electronics and the cooling circuit, since there are only two motors and two inverters, and the possibility to control in an independent way the right and the left rear wheel, exploiting the advantages of torque vectoring. The downsides of this architecture are the fact that the vehicle is RWD, thus having not perfect traction and having a limited

capability of regenerating energy during braking, and the packaging of two motors inside the vehicle chassis.

2.1.3. Four in-board motors

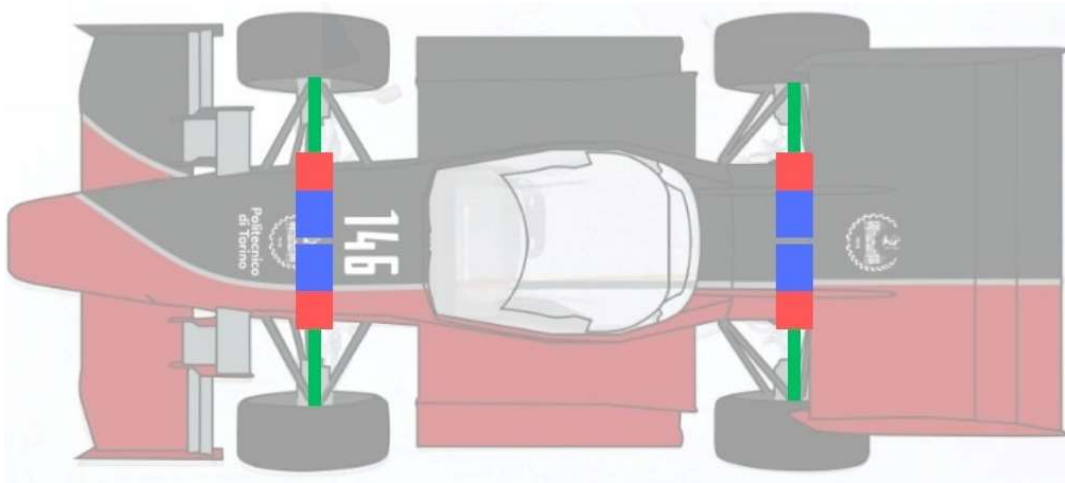


Figure 12. Four in-board motors scheme

The powertrain architecture with four in-board motors consists of four electric motors mounted inside the vehicle chassis; each of the motors powers independently one of the four wheels. This is the first layout analysed up to now that gives as result an all wheel drive vehicle: this aspect is beneficial for vehicle dynamics, since it is possible to exploit traction on all wheels, and for regenerative braking, since energy is recovered from every wheel. In addition, controlling each motor independently it is possible to define at every instant how to split the power between the front and the rear axle, to maximize traction in every condition, and between the right and left side of the vehicle, to maximize the performances during cornering thanks to torque vectoring, transmitting more torque to the out of the bend tires. All these advantages come at the expenses of an increased complexity, both in the physical components and in the control strategies. In fact, four motors need four inverters and consequently lots of high voltage cables and cooling hoses. Moreover, also the mechanical components increase in number and complexity, since there is the need to have four transmission, four semi shafts and eight constant velocity joints. All these aspects represent an issue regarding the packaging inside the vehicle chassis and the overall weight. The semi shafts increase the complexity of the wheel assembly, especially for the front steering wheels.

2.1.4. Two out-board motors

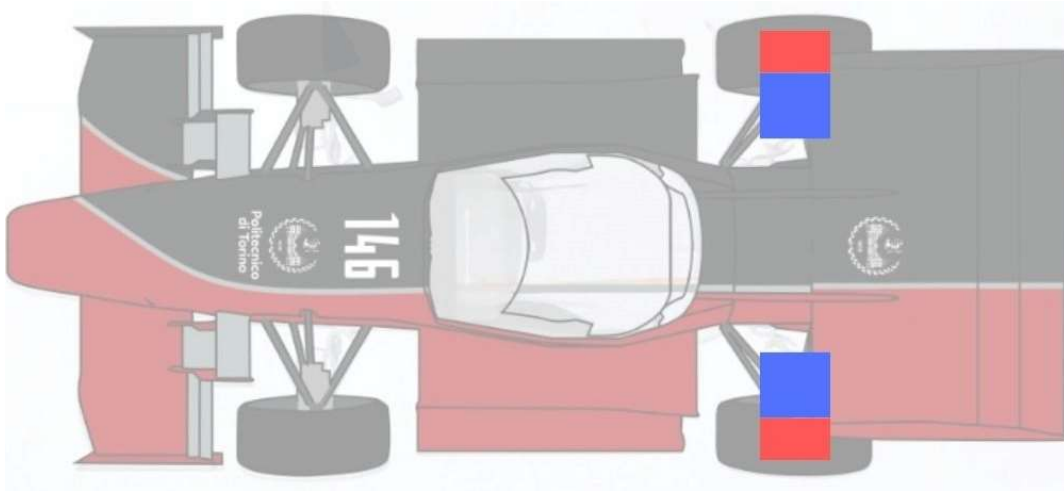


Figure 13. Two out-board motors scheme

The configuration with two out-board motors consists of two electric motors mounted directly to the uprights and controlled independently, making a rear wheel drive vehicle. This layout is similar to the one with twin in-board motors described above and shares many of its advantages and disadvantages. The main difference is that the motors in this case are not inside the vehicle's chassis, thus they don't represent a problem for the packaging inside the monocoque, but they increase the complexity of the packaging of the wheel assembly and the weight of the unsprung masses. By removing the need of drive shafts and constant velocity joints, the mechanical complexity and the overall weight decrease with respect to the equivalent configuration with in-board motors.

2.1.5. Four out-board motors

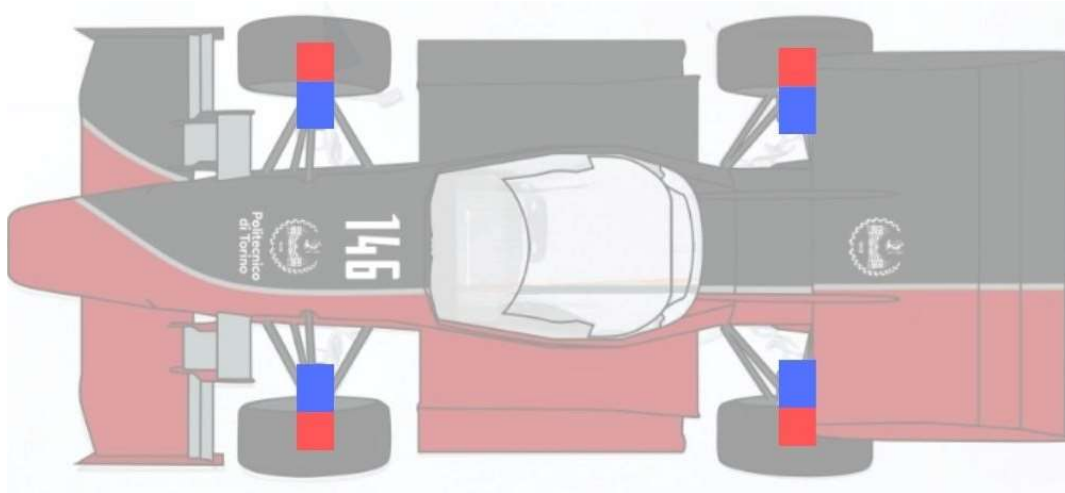


Figure 14. Four out-board motors scheme

The powertrain layout with four out-board motors consists of four electric motors, one for each wheel, directly mounted to the uprights and controlled independently. The result is an all wheel drive vehicle similar to the one with four in-board motors, thus having similar pros and cons. The difference with respect to the four in-board architecture is that the motors are not inside the vehicle body but are directly in-wheel, reducing the complexity of the chassis packaging at the expenses of a more difficult packaging of the wheel assembly and an increase of the unsprung masses. Avoiding the use of drive shafts and constant velocity joints, the mechanical complexity and the overall weight decrease with respect to the equivalent configuration with in-board motors.

2.1.6. Conclusions

After having analysed all the possible layouts, the one with four out-board motors results to be the best since it delivers optimal performances both in traction and regenerative braking in a very compact assembly, with high efficiency and with the possibility of accurately controlling the torque delivered to each wheel. The weight is evenly distributed over the four wheels and the number of complex mechanical components is kept to a minimum. The downsides of this solution are the wheel packaging and the weight of the unsprung masses, which can be dealt with to exploit the great advantages provided by this configuration.

2.2. AMK electric motors

Most electric Formula Student vehicles, especially the ones with four motors, are powered by alternating current three phase permanent magnets synchronous motors. A small number of teams uses custom designed motors, but most rely on commercial solutions specifically designed for Formula Student applications. The two main suppliers are AMK, which provides a kit composed of a fully operational set of four motors and four inverters, and Fischer, which only provides the motor, without shaft, bearings, encoder and inverters.

Fischer motor has a peak torque of 29 Nm and a maximum rotational speed of 20000 rpm. The mechanical design of the component offers great flexibility for the design of the transmission and for the integration inside the wheel assembly. Despite the great performances and the design freedom, to function the motor needs a third party or custom inverter, with all the problems related to the integration between the components. Moreover, all the necessary mechanical components should be designed from scratch, increasing the complexity of the project and the time needed for the design phase.

For these reasons the only viable option is AMK DD5-14-10-POW motors, that come in a plug and play kit with the inverters. These motors are three phase SMPM and deliver very solid performances in a compact package. The peak power is 35 kW, the peak torque is 21 Nm and the maximum rotational speed is 20000 rpm, achievable by flux weakening at 600 V. The component mass is only 3,55 kg. Considering the power limitation of 80 kW imposed by the rules in EV 2.2.1, AMK motors are more than enough; this excess power allows the control system of the vehicle to split in an optimal way the 80 kW between the four motors independently, for maximum traction and performance. The motor characteristic curves and efficiency map are shown below.

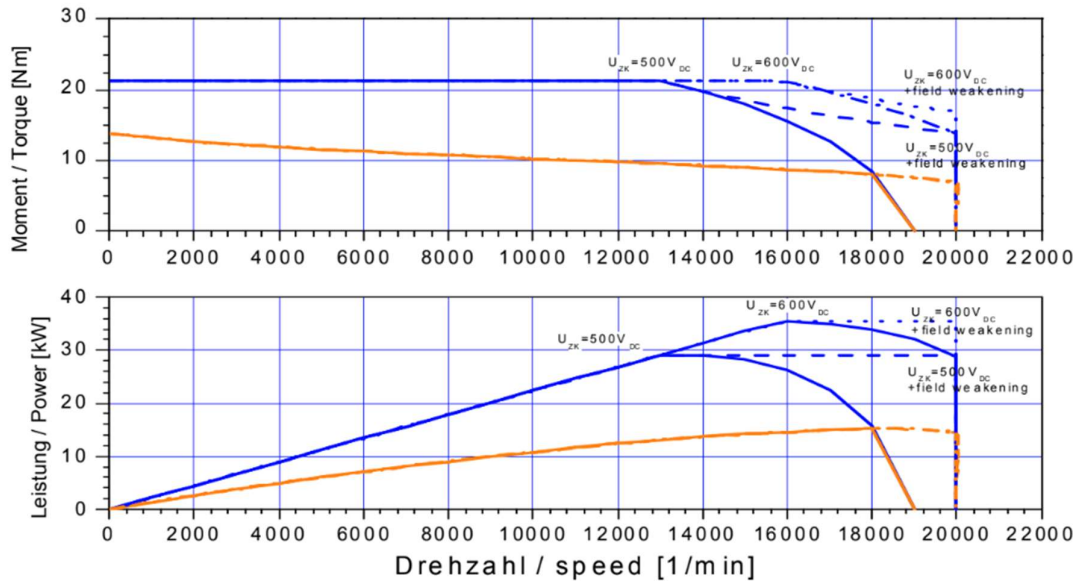


Figure 15. AMK motors characteristic curves

Efficiency [%]	Speed[RPM]																				
	500	1000	2000	3000	4000	5000	6000	7000	8000	9000	10000	11000	12000	13000	14000	15000	16000	17000	18000	19000	20000
1.3	66.61	68.99	72.60	74.93	76.30	76.95	77.13	77.03	76.80	76.57	76.45	76.47	76.68	77.06	77.56	78.11	78.60	78.87	78.75	78.02	76.44
2.7	62.00	67.25	75.23	80.44	83.51	85.03	85.49	85.31	84.84	84.35	84.05	84.06	84.44	85.17	86.14	87.20	88.09	88.50	88.04	86.25	82.58
5.4	49.16	57.41	70.10	78.58	83.81	86.64	87.79	87.91	87.52	87.02	86.72	86.83	87.42	88.49	89.90	91.42	92.70	93.30	92.65	90.09	84.85
7.9	39.49	48.98	63.76	73.86	80.32	84.07	85.91	86.52	86.47	86.23	86.13	86.39	87.13	88.35	89.91	91.57	93.00	93.70	93.11	90.51	85.10
10.4	32.49	42.42	58.04	68.94	76.14	80.54	82.96	84.05	84.41	84.49	84.63	85.06	85.91	87.18	88.77	90.46	91.91	92.68	92.21	89.84	84.78
12.5	26.93	36.87	52.66	63.90	71.55	76.46	79.38	80.97	81.76	82.20	82.62	83.25	84.21	85.52	87.11	88.77	90.21	91.03	90.73	88.70	84.23
14.4	22.65	32.34	47.90	59.18	67.06	72.33	75.68	77.70	78.91	79.71	80.41	81.24	82.31	83.67	85.23	86.85	88.27	89.14	89.01	87.35	83.53
16	19.08	28.33	43.35	54.44	62.40	67.92	71.62	74.05	75.66	76.82	77.81	78.84	80.04	81.43	82.98	84.55	85.94	86.85	86.89	85.61	82.47
17.4	16.19	24.94	39.29	50.05	57.94	63.60	67.56	70.33	72.29	73.79	75.08	76.34	77.68	79.13	80.65	82.12	83.35	84.07	83.95	82.56	79.41
18.5	13.80	22.08	35.71	46.05	53.76	59.41	63.53	66.54	68.82	70.65	72.26	73.80	75.33	76.85	78.31	79.54	80.34	80.41	79.40	76.85	72.28
19.6	12.60	19.54	31.67	41.66	49.75	56.16	61.10	64.78	67.39	69.10	70.09	70.52	70.52	70.25	69.82	69.35	68.95	68.70	68.69	68.98	69.65
21	9.10	14.27	24.08	33.05	41.01	47.84	53.47	57.85	60.99	62.93	63.76	63.58	62.57	60.93	58.90	56.76	54.84	53.50	53.14	54.22	57.20

Figure 16. AMK motors efficiency table

2.3. 10” wheels

As already mentioned above, one of the current trends in Formula Student is the reduction of wheel size, with many teams that are already using 10” rims instead of 13” ones, which were most common in the past. This design choice offers many advantages, and the future Squadra Corse’s vehicles will transition to smaller rims as well. In this section pros and cons of 10” rims will be analysed, taking as reference 10” OZ Racing magnesium alloy rims and Hoosier 16x7,5-10 slick tires, that are commercially available and widespread. Further improvements could be obtained with custom designed rims.

The main advantages related to the transition from 13” to 10” rims are:

- Weight reduction.

With respect to the configuration with 13” OZ Racing magnesium alloy rims and Pirelli 185/40 R13 tires used in SC22 EVO, it is possible to reduce the mass of each wheel by 15%, saving 3,4 kg on the whole vehicle mass. Most of this reduction comes from the rims, since Hoosier tires are wider and have a higher sidewall height.



Figure 17. Pareto diagram of SC22 EVO unsprung masses

Looking at the Pareto diagram analysing the contributions to the unsprung masses of the vehicle, it is possible to notice how rims and tires are one of the main contributors to the overall mass. For this reason, working on their mass reduction has an important impact on the whole vehicle and its performances.

- Rotational inertia reduction.

The smaller radial dimension of the wheel, combined with the lower mass leads to a reduction of the rotational inertia of 35%. This aspect is very important to improve the performance during accelerations and decelerations, reducing the apparent mass of the vehicle.

- Axle height reduction.

With 10” rims the axle is lowered by 36 mm, and consequently all the components that lie on the same axis, such as the motors, the transmissions, the uprights and the brake system. This effect results in a lower centre of gravity for the whole vehicle and a better dynamic behaviour.

- COG height reduction.
Smaller wheels have a lower centre of gravity and also force the height of other components to be lower as explained in the previous point.
- Unsprung mass reduction.
The wheels and all components that will benefit in terms of weight from smaller rims, such as uprights, brake discs and wheel hubs, belong to the unsprung masses. For this reason, the overall weight reduction of the vehicle is even more valuable since unsprung masses are very important for suspension, and consequently vehicle's, performances and tire grip.
- Yaw inertia reduction.
The wheel assemblies and the unsprung masses in general are quite far from the vehicle yaw axis, thus a weight reduction also translates in a reduction in yaw inertia. This aspect is very important for the cornering performances, agility and responsiveness.
- Lower transmission ratio.
The lower tire diameter reduces the needed reduction ratio to achieve the same traction force on the ground for the same input torque. This has an impact on geartrain design, reducing the overall stress on some components and allowing a more compact design.
- More vertical pushrod inclination.
The smaller and lower wheel forces the pushrod to be more vertical to reach the same spot on the chassis. This will result in a less loaded component, an advantage when designing the pushrod.
- Lower forces on brake system.
The lower wheel diameter reduces the needed tangential force on the brake discs to apply the same braking force on the ground. Consequently, also the force on brake calipers, and thus uprights, is decreased.
- Smaller uprights.
The smaller space inside the rims will force the uprights to have a more compact design. In particular will be mainly affected the height of the component, resulting in decreased weight and higher stiffness, which are some of the main targets for uprights design.
- Improved aerodynamics.

Smaller wheels might offer improved aerodynamic performance, due to reduced wheel well turbulence and lower frontal area.



Figure 18. 10" vs 13" wheels comparison

All these advantages come at the expense of a more complex packaging of the wheel assembly, due to the reduction in available volume inside the rims. For this reason, it will be needed to redesign many of the components of the assembly, including transmission, upright, suspensions and brake system. It is however clear from this analysis that a transition to 10" rims will be very effective in increasing the vehicle performances. Furthermore, the future development of custom rims would reduce the difficulties related to the wheel assembly integration, allowing to optimize the usage of space inside the rim to improve the packaging.

2.4. Laptime simulation and target transmission ratio

The fundamental function of the transmission is to adapt the torque and rotational speed coming as input from the motor to the ones suitable for the vehicle running. The parameter affecting this power transformation is the transmission ratio, defined as the ratio between the input and output rotational velocities, and its optimization is crucial to achieve excellent performances. In SC22 EVO the reduction ratio was 14,69, but the transition to 10" rims with consequent reduction of wheel radius from 239 mm to 203 mm imposes to re-evaluate this value.

The choice of the optimal transmission ratio is done by performing lap time simulations with the software Optimum Lap. During these simulations all the parameters are kept constant except for the reduction ratio, which is iteratively changed looking for the best performances in terms of lap time, energy consumption, acceleration performances,

maximum speed and score at events for every track of interest. In the software the vehicle is modelled as an AWD Formula Student vehicle, inserting the main data regarding aerodynamics, tires and the electric traction.

The first event analysed has been the acceleration, since it is very dependent on the amount of torque transmissible to the ground and to the top speed, which are contrasting criteria for the choice of the reduction ratio. Moreover, this event mainly relies on raw vehicle performances, so it is suitable to understand the effect of different transmission ratios. Looking at the results it is possible to notice that the transmission ratio giving the best time is around 13. This value represents a compromise between higher values, that guarantee higher peak acceleration but sacrificing the top speed achievable, and lower values, that allow to reach higher top speeds but excessively hampering the acceleration performances.

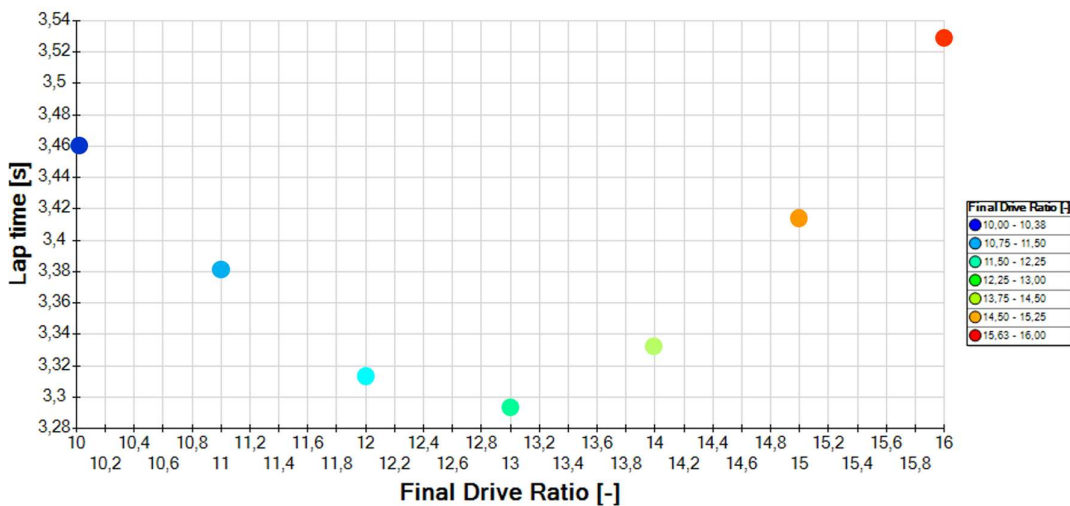


Figure 19. Acceleration lap time vs transmission ratio

Although very relevant for transmission design, acceleration event is not the most representative of normal track driving, which is more common and represents lots of the points awarded in a competition. For this reason, an autocross event is simulated over a track used some years ago at Formula Student Germany. As the endurance event consists of more laps with a track similar to the autocross one, the results can be used to assess the difference in performance for both events. Analysing the results obtained in terms of lap time, it is possible to notice that the optimal transmission ratio is around 12. For the endurance event it is also crucial to look at the energy consumption, a critical parameter for this long event. Considering this aspect, a low reduction ratio delivers better

performances but at the cost of an increased energy consumption. A trade off must be made between these two contrasting criteria.

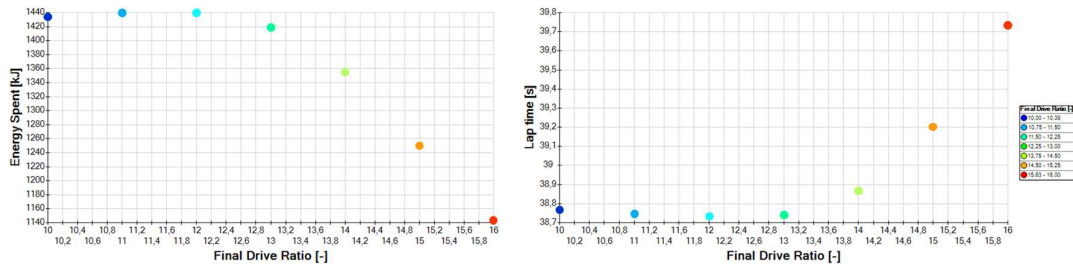


Figure 20. Autocross lap time and energy spent vs transmission ratio

Furthermore, to evaluate the performances of each transmission ratio in a competition, all the dynamic events have been simulated to find the value able to gain more points across all events.

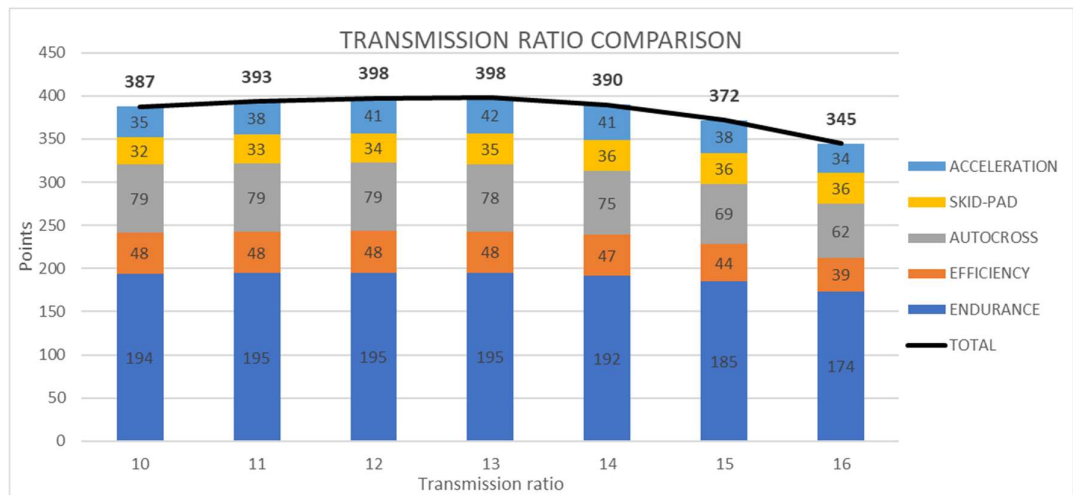


Figure 21. Competition scoring with different transmission ratios

After all the analysis, the optimal transmission ratio resulted to be 12,5. Reducing or increasing too much this value will reduce the vehicle overall performance.

Finally, it is possible to look at the traction model extrapolated from the software. It is possible to see that with a transmission ratio equal to the target, the vehicle is close to the traction limit, but it never overcomes it and is always able to transfer the torque to the ground without wheels slipping. This result confirms that the capabilities of the vehicle are exploited in an optimal manner. The top speed achievable is 120 km/h, suitable with Formula Student requirements and in line with SC22 EVO performances.

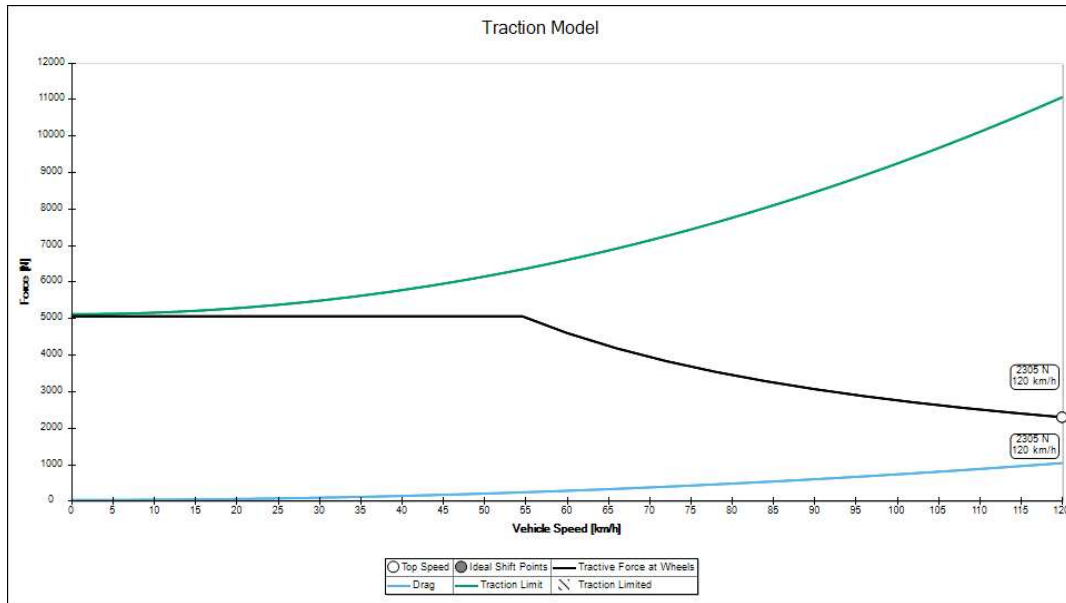


Figure 22. Traction model

2.5. Gearbox layout evaluation

The choice of the gearbox layout has a pivotal role in the design of the transmission for a Formula Student vehicle. The powertrain layout adopted, with electric motors out-board, implies that the transmission has to be integrated inside the upright. This need of having the transmission inside of a reduced volume, together with the aim of reducing weight, underlines the imperative to analyse various gearbox layouts comprehensively. Such analysis becomes crucial in identifying the gearbox layout that can offer the highest torque density with a high efficiency, ensuring an optimal balance between space constraints and weight reduction. The most suitable layouts include combinations of parallel axis gear systems, composed by one or more spur gear couple, and/or planetary systems and its different configurations. Epicyclic system include a combination of external and internal spur gears, to achieve extremely high transmission ratios in a compact volume.

The layouts taken into consideration for this analysis are:

- Two gear pairs in series
- Simple planetary system in series to a gear pair
- Simple planetary system

- Two planetary systems in series
- Compound planetary system

2.5.1. Two gear pairs in series

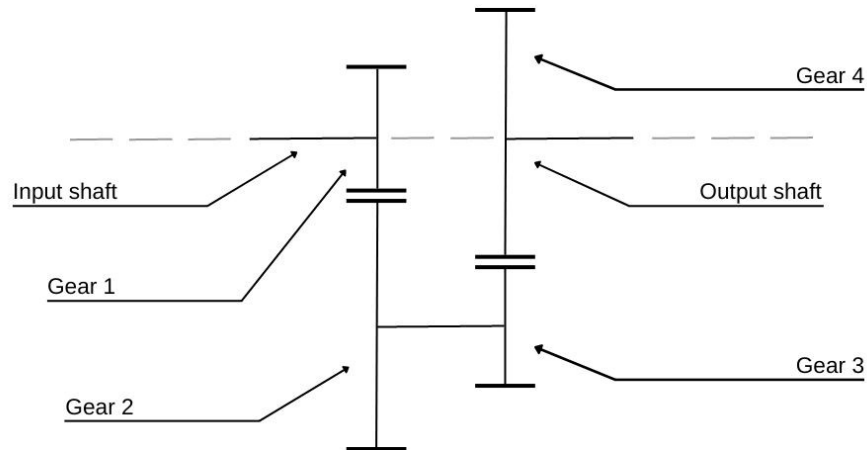


Figure 23. Two gear pairs in series scheme

The layout with two gear pairs in series consists of two couples of spur gears, where the output of the first stage is connected to the input of the second one. In this way, with a two stage reduction, it is possible to achieve high transmission ratios and, with a proper design, to have the output shaft coaxial with the input shaft. The transmission ratio can be calculated as:

$$i = \frac{Z_{G2}}{Z_{G1}} * \frac{Z_{G4}}{Z_{G3}}$$

The main advantages of this layout lie in the simplicity of the components adopted, and consequently on their design, and in the high efficiency of the transmission. On the contrary, while the desired reduction ratio could be achieved with this configuration, the volume of the resulting gearbox would be too big and irregular, causing problems for packaging and upright design. Moreover, opposite to planetary systems, in parallel axis systems all the torque follows the same path: this will result in more stressed and consequently bigger and heavier gears.

is quite complicated, but could be favoured by additive manufactured uprights and custom rims.

2.5.3. Simple planetary system

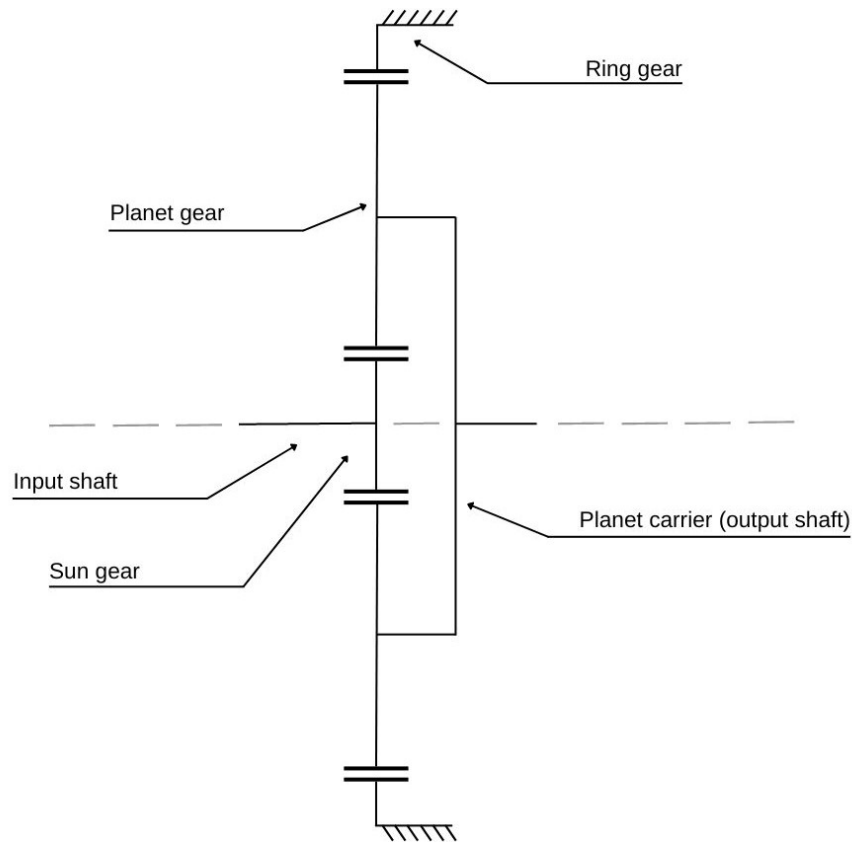


Figure 25. Simple planetary system scheme

The transmission architecture with a simple planetary system offers great performances with medium complexity. Unfortunately, even using a fixed ring gear to maximize the transmission ratio, it is not possible to achieve the target value of 12,5. The transmission ratio is calculated as follows:

$$i = \frac{Z_R}{Z_S} + 1$$

This solution would be the optimal one, since it reduces at a minimum the axial length of the gearbox and also the number of components is low, resulting in lower design effort and weight. The problem is that to achieve a reduction ratio of 12,5, the radial size of the

transmission would be much beyond the limits imposed by packaging and targets, making impossible to fit inside the uprights.

2.5.4. Two planetary systems in series

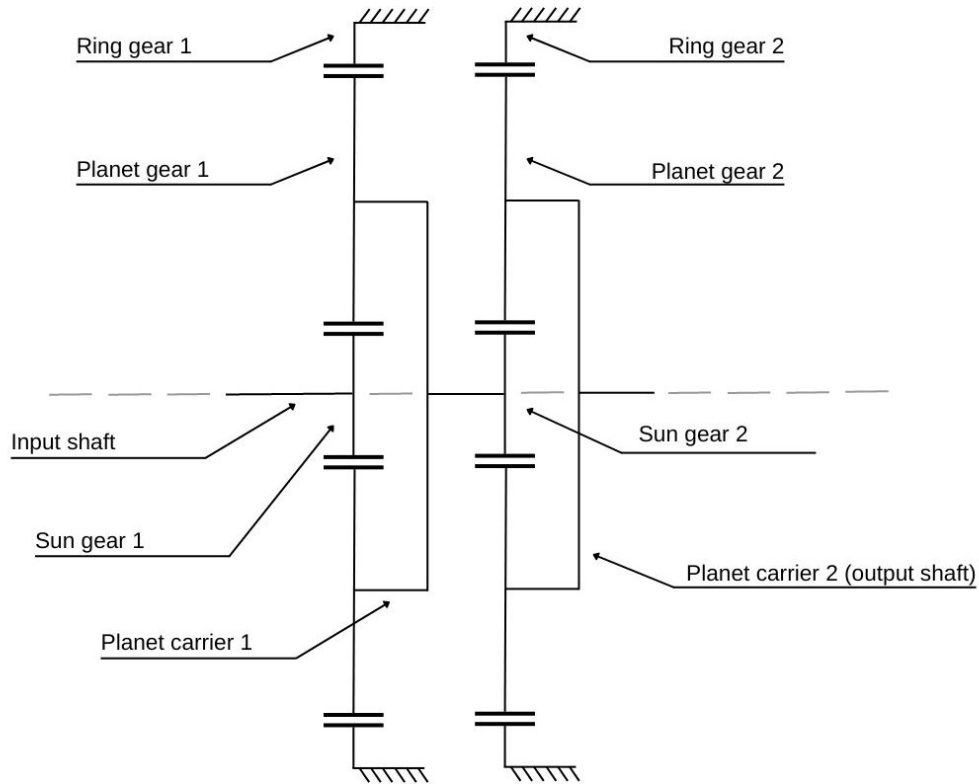


Figure 26. Two planetary systems in series scheme

The layout with two planetary systems in series, where the output of the first one is the input of the second one, is able to reach extremely high transmission ratios while maintaining a compact radial dimension. Considering both ring gears fixed, the input through the sun gear of the first epicyclic geartrain and the output through the planet carrier of the second one, the transmission ratio is calculated as:

$$i = \left(\frac{Z_{R1}}{Z_{S1}} + 1 \right) * \left(\frac{Z_{R2}}{Z_{S2}} + 1 \right)$$

The main advantage of this layout is the possibility to reduce the radial dimension, which can open the doors to a higher level of integration inside the wheel assembly, especially with custom rims. On the contrary the axial dimension is increased. Also, the number of

components is increased with respect to a simple planetary system, with a consequent increase in complexity, design effort and weight, and a reduction in overall efficiency.

2.5.5. Compound planetary system

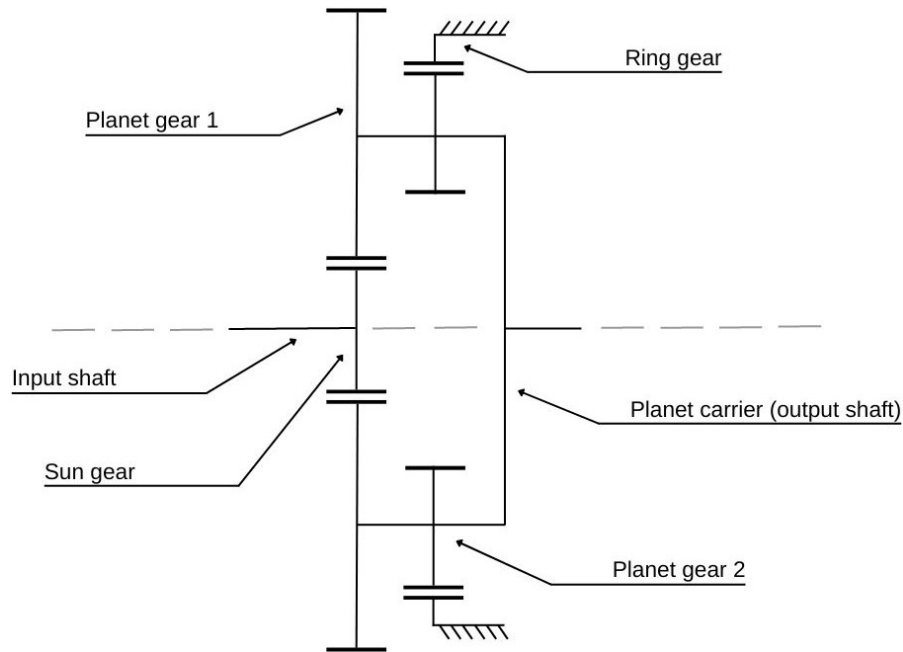


Figure 27. Compound planetary system scheme

In a compound planetary system, the torque is transferred from the sun, which is the input, to the first stage planet gear, that is rigidly fixed to the second stage one. The second stage planet gear meshes with the ring gear, which is fixed to maximize the transmission ratio, and the output is through the planetary carrier. The reduction ratio can be calculated as:

$$i = \frac{Z_{P1}}{Z_S} * \frac{Z_R}{Z_{P2}} + 1$$

With this layout it is possible to achieve a high reduction ratio thanks to the two stages, while maintaining relatively compact radial and axial dimensions. Also, with respect to the two planetary systems in series, which is similar to this solution, the number of components is reduced. This has positive effects on overall efficiency, weight and design complexity.

2.5.6. Conclusions

Analysing the characteristics of the solutions presented above, it is clear that the most suitable for this application is the compound planetary system. This layout is able to reach the target transmission ratio while still maintaining compact radial and axial dimensions, and minimizing the overall volume. The number of components, linked to weight and efficiency, is also in line with the desired performances. In fact, even though in a parallel axis gearbox it is possible to reduce the losses related to the gear meshing, since the number of engaged gear pairs is lower, this aspect is counterbalanced by the reduced number of components such as shafts and bearings and by the possibility of achieving a better lubrication in a compound planetary system. Moreover, the larger loads experienced by the gears in a simple spur gear pair will cause the gears to be larger to support higher forces; also bearings and shafts must be stronger to sustain the higher stresses, with an even higher increase in total mass. In contrast, in a planetary system the torque is split in different pathways, leading to less loaded components, which can then be smaller and lighter. In addition, radial forces are intrinsically balanced, lowering the overall load, and thus weight, on shafts and bearings.

2.6. Design constraints

After having defined the layout of the gearbox, it is necessary to define the design constraints to respect in this analysis. The required constraints can be divided into two main groups: geometric constraints and manufacturing & assembly constraints.

Geometric constraints depend on the kind of configuration chosen and how the gears relate the other elements of the assembly. Main geometric constraints can be found for sun and second stage planet gears. According to ISO 6336-3:2019 the gear rim thickness, the amount of material to support the teeth roots, should be greater or equal than 1,2 times the height of the teeth for external gears and 3,5 times the gear normal modulus for internal gears.

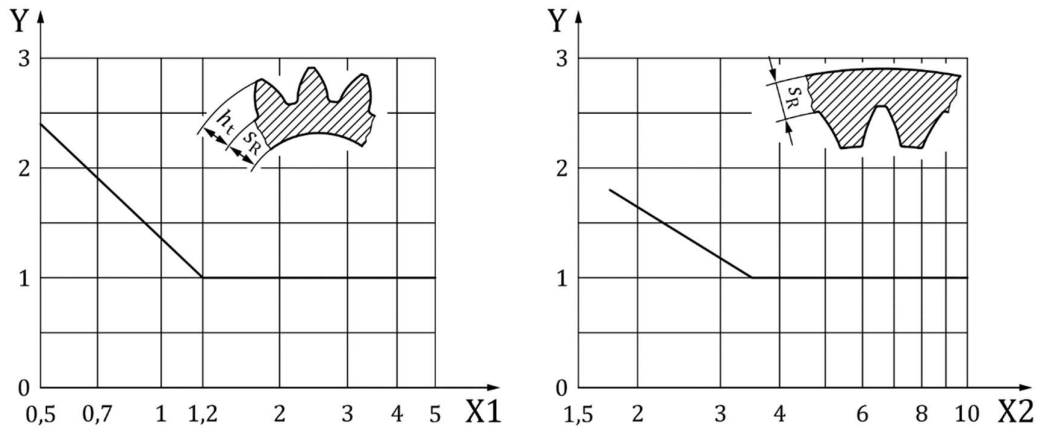


Figure 28. Rim thickness factor

For this reason, the diameter of the sun gear is limited by the outer radius of the motor spline to which is connected, and the second stage planet gear is constrained by the dimension of the pin shaft and of the roller bearings that must fit inside. Having a lower limit on the smallest gears dimensions effectively eliminates the possibility of reducing too much the gearbox radial dimensions.

Manufacturing and assembly constraints, on the other hand, are those which, if not respected, will cause the gear train not to be producible or not to function properly. These constraints are the minimum number of teeth for a given pressure angle α (with $\alpha=20^\circ$ the minimum number of teeth is 17) and the meshing rule, that reduces the number of possible combinations, stating that:

$$\frac{z_{P1} * z_R + z_S * z_{P2}}{N} = X$$

Where:

z is the number of teeth of each gear, depending on the subscript

N is the number of planet gears, and in this case is equal to 3

X is an integer number

If this rule is not respected, it will be physically impossible to assemble the gearset. Moreover, another assembly condition to respect is:

$$r_S + r_{P1} + r_{P2} = r_R$$

Where r represents the pitch radius of each gear.

Finally, to ensure correct meshing, it is essential for the three sets of planetary gears to be equally phased.

2.7. Preliminary sizing

The first step of the design process is a rough sizing operation, done with an Excel spreadsheet. In this preliminary calculation, many possible combinations of number of teeth are considered, to check whether all the constraints and targets are reached. This procedure allows to rapidly exclude the unfeasible or unsuitable configurations, reducing future unnecessary work in KISSsoft software.

From a first analysis it was noted that reaching the transmission ratio target was not possible within the maximum radial dimension target by using a normal modulus of 0,8 mm. As it can be noted from the transmission ratio formula of a compound planetary system, the ways to increase the transmission ratio are:

- Increasing the number of teeth of the first stage planetary gear or of the ring gear;
- Decreasing the number of teeth of the sun gear or of the second stage planetary gear.

By taking into consideration the radial dimension constraint, it is obvious that increasing the number of teeth of the first stage planet gear, thus its pitch diameter, is not a valid option. On the other hand, both the sun gear and the second stage planet gears are constrained regarding the minimum dimension as seen in paragraph 2.6. Additionally, due to the assembly constraints, it is not possible to change the dimension of a gear without having impact on the others.

Hence only three options remained:

- Reducing the normal modulus to 0,6 mm;

- Using a compound configuration with 0,6 mm modulus for the first stage and 0,8 mm for the second one;
- Keep the modulus at 0,8 mm and use an axial offset for the sun gear, to bypass geometrical constraint and further reduce its pitch diameter.

Reducing the gear module to 0,6 mm, it is possible to reduce the pitch diameter of every gear, thus reducing the overall size of the gears and consequently also the weight. This solution would still need to ensure compatibility with the previously explained constraints, however, talking about the sun gear pitch diameter, a lower modulus will allow to have smaller gears with respect to 0,8 mm modulus while keeping the transmission ratio constant. This solution is common to many FSAE top teams. However, this solution has the drawback of increasing the loads and the manufacturing complexity, since the gear teeth are smaller.

In a compound configuration the first stage would benefit for the reduced dimension given by the smaller normal modulus, while the second one would be bigger but less stressed due to the larger gears. However, this solution, together with the pros and cons of both 0,6 mm and 0,8 mm modules, introduces an additional difficulty in gear timing between the two stages.

The last possible solution would be to work around the motor spline constraint for the sun gear. By axially offsetting the gear out of the incumbrance of the motor spline it is possible to reduce its diameter without violating the geometric constraints. On the other hand, this configuration increases the axial length of the transmission and causes greater stresses on the sun gear and the motor shaft, which are loaded in bending.

After all these considerations, it was decided to adopt a normal modulus of 0,6 mm, which will allow to reduce as much as possible the radial dimensions of the gears. Moreover, without the need of an offset sun gear, also the axial dimension will be kept to a minimum. This rough sizing and its ability to deliver the desired performances will be later verified in KISSsoft.

2.8. Load spectrum and service life

The power and torque requirements of a Formula Student vehicle exhibit significant irregularities throughout its operational lifespan. Consequently, sizing mechanical components, especially gears, based solely on maximum load conditions could result in unnecessary oversizing and weight. Adding to this complexity, the torque demands can vary between positive and negative values, due to the integration of regenerative braking. For these reasons, it is imperative to conduct calculations using a reference load spectrum that is representative of the service life conditions. In any case, for completeness and for reference, also the calculation with the worst condition of 21 Nm and 20000 rpm is carried out.

The load spectrum utilized for these calculations is derived from an autocross event ran during the 2022 racing season, acknowledged as the most challenging operational scenario for the vehicle. In particular, it is considered the torque experienced by one of the rear wheels, that are the most stressed ones. This distinction primarily arises from the fact that the front wheels seldom bear sufficient vertical load to fully transmit the available torque to the ground. This phenomenon is further accentuated by the static weight distribution, that is slightly shifted towards rear wheels, and by the weight transfer during accelerations.

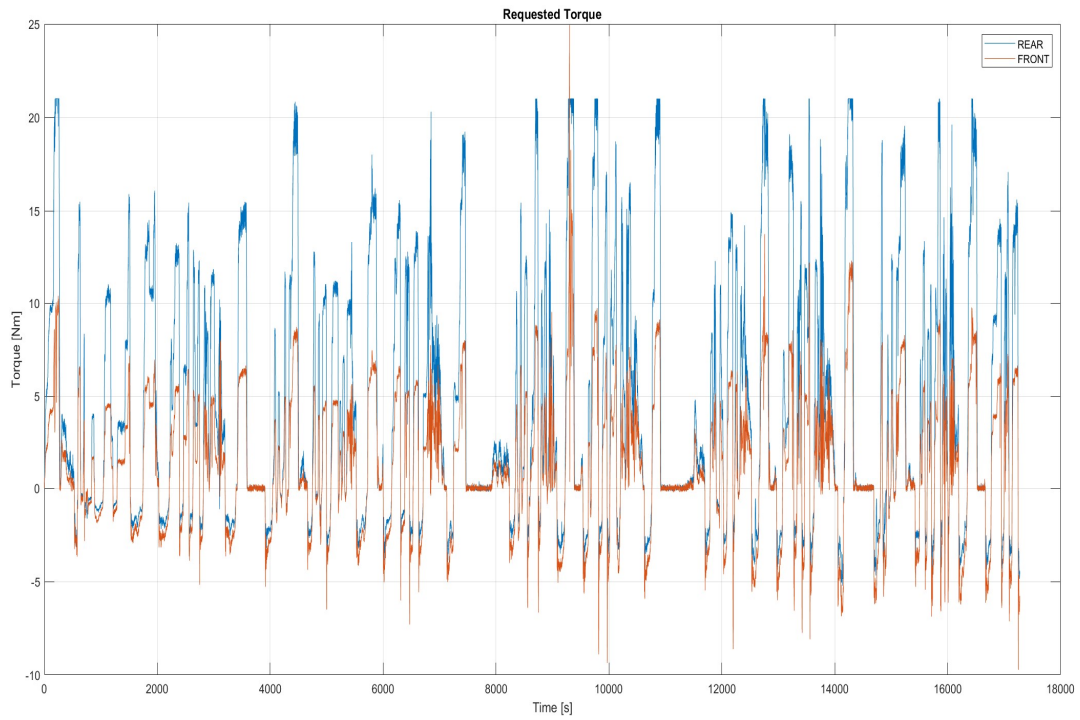


Figure 29. Requested torque during autocross

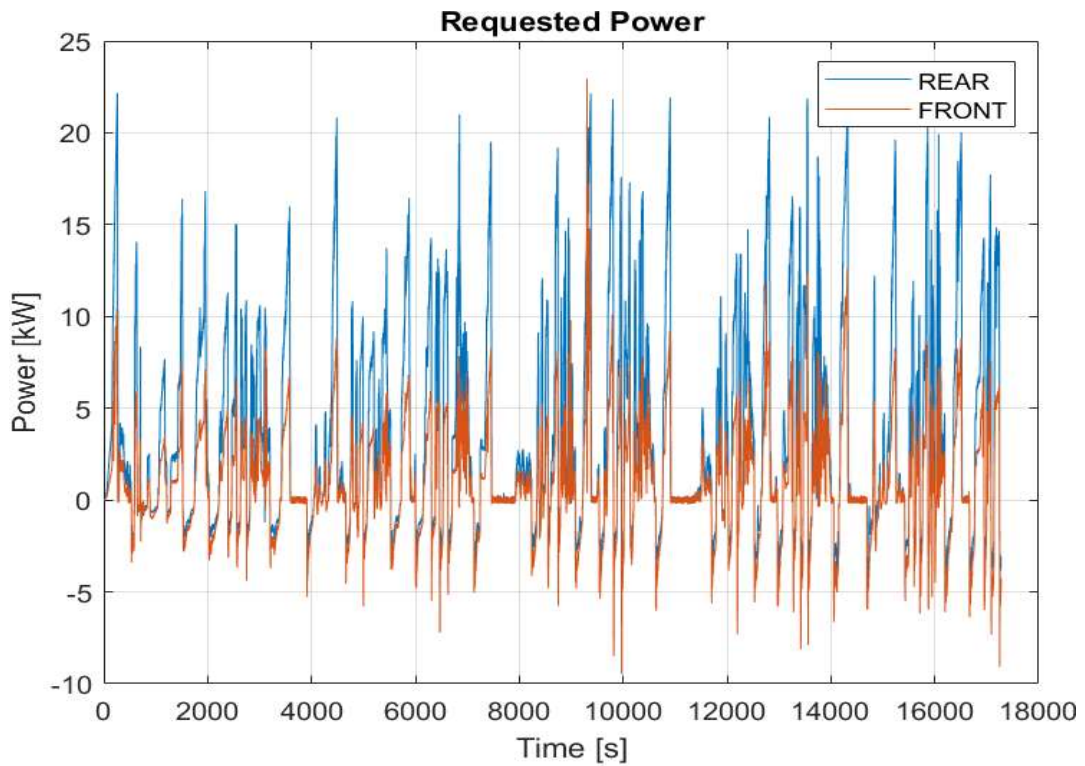


Figure 30. Requested power during autocross

Unfortunately, due to reliability issues, it is not possible to extract the required service life from the data of 2022 racing season. This value is therefore estimated based on previous experiences, considering:

- 3 races per season, for a total of 100 km
- 1000 km of tests among pre, mid and post-season testing

The average speed can be considered around 40 km/h, yielding a required service life of 27,5 h. As a new prototype is built every year, the strictly necessary working life of the vehicle is very short. Nonetheless the required life was set to 50 h, overestimating it a lot to account for even more testing (one of the long-term targets of Squadra Corse) and to give the possibility to eventually use the gearbox for two seasons, reducing costs and production times.

In conclusion the sizing process will be performed considering both the maximum nominal load, accepting lower safety factors since it is an excessively critical condition, and the load spectrum of rear wheels. The required life is 50 h.

3. KISSOFT TRANSMISSION MODEL

3.1. Introduction to KISSsoft and KISSsys

The design of the main elements of the transmission has been carried out with the help of KISSsoft software, supplied by KISSsoft AG that is one of the sponsors of Squadra Corse. KISSsoft is a very powerful engineering tool, providing designers cutting-edge calculation tools for machine design and sizing, according to most recent international standards.

The model of the transmission, fundamental for the design process, has been built in KISSsys. KISSsys, short for Kinematic Simulation System is an add-on of KISSsoft, that is used to model complex systems, such as an entire transmission, where many elements are linked together. The complete gearbox is modelled in KISSsys, that calculates the kinematics of the systems and then performs the analysis simultaneously for all machine elements, recalling the related KISSsoft modules inserted in the model build.

3.2. KISSsys transmission model

As defined in previous sections, the transmission is a compound epicyclic system with the input from the electric motor on the sun gear and the output to the wheel on the planet carrier, while the ring gear is fixed to the upright. In this section the KISSsys model will be described, detailing the building process and all the elements involved. With respect to previous years, the model has been refined, to exploit more of the potential offered by this software and to increase the accuracy of the results. In any case the results obtained should be validated via track testing.

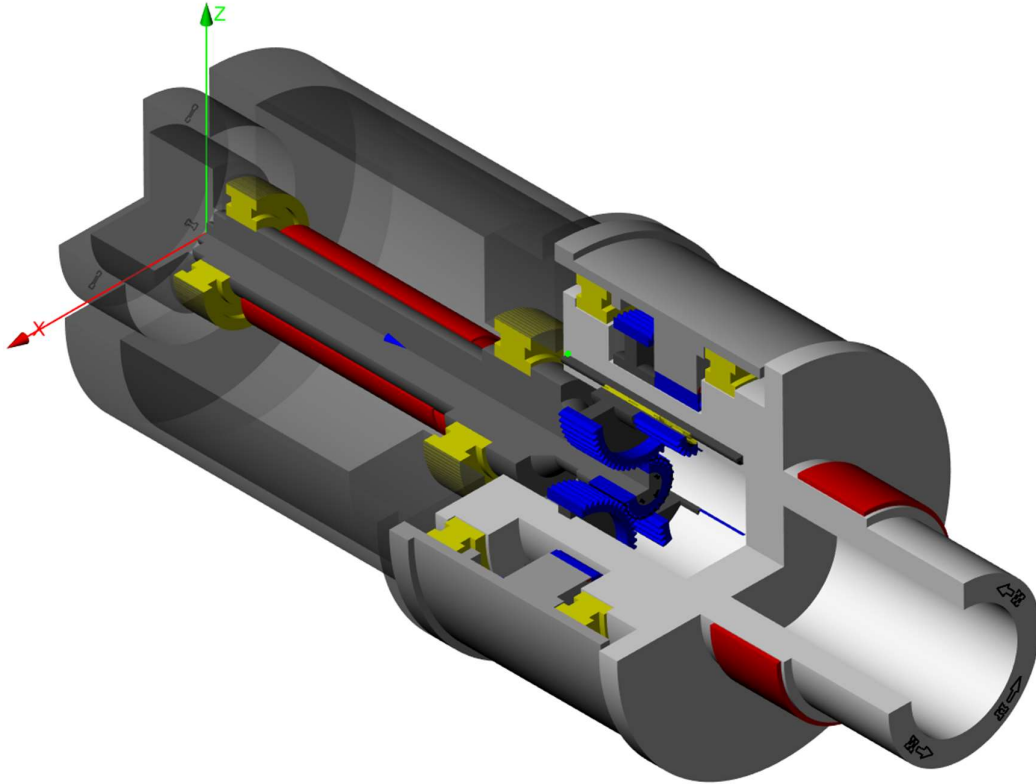
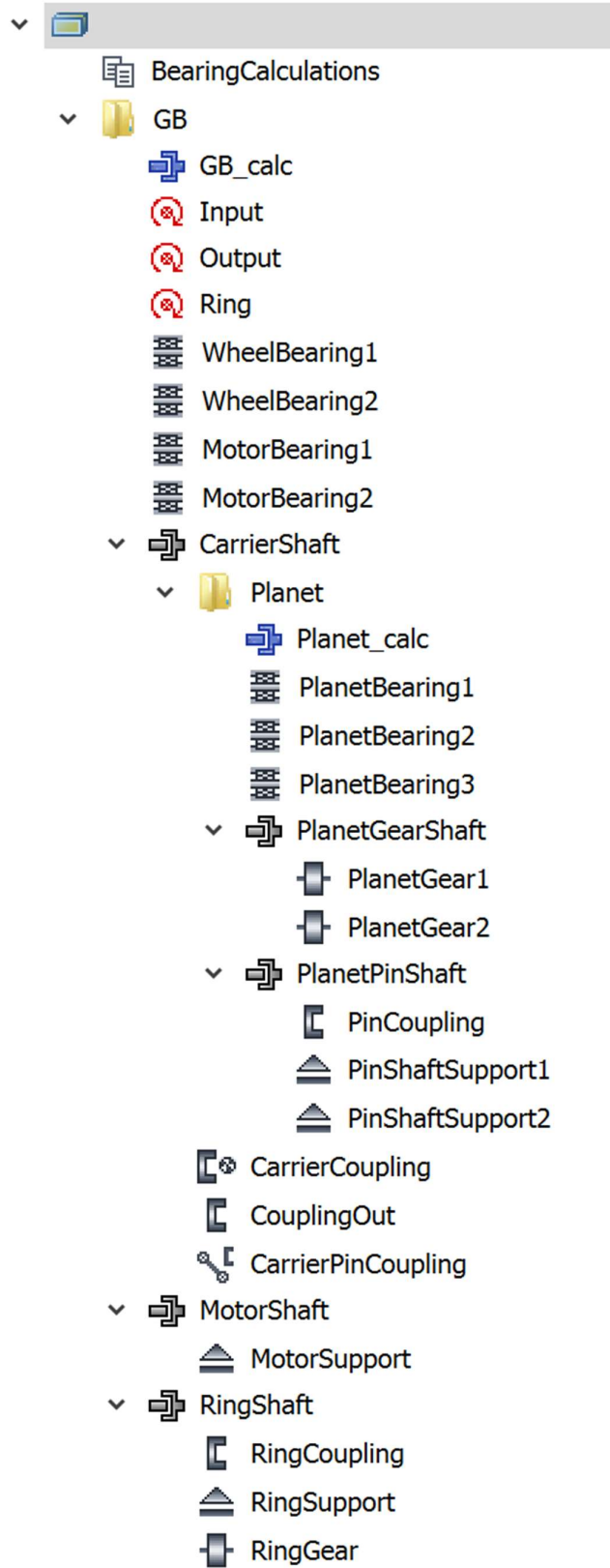


Figure 31. KISSsys transmission model 3D view

3.2.1. Model setup

The first step in the model build is to create the project folder, called *GB* in this case, that will contain all the elements of the transmission assembly.

The first elements that must be added to the gearbox are coaxial shafts, KISSsys elements that represent shafts with the same rotation axis and rotating at the same speed. The shafts involved in this model are the sun shaft (*SunShaft*), the motor shaft (*MotorShaft*), the ring shaft (*RingShaft*) and the planetary carrier shaft (*CarrierShaft*). Moreover, to the carrier shaft, the folder of the planets is added, which in turn contains the planet gears (*PlanetGearsShaft*) and the pin shaft (*PlanetPinShaft*). After the coaxial shafts have been created, the other machine elements, such as bearings and gears can be added on each shaft.



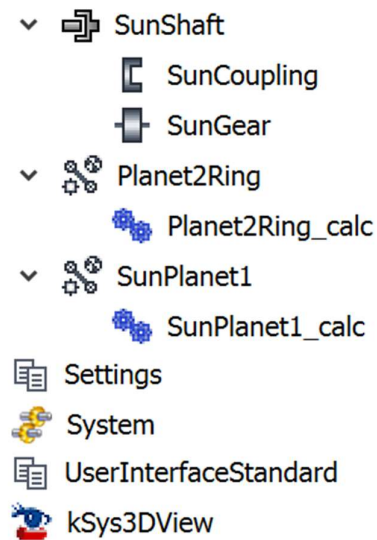


Figure 32. KISSsys transmission model tree

The sun shaft represents the sun gear and the motor output shaft to which it is rigidly linked. The elements in this coaxial shaft are:

- One coupling element, a general coupling between elements to transfer torque (*CouplingSun*). This coupling represents the input torque from the motor;
- One gear element (*SunGear*).

The motor shaft defines the motor stator and external housing. In this shaft the element added is:

- One support element, a general constraint removing one or more degrees of freedom (*MotorSupport*). It prevents the motor housing movements.

The ring shaft describes the ring gear and the part of the upright that contains the transmission. It is composed by:

- One coupling (*RingCoupling*), representing the torque transfer from the ring gear to the upright;
- One support (*RingSupport*), constraining the movement of the shaft;
- One gear (*RingGear*).

The planetary carrier shaft represents both the planetary carrier and the wheel hub. The coaxial shaft comprehends:

- One coupling (*CouplingOut*), defining the torque output from the gearbox through the carrier;
- One planet carrier coupling element (*CarrierCoupling*), a specific coupling for planetary systems.

The carrier shaft includes the planet folder, containing the planet gears coaxial shaft and the pin shaft. The planet gears shaft is composed by:

- Two gears (*PlanetGear1* and *PlanetGear2*), representing first and second stage planetary gears.

The elements in the pin shaft are:

- One coupling (*PinCoupling*);
- Two supports (*SupportPin1* and *SupportPin2*), constraining the motion of the pin shaft.

After all the main elements have been added to the model tree, it is needed to connect them in the proper way.

The gears are connected with a planetary gear meshing constraint element, the sun with the first stage planet (*SunPlanet1*) and the second stage planet with the ring gear (*Planet2Ring*). The use of the planetary constraint instead of the normal one allows the software to properly subdivide the torque to which each of the planets is subjected. In the configuration of these constraints, it is necessary to define the gears involved, the type of each gear (sun, planet or ring), the number of planets and the efficiency.

Connection roller bearings are KISSsys element used to describe the connection by means of bearings between different coaxial shafts in the model. To be defined, the shafts connected with the inner and outer raceways of the bearings must be specified. *WheelBearing1* and *2* represent the wheel bearings and connect the carrier shaft to the ring shaft. *MotorBearing1* and *2* are the bearings inside the motor that allow the relative rotation between the stator and the rotor; they connect the sun shaft to the motor shaft. *PlanetBearing1*, *2* and *3* are connection roller bearings contained inside the planet folder. They represent the three needle bearings between the pin shaft and the planet gears and connects the two relative coaxial shafts.

Finally, the planetary carrier and the pin shaft, which are rigidly linked and rotate together at the same speed, are constrained together with a coupling constraint element (*CarrierPinCoupling*), that imposes the rotational speeds of the two elements to be equal, without slip.

3.2.2. Kinematics

To calculate the gearbox kinematics, it is needed to define what are the input, output or fixed elements in the transmission. This can be done using the speed or force element, which allows to define the value of torque and/or speed of an element via the corresponding coupling. Moreover, it is possible to define if the element is the driving or the driven one. When the torque and/or speed are not constrained to a defined value, the software calculates them. The torque, even if not useful for the kinematics, will be utilized for the life calculations in KISSsoft.

In this particular design the input is through the sun gear, that is thus both speed and torque constrained to the peak values of 20000 rpm and 21 Nm respectively. It is needed to use the maximum values, so that they can be later scaled according to the load spectrum defined in section 2.8.

The ring gear is fixed, so its rotational speed is locked to 0 rpm, while the torque is not constrained.

The output of the system is through the planetary carrier, for which neither the speed nor torque are set, but are calculated by the software according to the transmission ratio.

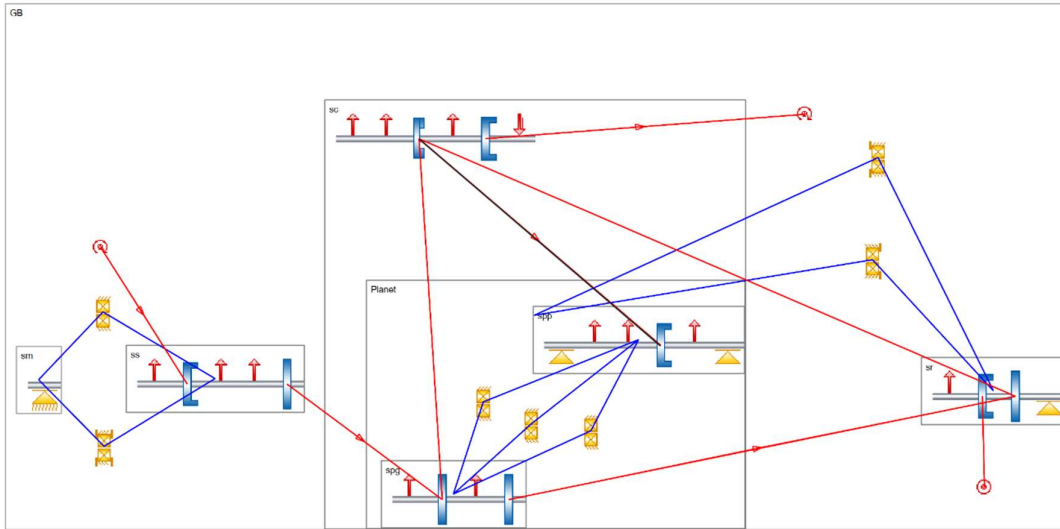


Figure 33. KISSsys model kinematic diagram

In the kinematic diagram it is possible to see a schematic representation of all the elements, connections and constraints, together with the power flow. Red lines represent the elements connected with a power flow, black lines represent connections without power flowing and blue lines are used to visualize the connection through connection roller bearings.

Following the red line, it is possible to visualize that power from the motor flows from the sun gear to the first planet gear; from there the power is split between the carrier and the second stage planet gear. From the second stage planet gear, the power flows to the fixed ring gear and into the carrier. The combined power is output from the planetary carrier to the wheel hub and then the wheel. The pin shaft is connected to carrier with a black line since the two components do not exchange power with each other, having the same rotational speed.

3.3. KISSsoft calculation modules

To perform the calculations, KISSsys model contains calculation modules that will run in KISSsoft. The two calculation modules used are the coaxial shaft calculation module and the gear pair one.

3.3.1. Coaxial shafts calculation module

The coaxial shafts module is used to design and to perform calculations on coaxial shafts. It is possible to design the shafts, inserting all the geometrical parameters and positioning on them the other machine elements, forces and constraints. Defining the materials of the shafts, the loads and required service life, it is possible to calculate the stresses and deformations of the components according to the chosen norm. Also the safety factors, service life and reaction forces of bearings are calculated in the same module. All these results can be then visualized with different diagrams and reports.

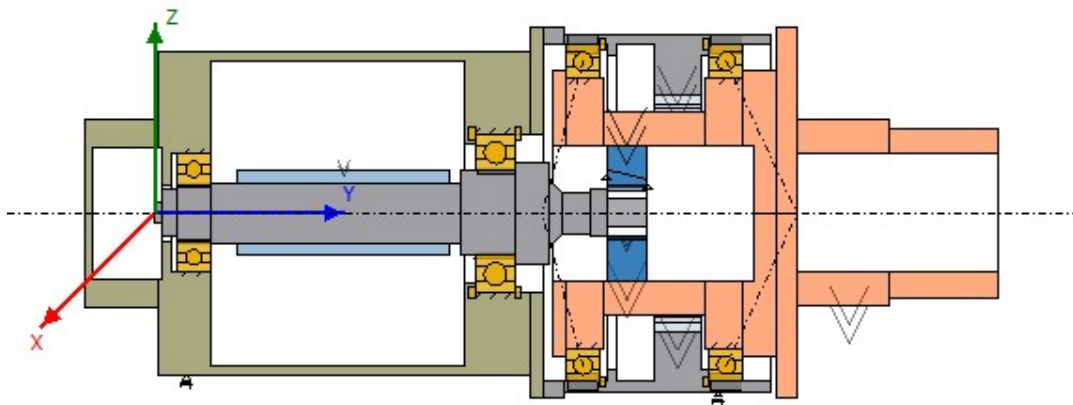


Figure 34. GB_calc coaxial shaft

In the model two coaxial shafts calculation modules are used:

- *GB_calc*, containing the motor shaft, the sun shaft, the ring shaft and the carrier shaft;
- *Planet_calc*, including the pin shaft and the planet gears shaft.

3.3.2. Gear pair calculation module

The cylindrical gear pair module is a tool designed to dimension and to assess the load-bearing capacity of a gear system. It operates by taking various geometric parameters as inputs, which can be inserted manually or directly calculated according to the requirements of the system. Additionally, KISSsoft provides the capability to reverse the process, being able to calculate the required gear dimensions based on a specified load rating and certain geometric constraints. The results of both dimensioning and verifications can be visualized with the help of numerous 2D and 3D graphs and reports.

Further details will be presented in the following sections, entirely devoted to gears design.

Each calculation module is related to a gear pair constraint, so in the transmission model two of these are present:

- *SunPlanet1_calc*, regarding the meshing of the sun gear with the first stage planet gear;
- *Planet2Ring_calc*, including the data of the second stage planet gear and of the ring gear.

3.4. Gear pair calculation

As said above, all calculations regarding the gears are performed inside the related KISSsoft calculation module. This tool is very powerful, but for its functioning a lot of data and information must be inserted in different tabs, subdivided between standard and special. The main ones are presented below.

3.4.1. Basic data

The *Basic data* tab contains all the fundamental information needed to define the gears. It is subdivided into two sections, *Geometry* and *Material and Lubrication*.

In the *Geometry* section, all the main geometrical dimensions must be inserted. These are:

- normal modulus
- pressure angle
- helix angle, if present
- centre distance
- number of teeth of each gear
- face width of each gear
- profile shift coefficient for each gear
- quality level according to ISO 1328:2013

All of these values can be inputted to the software, but some of them can be directly calculated according to the specific needs and requirements specified by the user. Furthermore, in this section it is also possible to define the internal geometry of gear components according to the shape and dimensions defined in the figure below.

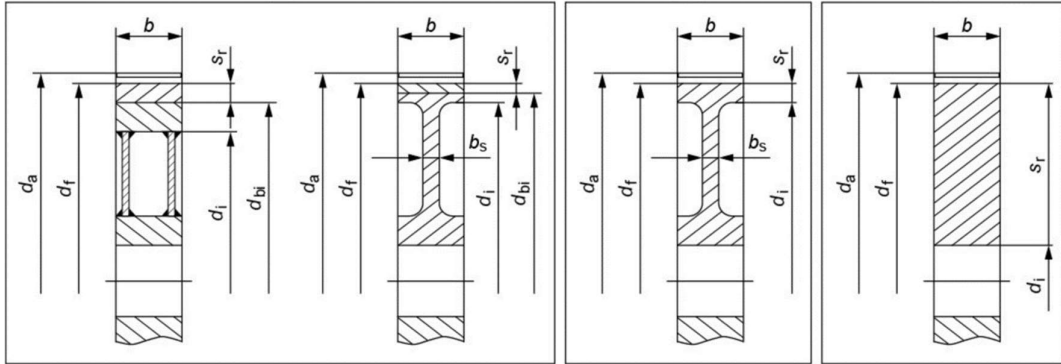


Figure 35. Gear internal geometry

In the *Materials and Lubrication* section all information regarding materials used for each gear, lubricant used with its working temperature and method of lubrication should be detailed.

3.4.2. Reference profile

The *Reference profile* tab includes data needed to define the shape of the gear teeth.

The profile can be defined with custom values, can be dimensioned from the software according to the specific requirements or can be chosen among different norms. The most common profile is the one described by profile A of ISO 53:1998, which has an addendum coefficient of 1, a dedendum coefficient of 1,25 and a root radius coefficient of 0,38.

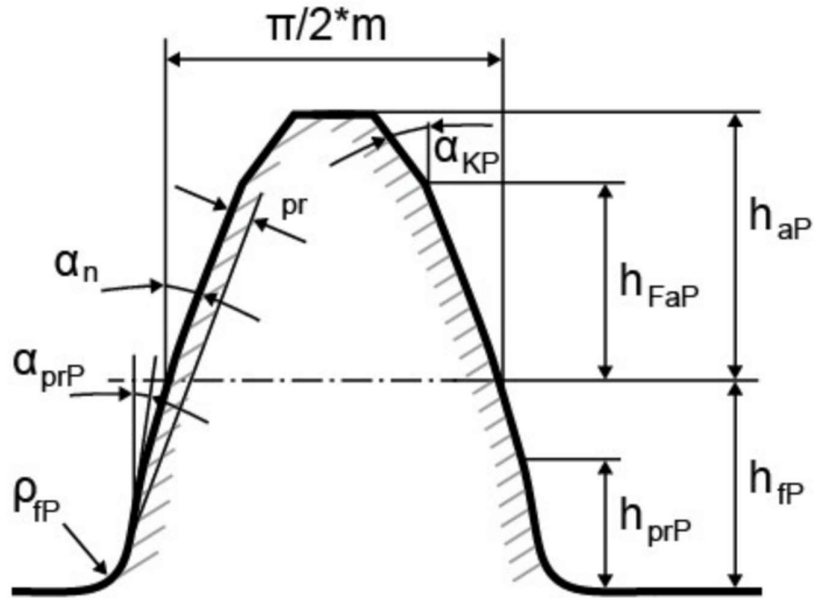


Figure 36. Gear reference profile

The profile of the teeth is then modified according to the tool used for gear cutting, whose dimensions and geometry can also be defined in this section.

The choice of the reference profile has a great impact on the teeth dimensions and strength.

3.4.3. Manufacturing

In the *Manufacturing* tab is possible to specify the manufacturing process for pre-machining and final machining.

It can also be checked whether special manufacturing processes such as power skiving or honing can be used. Also manufacturing deviations and modifications for each gear can be set in this section.

3.4.4. Tolerances

The *Tolerances* tab allows to define the tolerance class both for the gear teeth thickness and for the centre distance.

These values can be chosen according to tabulated data according to different norms. Moreover, in this section it is possible to set the tolerance for the teeth shape and the process to measure gears. The tolerance class must be chosen considering the material used, the application and the production process.

3.4.5. Modifications

In the *Modifications* tab it is possible to define all the modifications of tooth geometry.

This aspect is important to improve the contact between mating gears, reducing noise and peak stress on teeth. The possible modifications include face chamfering, tip and root relief, end relief and face crowning. The dimensions of the modifications can be entered by the user or calculated by the software and their design will be treated in detail in the microgeometry dimensioning section.

3.4.6. Rating

The *Rating* tab includes all the information for the calculation of the gears' life.

In this section it is possible to define the loading conditions, inserting the values for the torque and rotational speed, and the required service life. Then the calculation to be performed are chosen, together with the normative that should be applied with all the relative specific data.

The main calculations include the bending and pitting strength according to ISO, AGMA or DIN norms. There is also the possibility to choose the load spectrum to consider for the calculation.

3.4.7. Factors

Lastly, in the *Factors* tab it is possible to define the main factors involved in the majority of calculations.

The factors can be chosen by the user considering tables according to the operating conditions or directly calculated from the software. Main factors include the application

factor K_A , the dynamic factor K_V , the face load factor $K_{H\beta}$ and the alternating bending factor Y_M .

3.5. Spur gears load capacity

3.5.1. ISO 6336:2019 standard

The calculation of the resistance of the gears to the loads applied is one of the fundamental steps in the design process. The results are provided by KISSsoft according to the chosen standard, which in this case was ISO 6336:2019.

ISO 6336:2019 standard is the latest update of this norm, first written in 1997 and then updated to implement the newest discoveries. This standard is one of the most widespread regarding the mechanical design of gear components and provides a robust system for calculating the load capacity of cylindrical involute gears, both with external and internal teeth. The procedures in the ISO 6336 series provide rating formulae for the calculation of load capacity with regard to different failure modes, of which the most relevant ones are pitting and tooth root breakage, described in ISO 6336-2 and ISO 6336-3 respectively.

For each of the failure modes a different safety factor should be defined, S_H regarding pitting and S_F regarding tooth root breakage. In any case it can be calculated as:

$$S_{H/F} = \frac{\text{limiting stress number}}{\text{calculated stress}}$$

Both the limiting stress number and the calculated stress are affected by various factors, which influence the calculations and are defined in the norm according to geometrical, material and loading characteristics as result of research and experimental data.

Depending on how the factors are calculated, three different methods can be distinguished:

- Method A: calculations are based on factors obtained from rigorous data sources. These sources include full-scale load tests, precise measurements, or comprehensive mathematical analyses of the transmission system, often grounded in established operational experience. While it can provide the highest level of

accuracy, it is seldom used due to large amount of data regarding loading conditions and gear geometry needed with respect to methods B and C. Additionally, it requires significant resources and a costly experimental plan;

- Method B: factors are derived with sufficient accuracy for most practical applications. However, the key aspect is the explicit listing of assumptions made during factor determination. It is crucial to evaluate whether these assumptions align with the specific conditions of interest. This method is the most commonly used due to its adaptability and widespread applicability;
- Method C: involves calculations based on simplified assumptions for certain factors, with these assumptions explicitly stated. On each occasion, an assessment should be conducted to determine whether these assumptions apply to the existing conditions. While it sacrifices some accuracy in comparison to Method B, it prioritizes simplicity and speed. Method C is often chosen when a quick assessment or rough estimate suffices, especially in situations with limited data or resources.

The method adopted for this analysis is method B, since it provides accurate results without the need of complex testing and measurements.

Although the ISO 6336 standard is the most widely adopted norm for gear dimensioning, some experimental investigations has proved that this norm underestimates the strength and resistance of gears with a normal module of less than 1 mm.

According to these researches, a corrective factor of 1.29 should be applied when dealing with carburized gears with modulus of 1 mm or less, as their strength has proven to be even 30% larger than what is evaluated by the ISO 6336 norm. Despite this extremely conservative approach of the standard, KISSsoft is able to account for this effect when dealing with gears design.

3.5.2. Pitting

Pitting is a common gear failure mode that occurs as a result of surface fatigue due to the high Hertzian contact stresses generated during gears meshing. It manifests as the formation of small, localized craters or pits on the surface of a gear tooth.

Pitting is primarily caused by repeated contact stresses and surface wear during the gear's operation. Factors such as insufficient lubrication, high loads, and inadequate gear design can exacerbate pitting. Over time, these pits can grow larger, leading to material loss and potentially compromising the gear's structural integrity, ultimately resulting in the premature failure of gears. The failure is not catastrophic and can be easily spotted during maintenance operations.

The calculation of surface durability is based on the contact stress at the pitch point. The safety factor against pitting is defined as

$$S_H = \frac{\sigma_{HP}}{\sigma_H}$$

σ_H is the contact stress, calculated as

$$\sigma_H = X_1 \sqrt{\frac{F_t}{d_1 b} \frac{u+1}{u}} X_2$$

σ_{HP} is the permissible contact stress, calculated as

$$\sigma_{HP} = X_3 \frac{\sigma_{H \text{ lim}}}{S_{H \text{ min}}}$$

Where:

- X_1 , X_2 and X_3 are the products of different factors;
- F_t is the tangential force acting on the gear tooth;
- d_1 is the gear reference diameter;
- b is the gear face width;
- u is the gear ratio;
- $\sigma_{H \text{ lim}}$ is the maximum allowable pitting stress of the material;
- $S_{H \text{ min}}$ is the minimum required pitting safety factor.

3.5.3. Tooth root breakage

Tooth root breakage, also known as tooth root fracture or tooth bending fatigue failure, occurs when the root area of a gear tooth fails due to cyclic bending stresses or due to an

excessive overload. This type of failure typically begins as small cracks at or near the base of the gear tooth and gradually propagates through the material until the tooth breaks.

Tooth root breakage is influenced by factors such as excessive loads, insufficient gear size, inadequate material strength, and improper gear geometry. It is a serious gear failure mode as it can lead to catastrophic gear failure, with consequent damages on the whole assembly.

Tooth root stress is the maximum tensile stress at the surface in the root fillet due to the bending effect. The safety factor against tooth root breakage is defined as

$$S_F = \frac{\sigma_{FP}}{\sigma_F}$$

σ_F is the tooth root stress, calculated as

$$\sigma_F = Y_1 \frac{F_t}{b m_n}$$

σ_{FP} is the permissible contact stress, calculated as

$$\sigma_{FP} = Y_2 \frac{\sigma_{F \text{ lim}}}{S_{F \text{ min}}}$$

Where:

- Y_1 and Y_2 are the products of different factors;
- F_t is the tangential force acting on the gear tooth;
- b is the gear face width;
- m_n is the gear normal modulus;
- $\sigma_{F \text{ lim}}$ is the maximum allowable bending stress of the material;
- $S_{F \text{ min}}$ is the minimum required safety factor for tooth root stress.

3.6. Material choice

The selection of the material for gears manufacturing is very relevant as it forms the fundamental basis for their overall mechanical capabilities. Gears must withstand substantial loads, intense friction, and impact stresses.

The targets for this transmission design are to reduce the weight and size of the components, while increasing the durability of the assembly and the service life. It is clear that one of the possible ways to achieve these targets is to choose properly the material used.

An evaluation regarding the implementation of aluminium alloy gears has been carried out, but the lower mechanical properties of this material led to excessively bulky components with anyway a low resistance.

As a result, steel alloys represent the most suitable material for this application. In order to attain the requisite strength and resistance to friction, it is essential to harden the steel to a hardness level of 55 HRC or higher. This can be accomplished through various methods, including carburizing and nitriding. Apart from the necessary hardness of the tooth surface, the remainder of the gear structure necessitates a high material strength capacity.

Carburization and nitridation are case hardening processes, thus very effective to reach the desired material performances. During these processes the surface is hardened, while the core of the material remains still quite flexible, preventing brittleness of the tooth. These processes happen at high temperature in a controlled environment, thus causing some distortion on gear teeth and requiring a finishing operation after the surface treatment to obtain the desired quality. This effect is minimized for small gears, since the exposure to high temperature is minimized due to the low thickness of the hardened layer.

The surface hardness has a great impact on the allowable stress, both for pitting and tooth root breakage. To have the smallest possible gears with the highest possible resistance it is evident the benefit of using the most performing material available.

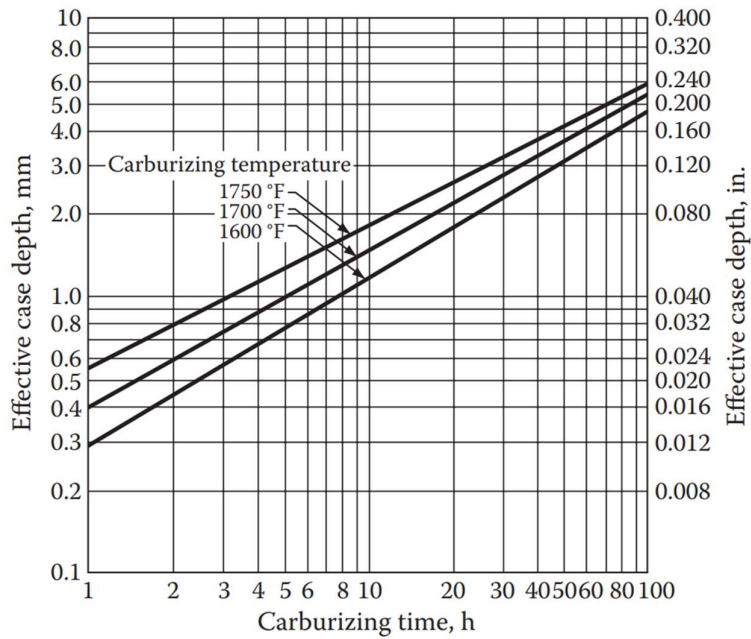


Figure 37. Carburizing process duration and temperature

Different steel alloys have been evaluated, comparing their mechanical characteristics and balancing them with availability and cost. The choice of the material has been done concurrently with the macrogeometry sizing, described in the next section, checking that the chosen material was able to provide the needed performances.

As carburizing is the surface treatment yielding the most promising characteristics, steels with this treatment have been taken into account. The alloys considered have been:

- 18NiCrMo7, a carburizing steel that was used in SC22 transmission. It is a very common gear material and is largely available at a relatively low price. Its mechanical performances are decent and are listed in the table below. The properties of 18NiCrMo7 will be considered the baseline for the comparison.

18NiCrMo7	
Treatment	Carburization
Density	7,85 g/cm ³
Elastic modulus	210 GPa
Yield strength	850 MPa
Ultimate tensile strength	1100 MPa
Surface hardness	60 HRC
Core hardness	40 HRC

Table 2. Steel 18NiCrMo7 characteristics

- BS S156, a high performance carburizing steel designed especially for aerospace applications. The mechanical characteristics are better with respect to the ones of 18NiCrMo7, but the surface hardness achievable is not as high. The availability of the material can be problematic. The properties are shown in the table below.

BS S156	
Treatment	Carburization
Density	7,8 g/cm ³
Elastic modulus	205 GPa
Yield strength	1030 MPa
Ultimate tensile strength	1320 MPa
Surface hardness	55 HRC
Core hardness	40 HRC

Table 3. Steel BS S156 characteristics

- Ferrium C61, a high performance carburizing steel offering high mechanical properties, high core strength and extremely high fatigue and wear resistance. It is a special steel designed for aerospace and high performance motorsport

applications. All the characteristics are improved with respect to 18NiCrMo7 and S156 alloys, but the price increases. Its properties are listed below.

Ferrium C61	
Treatment	Carburization
Density	7,97 g/cm ³
Elastic modulus	205 GPa
Yield strength	1550 MPa
Ultimate tensile strength	1650 MPa
Surface hardness	62 HRC
Core hardness	48 HRC

Table 4. Steel Ferrium C61 characteristics

- NC310YW, a super high performance carburizing steel with extreme strength characteristics and a density lower than a normal steel. Its hardening characteristics are very good as this is an alloy designed for use in high performance gear solutions, but not quite reaching the hardness of Ferrium C61. The downsides are the extremely high cost and the very low availability. The main mechanical properties are shown in the table.

NC310YW	
Treatment	Carburization
Density	7,66 g/cm ³
Elastic modulus	202 GPa
Yield strength	1790 MPa
Ultimate tensile strength	2150 MPa
Surface hardness	60 HRC
Core hardness	42 HRC

Table 5. Steel NC310YW characteristics

After having analysed these possible materials, the choice has fallen on Ferrium C61 for all gears. 18NiCrMo7 was not able to sustain the stresses involved in the gear meshing with a sufficient safety factor, thus its application was not possible. S156 had a sufficient strength to bear the loads of the first reduction stage, but not for the second one. Moreover, its low availability, combined with a medium price tag, made it not suitable for this application. NC310YW would be the best choice looking at the mechanical properties, but unfortunately it is extremely expensive, up to 100 times a normal steel, and it is difficult to find on the market.

Finally, Ferrium C61 represents the right compromise for this application, providing very high performances in terms of strength and durability and having a better availability. The cost of this material is quite high, but the impact of the raw material on the total cost of the transmission is limited and this effect could be counterbalanced by the longer service life achievable.

3.7. Macrogeometry dimensioning

The dimensioning of the macro geometrical parameters of the gears has been carried out using an iterative approach in KISSsoft. The process is done starting from the rough dimensioning performed in paragraph 2.7 and then using the KISSsoft macrogeometry sizing function.

Sizing function proposes possible gear teeth configurations based on the data entered for the reduction ratio and the load applied. The purpose of macrogeometry sizing is to ascertain the possible range of suitable solutions, all sized for the specified torque, according to all the specified required safeties and to the parameters inserted in the relative gear pair calculation module. It is needed to specify the range of variations of some parameters, such as the number of teeth, the face width and the centre distance. The program displays a number of different solutions among which the user can choose.

This procedure has been carried out several times both for the first and for the second stage gear pairs, iteratively improving the precision of the results until a solution satisfying the targets was found.

As seen before in section 3.6, the material chosen is Ferrium C61 carburized for all the gears. A pressure angle of 20° was selected for this gearbox design, as it offers advantages in terms of both efficiency and ease of manufacturing. Notably, an increase in the face width of the driving wheels (which in this particular transmission layout are the sun gear and the second stage planet gears) relative to the driven gears was decided upon. This adjustment was made to ensure that the minimum calculated face width always remains in contact, preventing a reduction in the contact surface under load conditions.

The normal modulus for every gear pair was set to 0,6 mm, as described in section 2.7.

The profile shift coefficient has been calculated by the software to optimize the specific sliding between gear teeth, maintaining constant the centre distance.

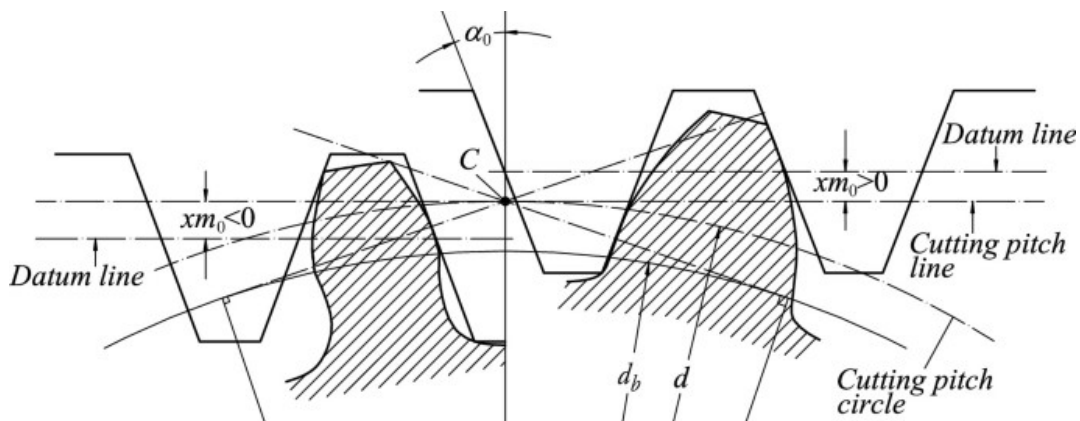


Figure 38. Profile shift coefficient

In adherence to ISO 1328:2013 standards, a quality level of 5 has been designated for all external gears. This quality level can be achieved by grinding the surface of teeth. However, the ring gear cannot be ground due to the complexity of being an internal gear with an extremely fine modulus, so its quality level has been set to 7.

Regarding lubrication, ISO-VG 46 oil has been chosen for the gearbox, with a more detailed discussion of lubrication in section 5.2.1. The lubrication method employed is *oil bath lubrication*, which aligns with the actual working conditions of the gearbox.

The selected reference profile is ISO 53:1998 Profile A, with specific coefficients: a dedendum coefficient of 1,25, an addendum coefficient of 1,00, and a root radius coefficient of 0,38.

To ensure precision and reliability, the tooth thickness tolerance conforms to class DIN 3967 d26, following Niemann's proposal. This tolerance class is well-suited for standard machine parts with a module falling within the range of 0,5 to 3 mm.

The centre distance tolerance has been set to 5J, according to the proposal of DIN 58405 for hardened steel gears.

For the dimensioning phase, the load condition considers the peak input values of 21 Nm of torque and 20000 rpm. This very high load, never actually reached in real applications, is important to achieve sufficiently resistant and durable gears.

The required service life for the gearbox has been established at 50 hours, with a minimum safety factor of 1 both concerning pitting and tooth root failure.

After some calculation loops, it was possible to find the optimal solution regarding the main geometrical parameters for the gears. The main results are summarized in the following tables both for the first and second reduction stage.

First reduction stage		
	Sun Gear	Planet Gear 1
Normal modulus - m_n	0,6 mm	
Pressure angle - α	20°	
Centre distance - a	25,2 mm	
Number of teeth - z	25	59
Profile shift coefficient - x^*	0,2293 mm	-0,2293 mm
Face width - b	12 mm	11,5 mm
Quality level	5	
Material	Ferrum C61	

Table 6. First reduction stage data

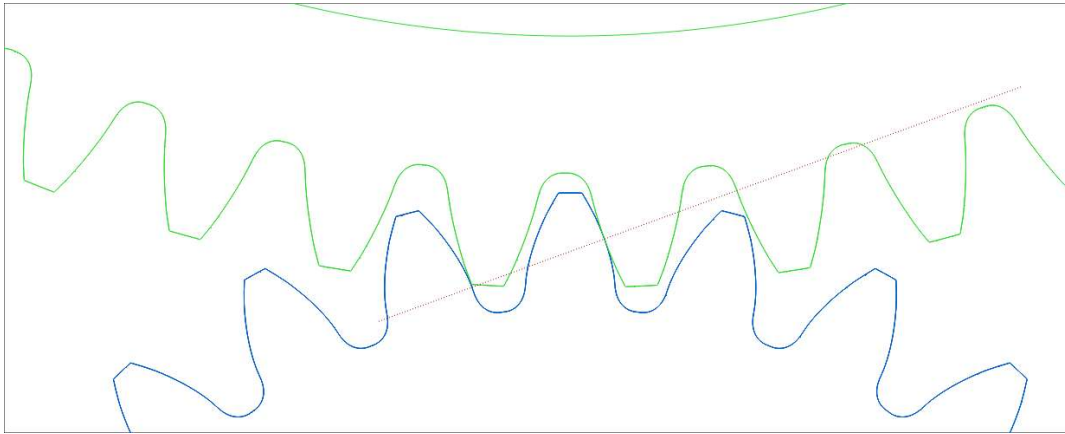


Figure 39. First stage meshing gears

Second reduction stage		
	Planet Gear 2	Ring Gear
Normal modulus - m_n	0,6 mm	
Pressure angle - α	20°	
Centre distance - a	-25,2 mm	
Number of teeth - z	21	-105
Profile shift coefficient - x^*	0,4891 mm	-0,4891 mm
Face width - b	14,5 mm	14 mm
Quality level	5	7
Material	Ferrum C61	

Table 7. Second reduction stage data

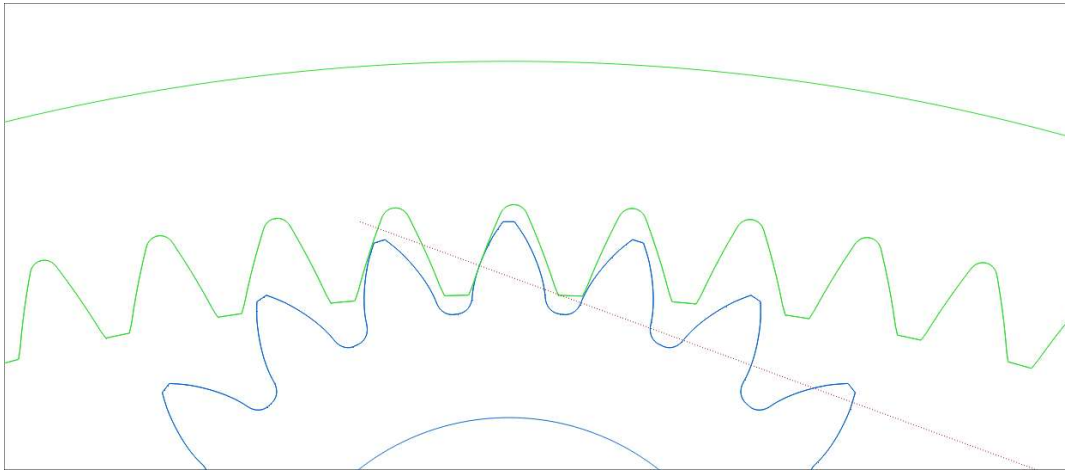


Figure 40. Second stage meshing gears

The reduction ratio obtained with this configuration is 12,8, which is quite close to the target one of 12,5.

3.8. Microgeometry dimensioning

The basic tooth profile is an involute of a circle. Under normal operating conditions this profile departs from the theoretical configuration due to the load applied during gear meshing between teeth and the deflection of machine elements, shafts and teeth themselves.

To mitigate the effect of these deformations, it is possible to modify the involute profile in the design phase, trying to optimize the shape of teeth under load and to achieve specific targets.

Tooth profile modifications act both on the radial and axial profile of the tooth and the most common and widespread options are tip and root relief and crowning respectively.

Tip relief is a modification of gear tooth profile that serves the essential purpose of promoting a more consistent load distribution during the meshing process. This refinement is pivotal for achieving smoother and more predictable meshing actions, offering a range of advantages, notably in terms of noise reduction and enhanced gear longevity.

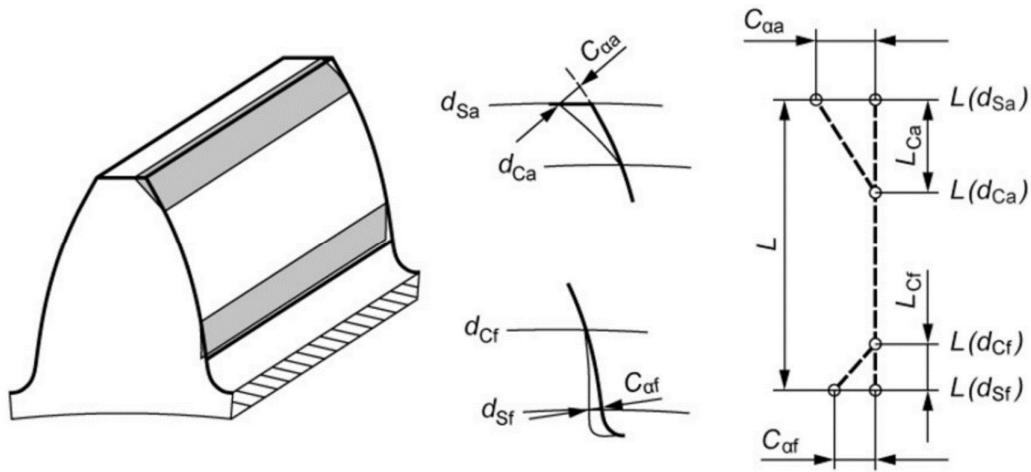


Figure 41. Tip and root relief modifications

When applied to the driven gear, tip relief is specifically engineered to address the initial stage of meshing. It works to decrease the impact force as one gear tooth initiates engagement with another, thereby softening this contact. For the driving gear, tip relief is directed toward the final phase of meshing. It aims to attenuate the impact force as one gear tooth disengages from another, ensuring a smoother separation process. Typically, due to these advantages, tip relief is incorporated into both the driving and driven gears within a gear system.

Crowning modification involves introducing a slight convex curvature along the width of the gear teeth, as opposed to having perfectly straight profiles. The primary objective of crowning is to address the uneven distribution of loads across gear teeth. Crowning helps distribute these loads more evenly along the width of the teeth, mitigating localized stress concentrations. Moreover, crowning ensures that the central section of the gear teeth makes initial contact during meshing. This enhances the gear's resistance to issues like pitting, wear, and scuffing, leading to improved gear durability and performance.

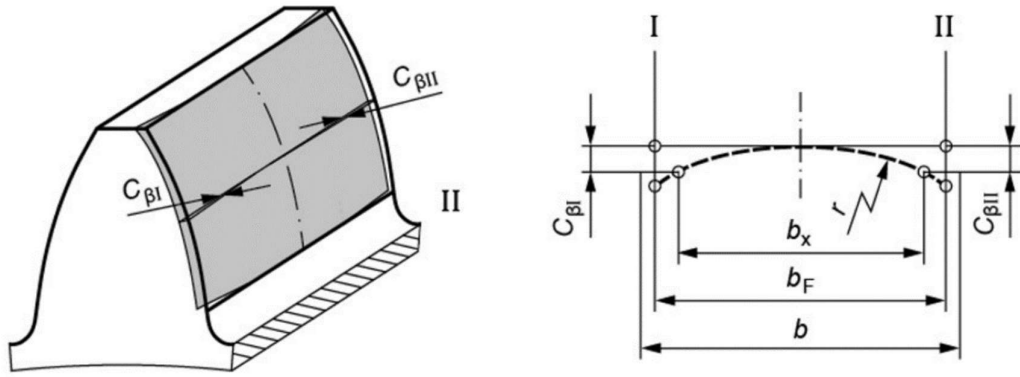


Figure 42. Crowning modification

KISSsoft offers the microgeometry dimensioning tool, a very powerful instrument for the design of tooth profile modifications. The user can define which of the possible modifications to apply and the software calculates the optimum values according to the gears geometry and loading conditions. It was decided to have tip relief and crowning on all gears.

For the first reduction stage the optimal tip relief was calculated according to the linear method and resulted to be of $8 \mu\text{m}$ (C_a in figure 41) with a length of $6 \mu\text{m}$ (L_{Ca} in figure 41). The optimal crowning C_β was obtained with a value of $2 \mu\text{m}$.

It is possible to notice the effects of these modifications looking at the graphs below, representing the normal force acting on the tooth flank before and after the application of the modified profile. Before the modifications, the load distribution graph displayed concentrated stress areas, with uneven contact patterns and elevated stress levels at certain points along the tooth profile. This often results in premature wear, noise, and reduced gear life.

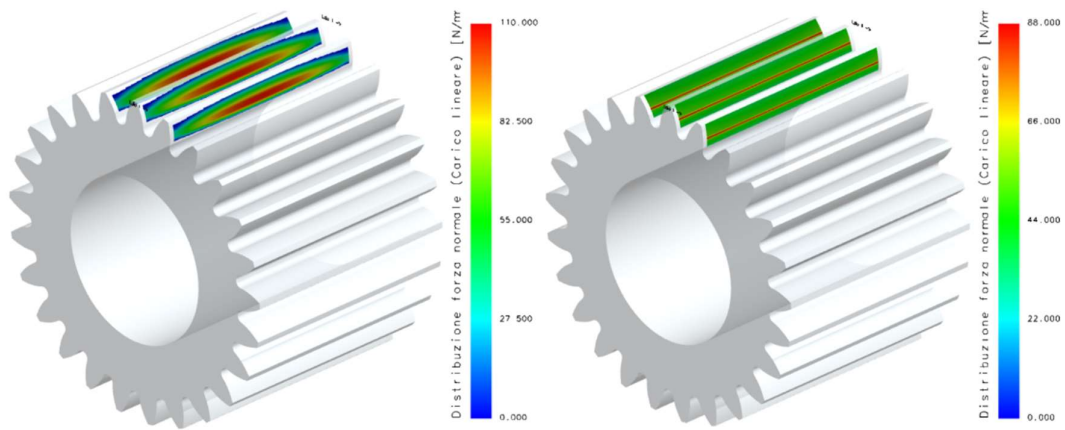


Figure 43. First stage normal load distribution after (left) and before (right) profile modifications

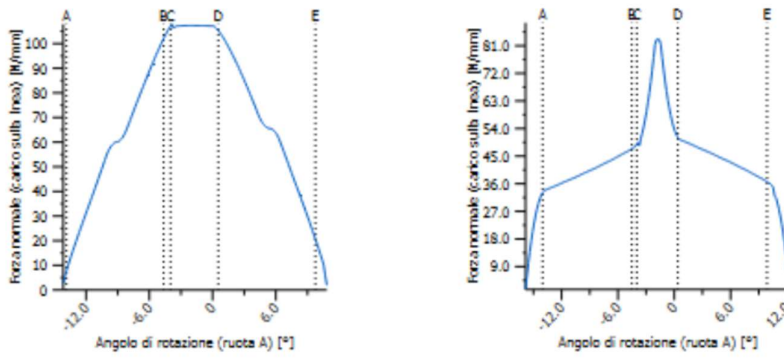


Figure 44. First stage normal force on tooth after (left) and before (right) profile modifications

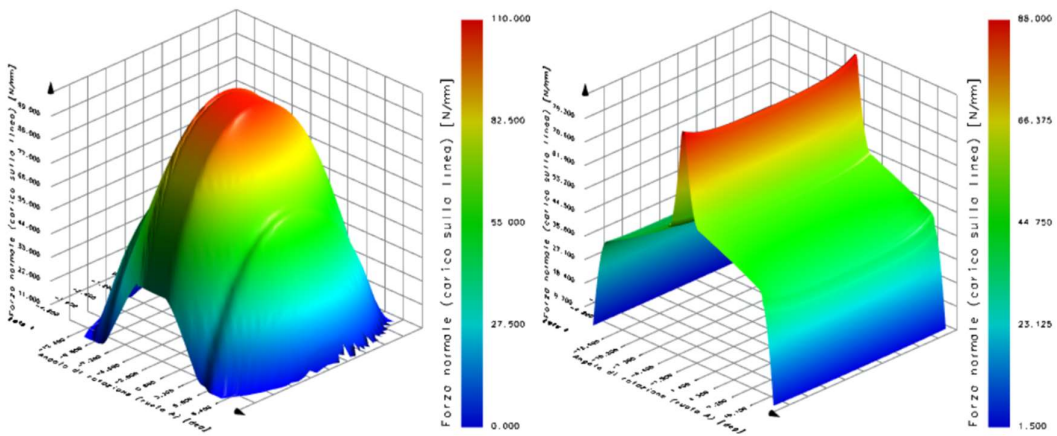


Figure 45. First stage normal force on tooth after (left) and before (right) profile modifications 3D view

However, after the profile modifications were implemented, the load distribution graph underwent a remarkable transformation. The modifications led to a more uniform and balanced distribution of load across the entire tooth profile. Stress concentrations were significantly reduced, and the graphs showed a smoother, more symmetrical curve, reflecting an even transmission of forces. This enhancement not only ensures a longer lasting and quieter gear operation, but also enhances the gear's overall efficiency and reliability.

Also for the second stage the linear method has been chosen and a tip relief of $13\ \mu\text{m}$ (C_a in figure 41) with a length of $6\ \mu\text{m}$ (L_{Ca} in figure 41) is obtained. The optimal crowning resulted to be with $C_\beta = 1\ \mu\text{m}$.

In the following, as for first the first stage, also for the second stage are shown the plots of the normal forces acting on the tooth flank both with and without profile modifications.

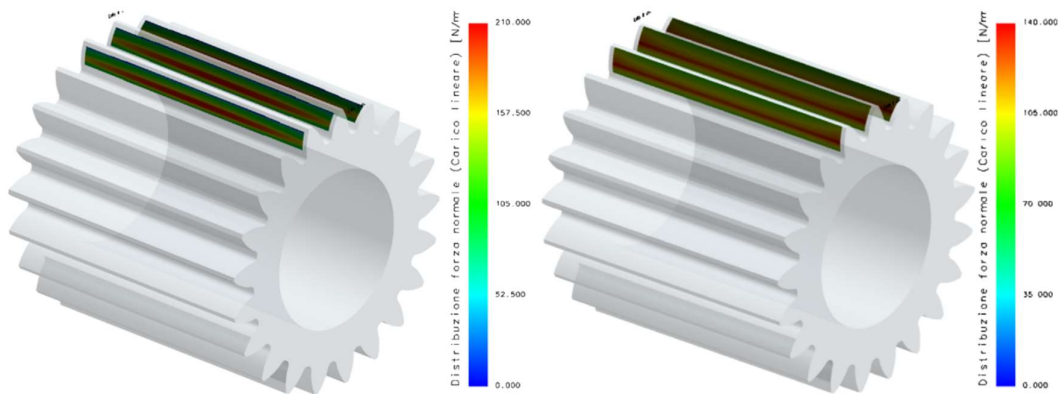


Figure 46. Second stage normal load distribution after (left) and before (right) profile modifications

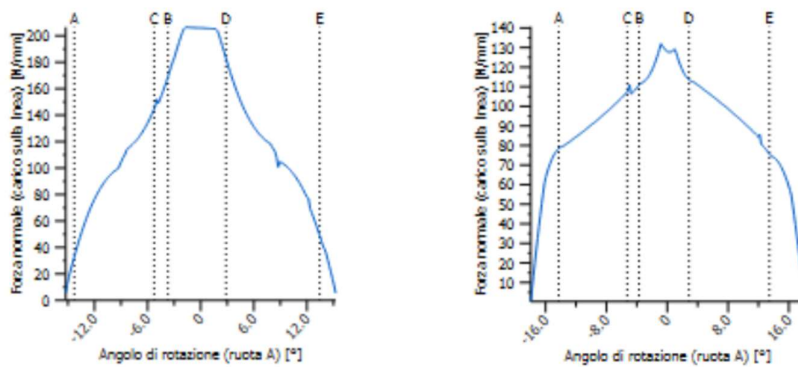


Figure 47. Second stage normal force on tooth after (left) and before (right) profile modifications

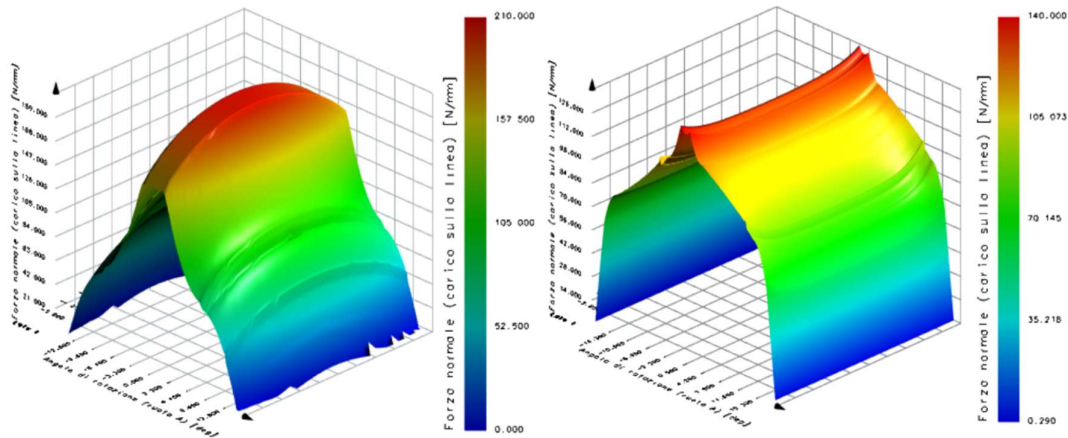


Figure 48. Second stage normal force on tooth after (left) and before (right) profile modifications 3D view

Also in this case it is evident the effect of profile modifications on the load distribution, reducing peaks of concentrated forces in favour of a smoother and better distributed load exchange area. The result is a smoother gear engagement, with benefits for noise emissions, gear lifetime, efficiency and reliability.

3.9. Gear life calculation: peak load

After having defined the geometrical macro and micro dimensions of the gears, it is possible to proceed with the life calculation.

This process consists in running the calculation on the entire gear pair module in KISSsoft, receiving as results the safety factors defined in ISO 6336:2019 according to the defined load conditions and parameters. The outputs of the software also include a large number of graphs and reports, useful to better understand and visualize the obtained results. The target is to have all safety factors greater than 1.

To perform the calculation, it is needed to define all the necessary corrective factors influencing the final results.

The application factor K_A compensates for any uncertainties in loads and impacts. Following tabulated values presented in ISO 6336-1, it has been set to 1,0. This has been done since for the calculation at maximum nominal torque and power the loading condition is already very conservative, and regarding the load spectrum calculation the knowledge of the loading condition is quite detailed with low possibility of changes.

The internal dynamic factor makes allowance for the effects of gear tooth accuracy and modifications as related to speed and load. It is calculated by the software according to the loading conditions.

The transverse load factor $K_{H\alpha}$ accounts for the effect of the nonuniform distribution of transverse load between several pairs of simultaneously contacting gear teeth. It is calculated by KISSsoft.

The mesh load factor K_{γ} takes into consideration the uneven load distribution across multiple planets or idler gears, especially in planetary systems. Its value has been set to 1,0, since it has been assumed that the power is equally subdivided between planets and the corrected values of torque have been used for the calculations.

The alternating bending factor Y_M is used to adjust the basic fatigue strength of a gear tooth when it experiences fluctuating loads. It is specifically applied to account for the alternating nature of the bending stresses that occur as gear teeth engage and disengage during each rotation. The value was set to 0,65, considering an oscillating operating mode as seen in the picture below.

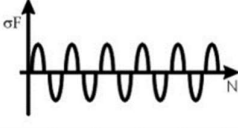
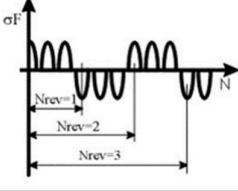
Operating Mode	Alternating Bending Factor (Mean Stress Influence Factor) Y_M	Load Direction
Pulsating	1	
Alternating	0.7 ⁽¹⁾ 0.65 ⁽²⁾	
Oscillating	$0.85 - 0.15 \cdot \frac{\log N_{rev}}{6}$ ⁽¹⁾ $0.85 - 0.20 \cdot \frac{\log N_{rev}}{6}$ ⁽²⁾ ($1 \leq N_{rev} \leq 10^6$) 0.7 ⁽¹⁾ 0.65 ⁽²⁾ ($N_{rev} \geq 10^6$)	
<small>(1) Linke, H.: Stirnradverzahnung, Carl Hanser Verlag, 1996. (2) Linke, H.: Stirnradverzahnung, Carl Hanser Verlag, 2010.</small>		

Figure 49. Alternating bending factor

The face load factor $K_{H\beta}$ takes into account the effects of the nonuniform distribution of load over the gear face width. The calculation requires detailed knowledge of the

deformation of teeth and shafts under load, so its value is determined by KISSsoft giving as input the profile modifications along the face width adopted and the type of pinion gear. Looking at the figure, the pinion gear type changes between the two reduction stages according to ISO 6336; first stage pinion is of type *C*, while second stage one is of type *B*.

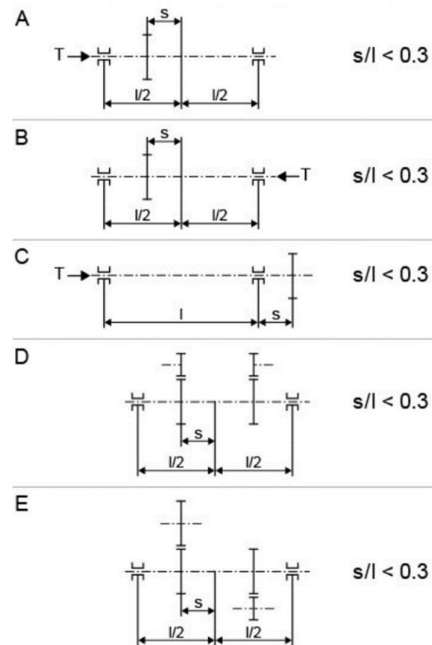


Figure 50. Type of pinion gear according to ISO 6336

The calculation has been carried out considering the maximum nominal load of 21 Nm and a rotational speed of 20000 rpm. The safety factors obtained for all the gears regarding both pitting and tooth root failure are shown in the table below.

	Sun Gear	Planet Gear 1	Planet Gear 2	Ring Gear
S_F	3,1	2,9	1,5	1,5
S_H	1,2	1,3	1,1	1,2

Table 8. Gears safety factors at peak load

Analysing the results, it is possible to notice how the second reduction stage is more stressed due to the higher loads applied. In any case all the safety factors reach the imposed target.

Below the graph of the specific sliding is shown for the two reduction stages.

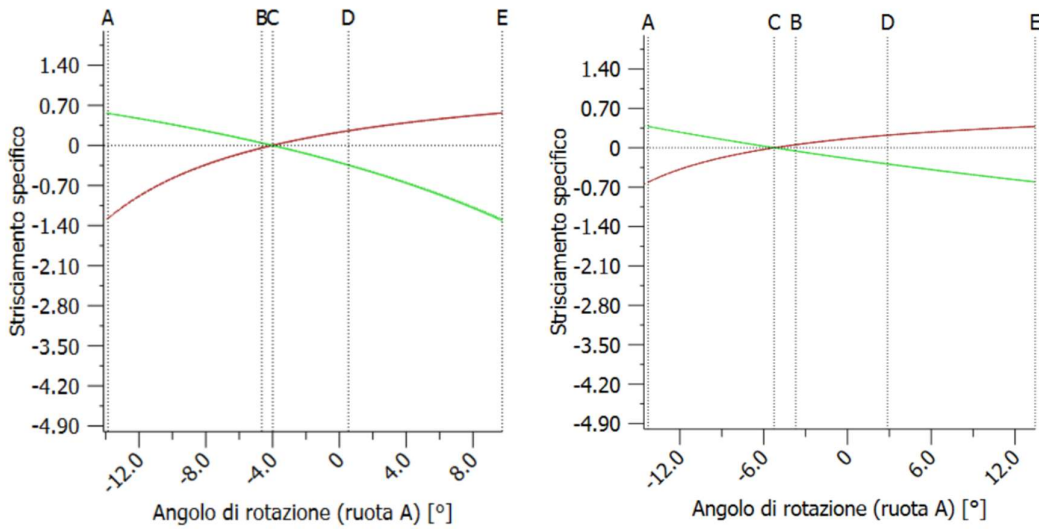


Figure 51. First (left) and second (right) stage specific sliding

The graphs depicting the bending and contact stresses applied on a gear tooth, along with the corresponding safety factors as a function of gear lifetime, provide a comprehensive insight into the gear's performance and reliability.

The bending stress graph showcases the bending stress experienced by the gears' teeth. It is noticeable that the second stage experiences higher bending stress, due to the higher forces exchanged. Looking at the 3D stress distribution, it is possible to visualize the most stressed areas, related to the load application points and to the contact surface.

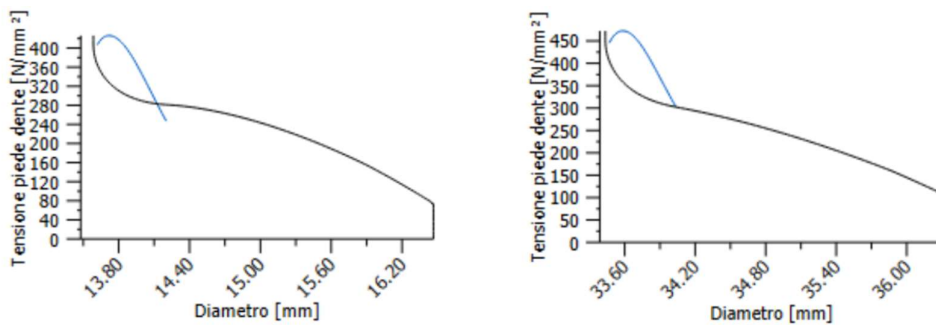


Figure 52. Root stresses for sun gear (left) and for first stage planet gear (right) at peak torque

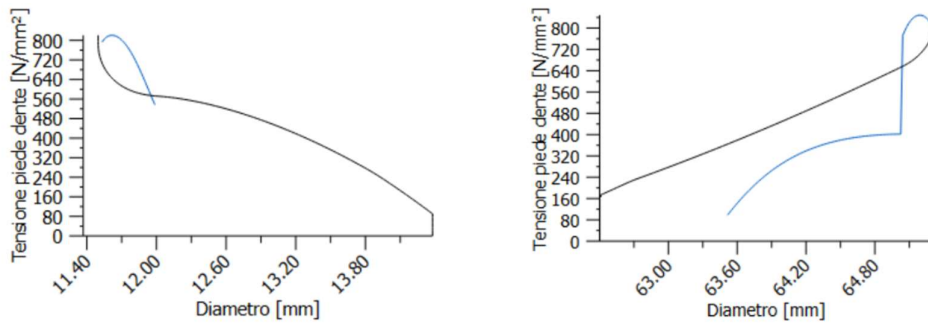


Figure 53. Root stresses for second stage planet gear (left) and for ring gear (right) at peak torque

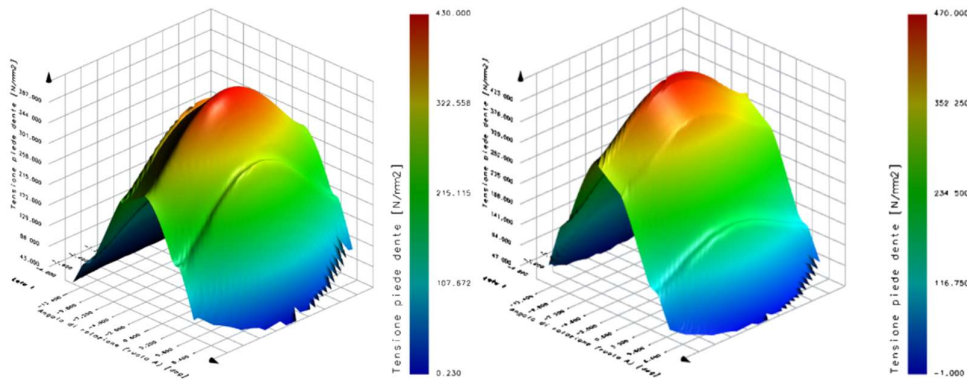


Figure 54. 3D stress distribution for sun gear (left) and for first stage planet gear (right) at peak torque

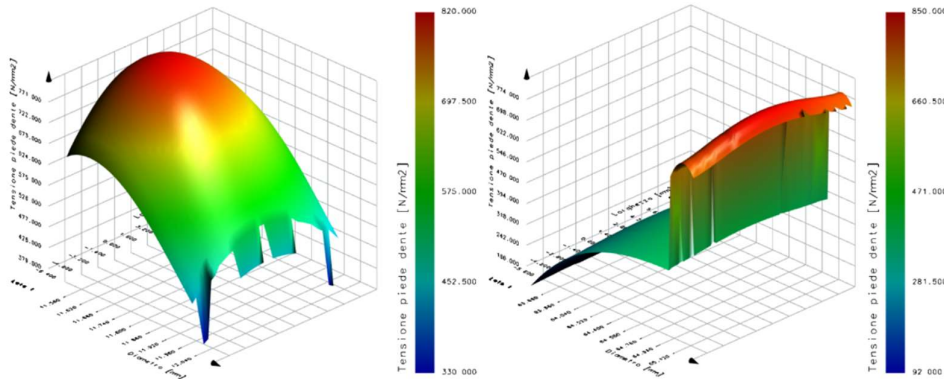


Figure 55. 3D stress distribution for second stage planet gear (left) and for ring gear (right) at peak torque

The contact stress graph illustrates the pressure distribution on the gear tooth's contact surface. Again, the values are higher for the second stage.

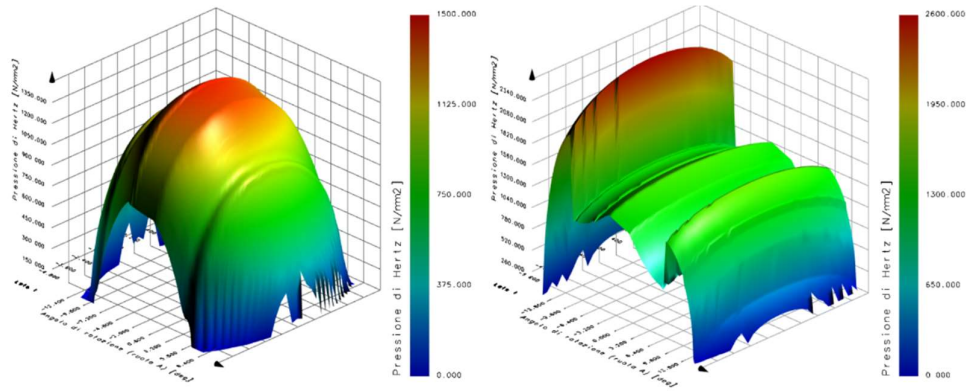


Figure 56. 3D contact pressure distribution for first (left) and second (right) stage at peak torque

The safety factors, plotted over the gears' lifetime, provide a view of the gears' resistance, indicating how they respond to stress fluctuations over time. Safety factors for second stage are lower as result of the higher bending and contact stresses. Pitting safety factors are lower and approach 1 after the desired service life of 50 hours.

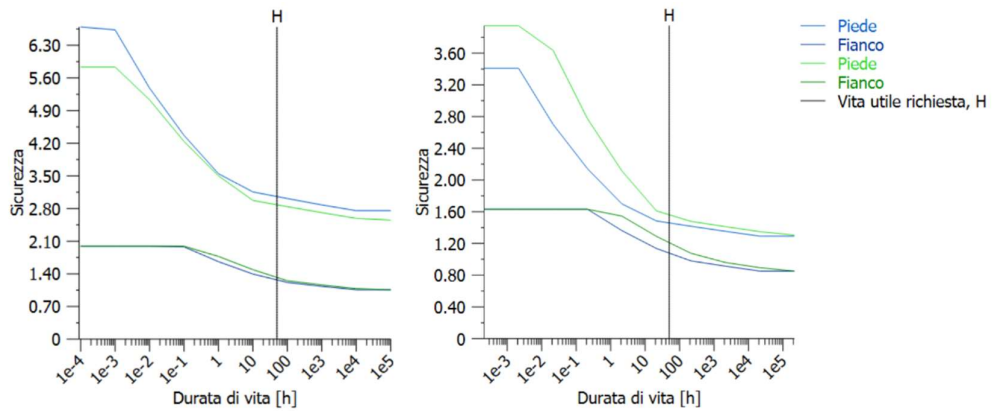


Figure 57. Safety factors for first (left) and second (right) stage

Additionally, the proposed hardness curves are shown, offering valuable information about the material's surface resistance needed to sustain the applied loads.

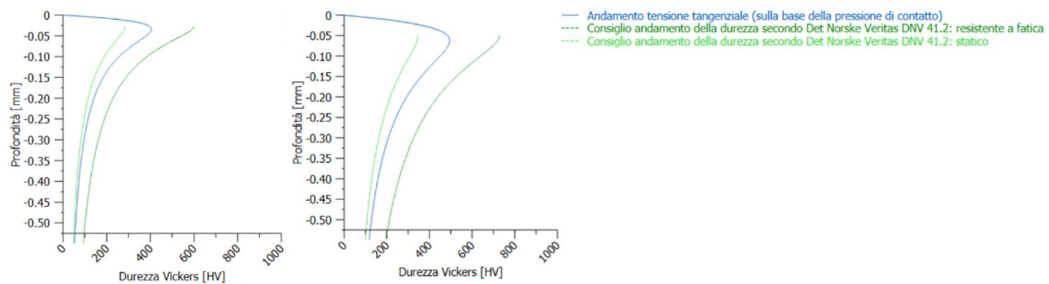


Figure 58. First (left) and second (right) stage hardness curve recommendation

3.10. Gear life calculation: load spectrum

The second calculation has been carried out considering the load spectrum defined in section 2.8, that scales the peak values of 21 Nm and 20000 rpm according to the real conditions faced during an autocross event. This loading condition is more representative of the real operating range during the transmission life, while still maintaining the conservative approach.

The safety factors obtained for all the gears regarding both pitting and tooth root failure are shown in the table below.

	Sun Gear	Planet Gear 1	Planet Gear 2	Ring Gear
S_F	4,0	4,0	2,0	2,5
S_H	1,7	1,8	1,5	1,7

Table 9. Gears safety factors with load spectrum

Looking at these results, it is clear that the safety factors obtained have increased. The second stage remains more critical than the first one, but all gears are verified with a sufficient margin and durability.

The graphs showing the bending and contact stresses highlight the lower loads applied with respect to the nominal loading condition, resulting in higher safety factors.

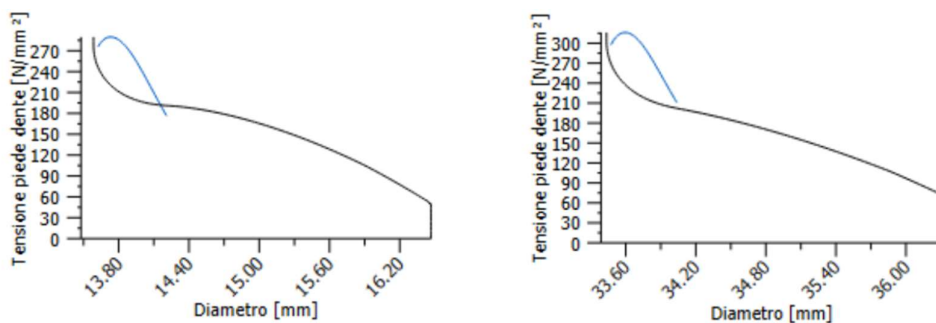


Figure 59. Root stresses for sun gear (left) and for first stage planet gear (right) with load spectrum

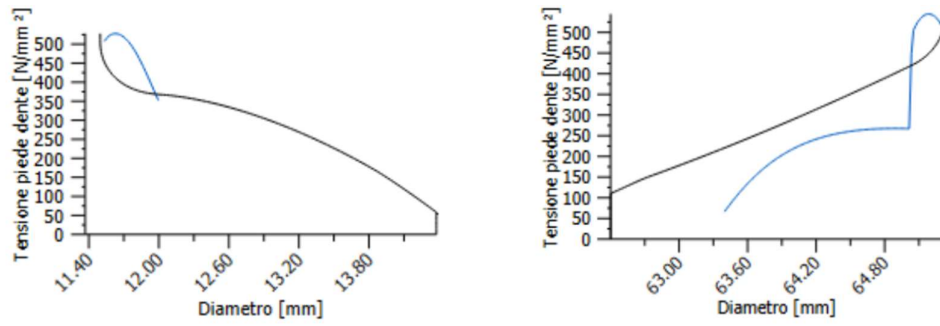


Figure 60. Root stresses for second stage planet gear (left) and for ring gear (right) with load spectrum

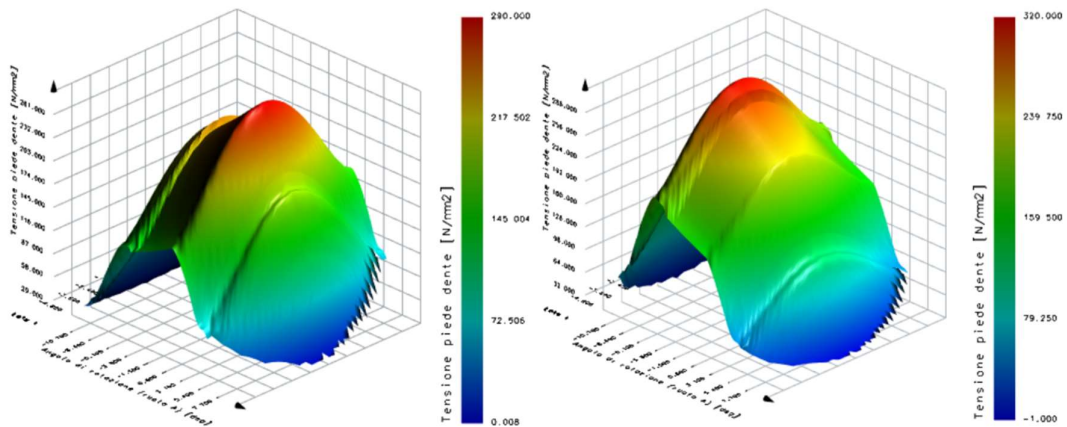


Figure 61. 3D stress distribution for sun gear (left) and for first stage planet gear (right) with load spectrum

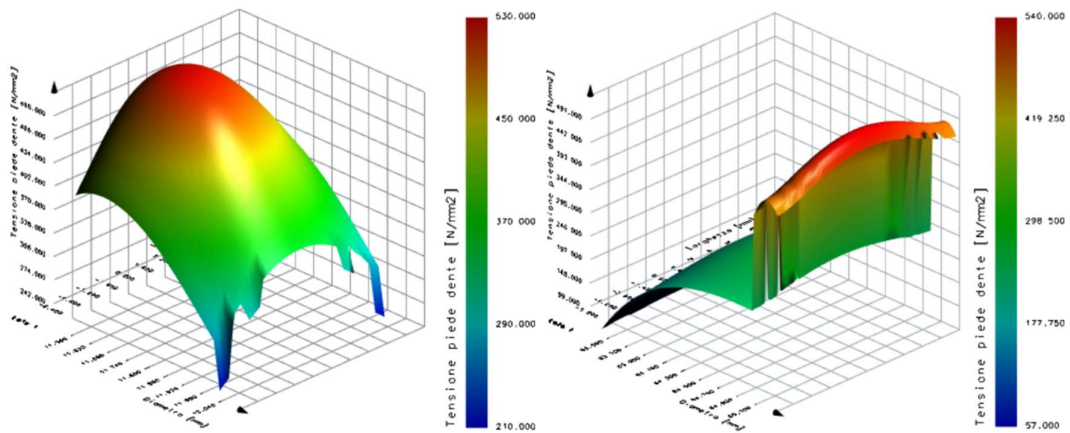


Figure 62. 3D stress distribution for second stage planet gear (left) and for ring gear (right) with load spectrum

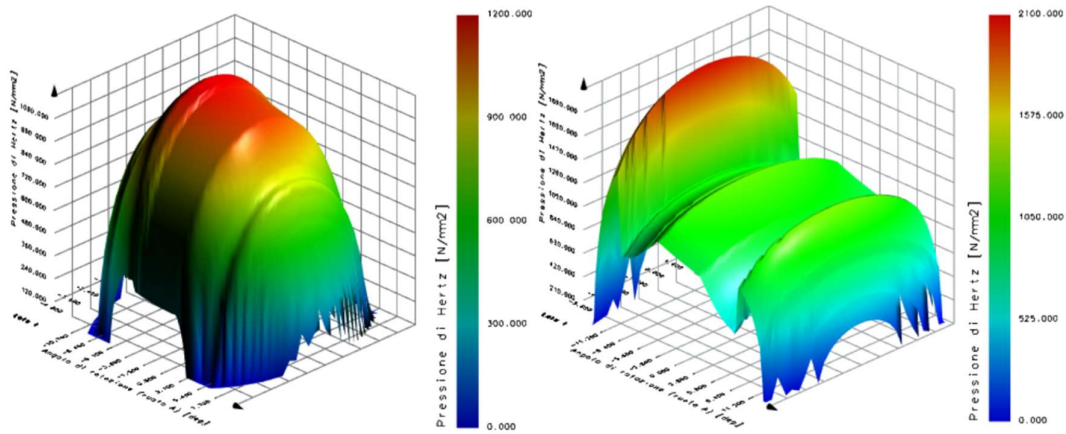


Figure 63. 3D contact pressure distribution for first (left) and second (right) stage with load spectrum

3.11. Efficiency

The efficiency of the gearbox plays an important role in the design of a transmission system: this is true also for applications in Formula Student, where an increased efficiency could result in improved performances and reduced battery consumption, since less power is lost passing from the motors to the wheels. Moreover, an efficient transmission also reduces wear and heat generation, with a beneficial effect on durability and reliability.

3.11.1. Power losses

The efficiency of a gearbox can be defined as the ratio between the output power and the input one, thus being able to identify the losses is crucial for the efficiency calculation.

Power loss in a double stage epicyclic geartrain, as the one designed in this work, arise from gears, bearings and seals losses. Gears and bearings losses can be further subdivided into load independent losses, which do not scale with the transmitted power, and load dependent ones, which increase when the torque transmitted increases. Load independent losses are influenced by operating conditions and internal housing design, and are mainly related to lubricant viscosity and density, as well as immersion depth of the components inside the oil bath. Load independent losses of gears can also be referred to as gear churning losses. Load dependent losses are influenced by transmitted torque, coefficient of friction and sliding velocity between components.

The total gearbox losses are then the sum of all these different contributions:

$$P_{TOT} = P_{VZ0} + P_{VZ} + P_{VL0} + P_{VL} + P_{VD}$$

Where

- P_{VZ0} are the gears churning losses
- P_{VZ} are the gears meshing losses
- P_{VL0} and P_{VL} are the bearings losses, respectively load independent and dependent
- P_{VD} are the seals losses

When the gearbox is working at nominal load, the load dependent gear losses due to the sliding friction between the teeth flanks are dominant. When operating at part load and high rotational speed, load independent losses, due to the friction of the moving components immersed in oil, become more important as contribution to the total losses.

Also working temperature is an influencing factor when talking about the gearbox efficiency, due to its effect on lubricants' properties.

3.11.2. Efficiency model

The calculation of the efficiency of the gearbox can be performed in KISSsys, developing a specific model starting from the one used for the gears design and calculations presented before. It is possible to use a devoted template embedded in the software, which calculates the efficiency and other related parameters starting from the transmission model and some additional information given by the user about working conditions.

The calculation is performed by the software according to ISO TR 14179 norm. It is then possible to define all the needed parameters.

The housing is generated by the software as a simple cylinder enclosing all the gears and bearings. The material chosen for the housing has been an aluminium alloy with a thickness of 6 mm, values extracted from the upright design of the SC22 EVO. It has also been possible to set the surface treatment of the housing, which has an influence on the heat exchange with the environment: in this case has been defined as an oxide layer, consistent with the anodization process to which the upright is subjected. A radial shaft seal is automatically added by the software, because not all the components are fully enclosed in the case volume modelled (in light blue in the figure below), with the

characteristics of a "general oil seal" described by ISO TR 14179-2. It is also possible to define additional settings regarding the housing geometry, which influence the heat transfer coefficient and thus the lubricant temperature.

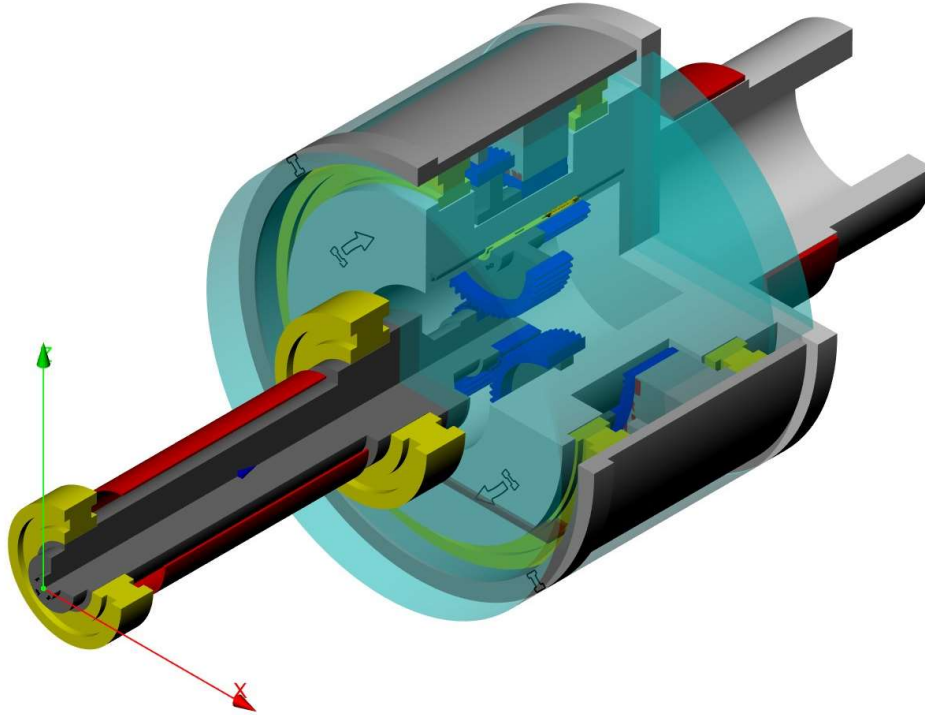


Figure 64. KISSsys transmission model 3D view for efficiency analysis

It is then possible to define the ventilation conditions, which describe the air motion around the casing. In this case has been set an air motion at 10 m/s, which represent the air flow hitting the upright at the average speed of the vehicle during its lifetime.

The lubrication has been set as oil bath lubrication, with an oil temperature of around 60°C. The oil level and oil viscosity are set according to the values explained in the lubrication section.

It would also be possible to define the characteristic of the oil cooler, which is obviously not present in this application.

The results of the calculation indicate an overall efficiency of the gearbox of 97,7% and of 98,7% for the gear meshing. These values have been calculated with the maximum torque input and maximum rotational speed, thus in favourable conditions for efficiency, but are in any case quite impressive for a gearbox with two reduction stages.

The main contributions to the total losses in this working condition come from the gears meshing losses and from the bearings losses, which dissipate around 590 and 375 W respectively. The effect of churning losses and seals losses is negligible with respect to the other contributions, since the calculations are performed at high load, where load independent losses are less meaningful.

4. GEARTRAIN COMPONENTS DESIGN

After the definition of the main geometrical parameters carried out in KISSsoft it is possible to proceed with the design and engineering of the physical components involved in the transmission assembly.

4.1. Sun gear

The sun gear represents the input for the gearbox, receiving the torque from the electric motor and transmitting it to the first stage planet gear.

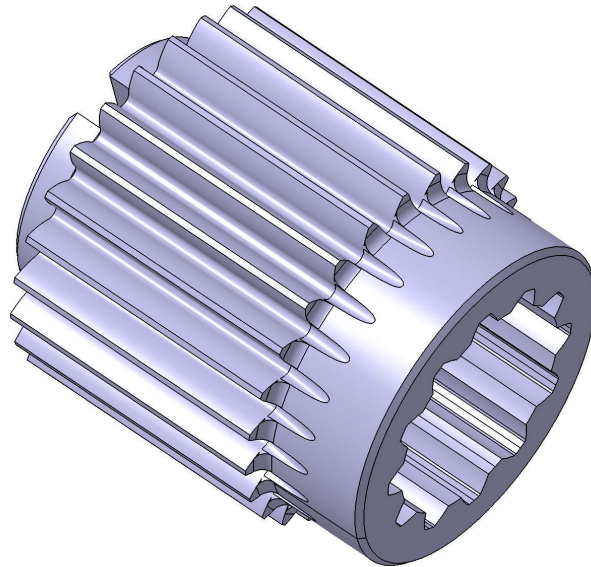


Figure 65. Sun gear

The material chosen for the sun gear is Ferrum C61 with carburization treatment. The case hardening depth is established at a range of 0,2 - 0,3 mm. This range exceeds the minimum depth determined by the calculation results, which falls within the range of 0,12 - 0,15 mm. However, it remains below the maximum depth specified by ISO 6336 norm, since higher values would increase the risk of embrittlement of the tooth tip and lower the allowable stress.

$$CHD_{max} = 0,4 * m_n = 0,4 * 0,6 \text{ mm} = 2,4 \text{ mm}$$

Where:

- CHD_{max} is the maximum case hardening depth
- m_n is the gear normal modulus

Additional material is incorporated into the design to accommodate material removal during the subsequent grinding process, estimated to be in the range of 0,05 – 0,1 mm.

4.1.1. Motor interface

The AMK electric motor's output shaft is designed with a male spline conforming to DIN 5480 standards, specifically DIN 5480 - W11 x 0,8 x 30° x 12 x 7h.

The spline nomenclature indicates that the nominal diameter is 11 mm, the normal modulus of the teeth is 0,8 mm, the pressure angle is 30°, the number of teeth is 12 and the flank mating tolerance is 7h. This spline configuration is illustrated in the figure below.

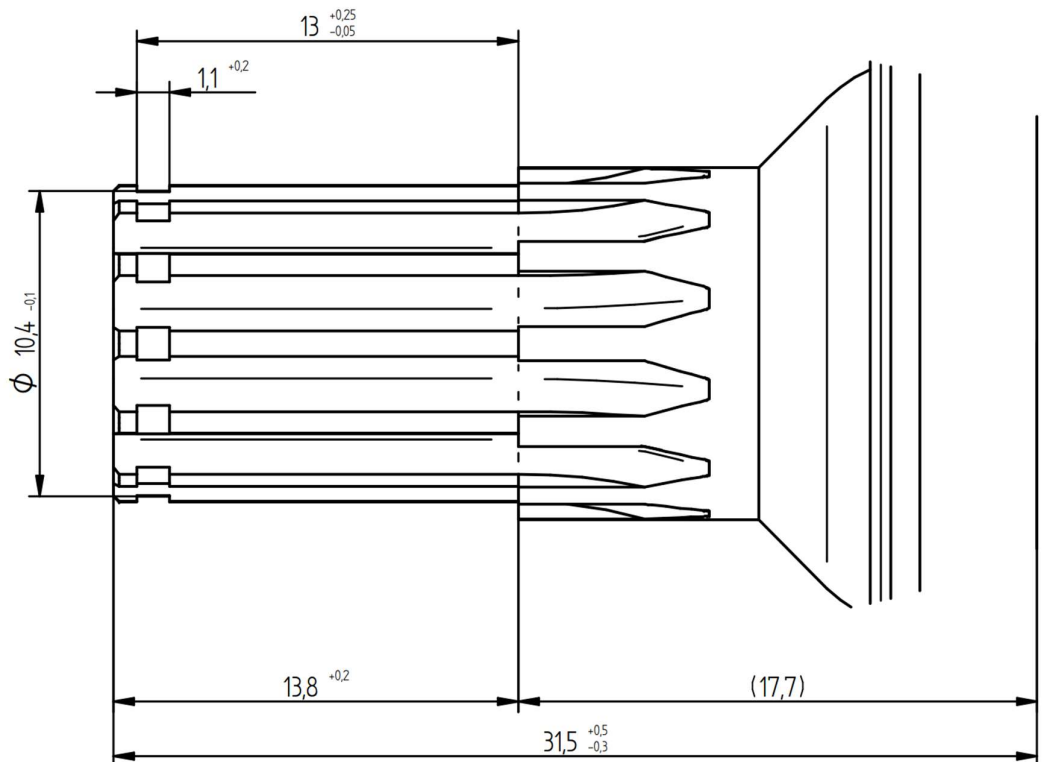


Figure 66. Motor output spline

To reduce the component's overall size and consequently its weight, in this layout the female spline with dimensions equivalent to the motor's one is directly obtained into the sun gear.

Due to the design adopted, that can be seen in the section view in figure 68, it is not possible to use a machining operation for the manufacturing of the female spline, since there is not enough room to allow the tool exit after machining. For this reason, the inner spline of the gear can be realized by means of EDM, Electrical Discharge Machining, an electro-erosion process that allows material removal without passing through the whole component.

The splined connection locks all the sun gear degrees of freedom, except for the axial movement. It is then needed to establish a method for keeping the sun gear attached to the motor's output shaft.

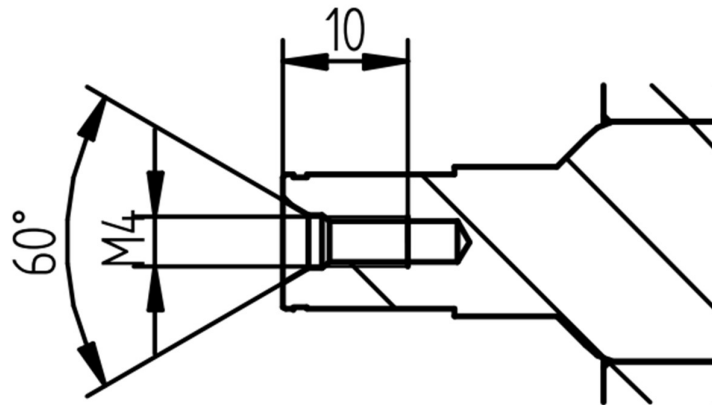


Figure 67. Motor output spline section view

The shaft geometry offers two viable options: using a circlip in the groove showed in figure 66, or employing an M4 screw in the threaded hole shown in figure 67. In this particular application the circlip option is not feasible due to the excessive axial size of the sun gear with respect to the splined shaft, consequently it was decided to use a screw. It's essential to note that, since all the torque is transmitted through the spline, the axial force applied during screw tightening doesn't need to sustain the transmitted torque but only to keep the gear in place.

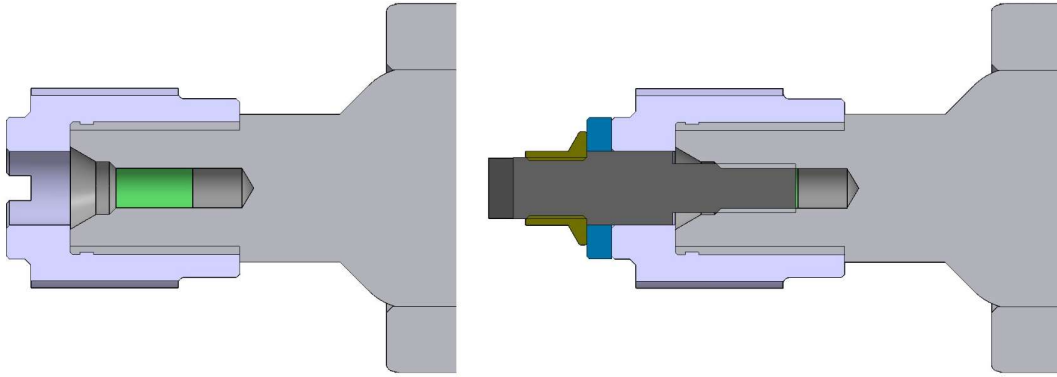


Figure 68. Sun gear mounting section view

This screw must have a positive locking mechanism to avoid unintentional loosening, according to FSAE rule T10.2.1. In the past, the solution adopted was safety wiring applied between the head of the screw, which was radially drilled, and the sun gear, which also had radial holes to accommodate the safety wiring. Although very easy and lightweight, this solution was not effective in avoiding the screw loosening, with consequences on the correct gears alignment and meshing and ultimately on gears life.

The strategy implemented to ensure positive locking includes a machined stud, a custom washer and a k-nut and can be seen in the following figure.

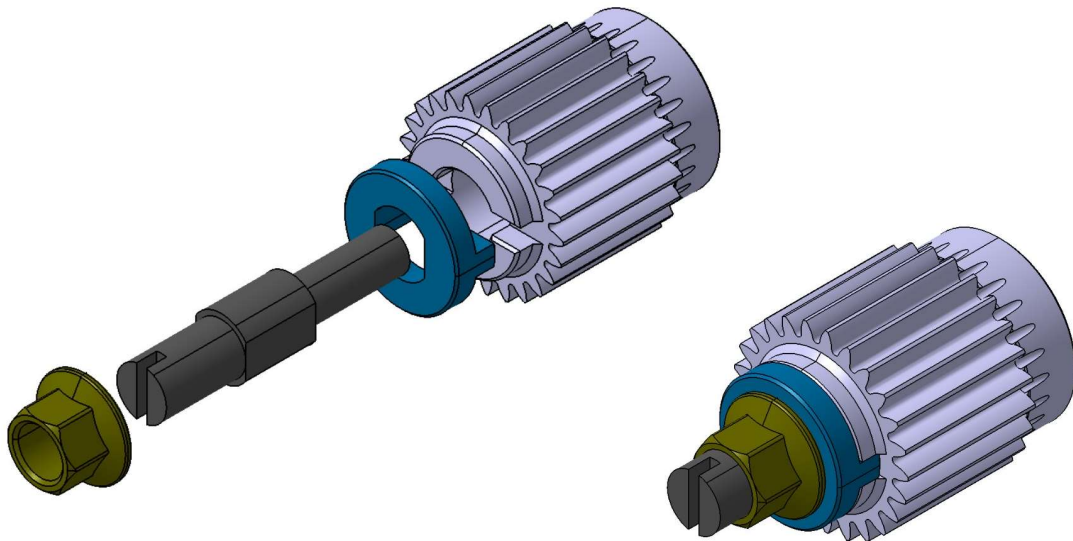


Figure 69. Sun gear positive locking mechanism

The stud is composed by a central part, with circular section with two flat faces, and by two threaded ends. The washer has two teeth, mating with equivalent slots on the sun gear, and the central hole with two flat sides, mating with the central part of the stud. The

stud is screwed to the motor shaft and the action of the flat faces and the washer avoids loosening. Finally, the k-nut tightened on the other threaded section of the stud locks the axial movement of the sun gear while guaranteeing positive locking.

4.1.2. FEM analysis

To check the performance of the component under load a FEM analysis is performed in Hypermesh. A simplified version of the sun gear has been used, to avoid longer computational time and the need of a more refined mesh. The mesh size has been set to 0,2 mm. The model was set up as follows:

- Constraint locking all the degrees of freedom except for the axial rotation applied to the spline internal surface, only on one side of each tooth to better simulate the contact condition. The single point constraint (SPC) is applied to the dependent node of a RBE3 element through a zero length CBUSH element. The independent nodes of the RBE3 are on the spline surfaces. The use of RBE3 and CBUSH avoids an excessive and unreal stiffening of the part that would happen using RBE2 rigid elements.
- Constraint locking the axial displacement applied to the front surface of the gear, where there is the contact with the washer. Again the SPC is connected to the RBE3 element through a CBUSH element.
- Three forces applied, each on one of three teeth equally spaced of 120° with each other. The forces considered represent the condition in which the three first stage planets mesh with the sun gear with the maximum input torque from the motor. The forces are connected to the teeth surfaces with three RBE3 elements.

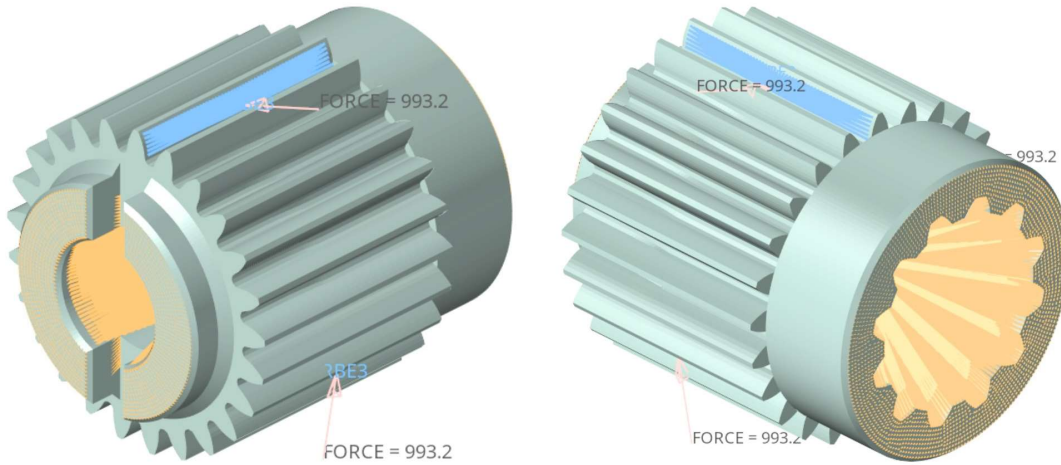


Figure 70. Sun gear FEM model

All these conditions have been applied together in a single loadstep and the results can be seen in the following images. The maximum stress reached at maximum load conditions and assuming three teeth in contact is 261 MPa. The maximum displacement is 6,7 μm . Even in the case of improper assembly or unlikely improper contact in which only one tooth is meshing in the whole transmission, the highest stress is still well below the material yield stress.

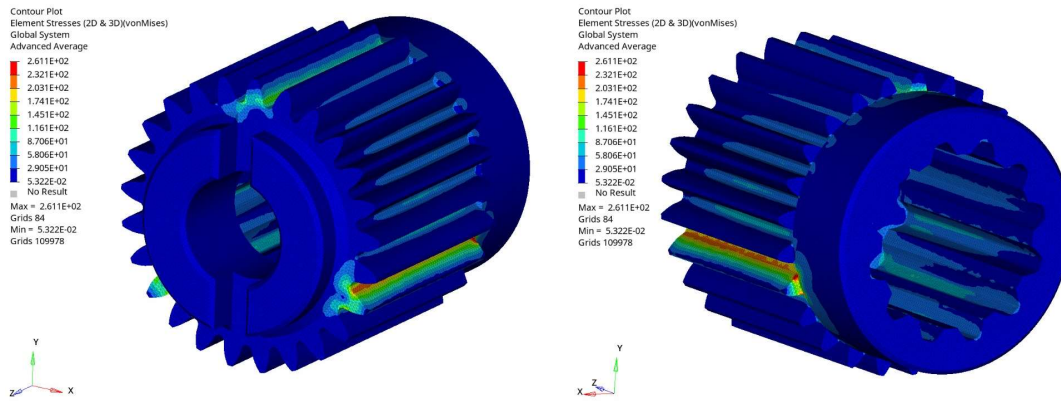


Figure 71. Sun gear Von Mises stress

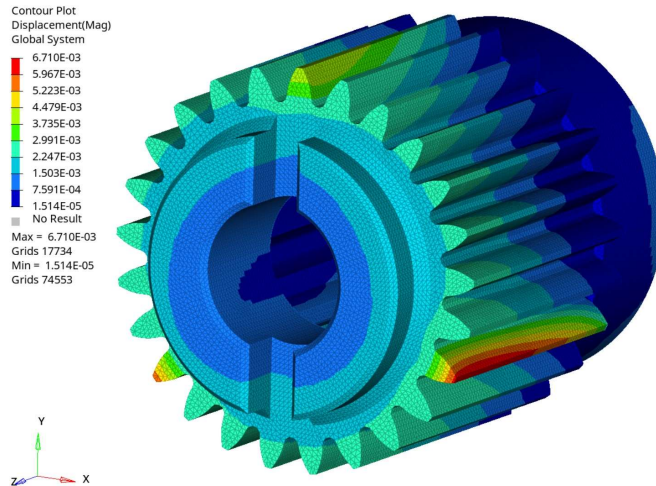


Figure 72. Sun gear displacement

The static safety factor is satisfactory and is given by

$$SF = \frac{R_{p0,2}}{\sigma_{max}} = \frac{1550 \text{ MPa}}{261 \text{ MPa}} = 5,94$$

4.2. Planet gears assembly

The planet gears assembly, which can be seen in the figure, is composed by the two planet gears, first and second stage, the planet pin shaft, the bearings and the shims.

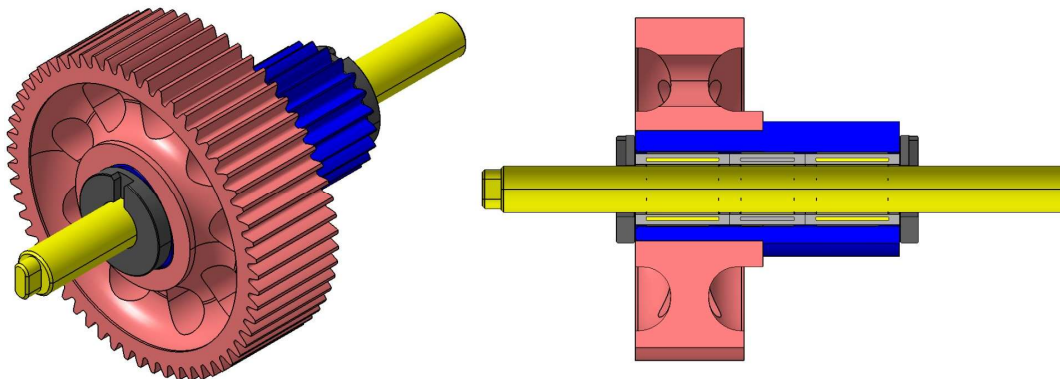


Figure 73. Planet gears assembly

The two planet gears have been designed as separate components, to be assembled together after manufacturing. This approach is chosen because it enables the reduction of the axial dimension of the planetary gears' assembly. If the gears were manufactured

as a single piece, they would occupy significantly more space due to the necessity of providing axial clearance for the smaller gear, which is required to allow the tool's passage during both the gear cutting and grinding processes. Moreover, the raw material needed would be increased, with higher costs. The two planetary gears are connected with a P3G profile, which will be treated in section 4.2.1.

The two planetary gears assembled are connected to the planetary carrier and to the hub by means of the planet pin shaft, and they are supported onto this shaft through three needle roller bearings to allow the relative rotation. The shaft is integral with the planet carrier and wheel hub, while the gears can freely rotate.

The planet shims are used to avoid damaging the planet carrier and wheel hub when gears are spinning, due to the high surface hardness of the carburized steel. To achieve this objective, the shims are secured in place with an anti-rotation pin, connecting them to both the hub and the planetary carrier on one side, while allowing them to slide against the planetary gears on the other side.



Figure 74. Planet shim

Careful consideration has been given to the selection of shims material and heat treatment, which is 100Cr6 steel, hardened to 52 - 58 HRC to prevent wear and damage during operation.

4.2.1. P3G connection

The connection between the first and second planet gears must be able to transfer torque between the two and to correctly locate one gear with respect to the other one. In fact, the

two planetary gears must be properly timed with the correct angular position, to guarantee a correct meshing and assembly.

It was decided to adopt a polygonal shaft connection with a P3G profile according to DIN 32711-1:2009. This solution requires some slight interference to guarantee the press fit and a larger contact surface between the two planets, since the torque transfer happens by friction between the mating surfaces.

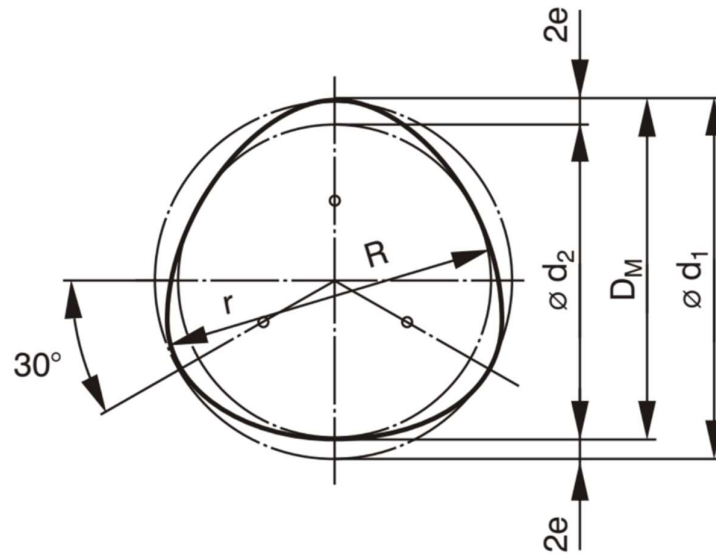


Figure 75. P3G profile

The correct mesh timing can be ensured during the design phase, such that the manufactured profile is self-centring and aligned with the gear teeth. The polygonal connection was chosen as it is easier to manufacture with respect to a splined profile and it better distributes the stresses compared to a key connection, while it guarantees a good torque capacity and precision.

The P3G profile with 3 lobes was chosen since it delivers better performances with respect to the four-lobe P4C equivalent in a high torsional stress application, due to the high stress concentration in the corners of the P4C connection.

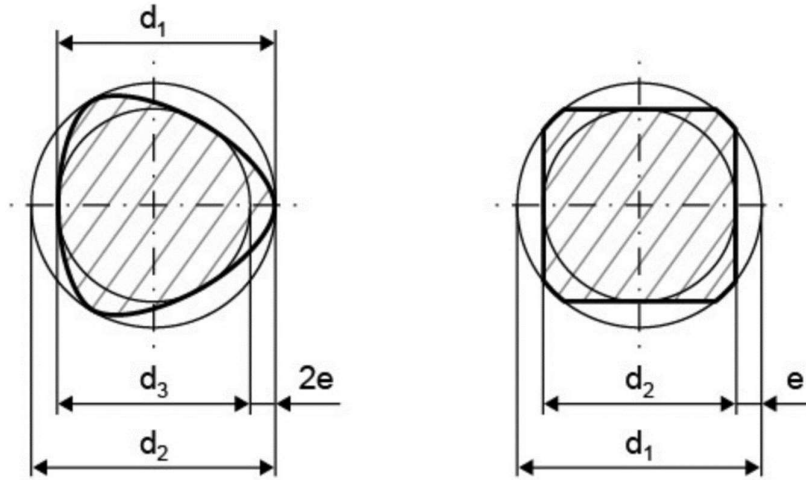


Figure 76. P3G vs P4C polygonal profile

The polygon connection and the pressure fit have been studied in the specific KISSsoft calculation module, which, receiving as inputs the geometrical and operational conditions of the connection, outputs the safety factors against sliding. After a few iterative loops, in order to guarantee the maximum torque transmission between the two gears, it was decided to use a location interference H6 - p6; this provides an evenly distributed stress without generating critical peaks in local areas and, being a moderate interference joint, also the assembly accuracy can be preserved.

4.2.2. First and second stage planet gears

The first stage planetary gear receives torque from the sun gear, then transfers it to the second stage one through friction in the P3G connection described above. The gears are supported by the planet pin shaft, on which they can freely rotate thanks to the presence of needle roller bearings.

To maintain the assembly as compact as possible, the smaller second stage planet gear hosts the male polygonal profile and the hole for the pin shaft, while in the first stage planet gear the female polygon profile is machined.

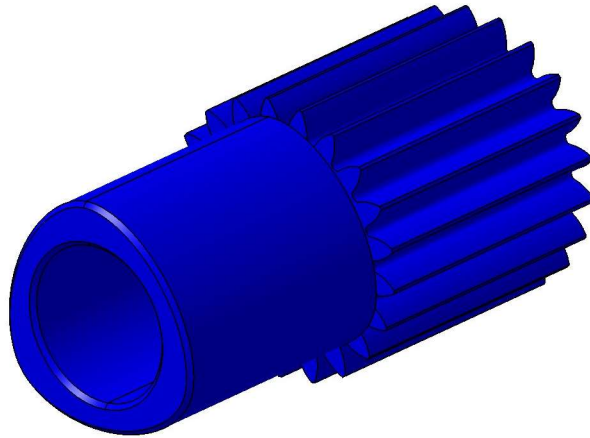


Figure 77. Second stage planet gear

The material chosen for the gears is Ferrum C61 with carburization treatment. The case hardening depth is set to 0,2 - 0,3 mm, a value in between the proposed depth coming from the calculations and the maximum case hardening depth presented before. Additional 0,05 - 0,1 mm of material is added to the design to accommodate material removal during the subsequent grinding process.

The first stage planet gear, due to the larger dimensions, can be optimized to reduce the component weight, while maintaining it stiff and resistant. This process was performed with a finite element analysis with Altair suite.

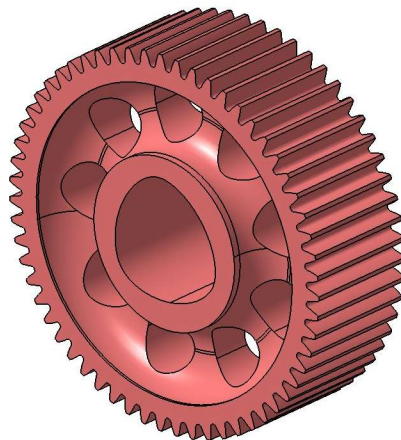


Figure 78. First stage planet gear

The result of the optimization was a very complex design, but it was decided to adopt a simpler solution with nine holes. This configuration is much simpler from the manufacturing point of view and the performances are similar to the optimized design.

Special attention has been given to ensure that a minimum of 3 - 4 mm of material is retained in all areas. This guideline is applied to prevent excessive distortions during the case hardening process.

The design and the feasibility of the drilled holes is then verified with a FEM analysis in Hypermesh. The component was meshed with an element size of 0,2 mm and the model has been set up as follows:

- Constraint locking all the degrees of freedom applied to the P3G polygonal connection surface. The SPC is applied to the dependent node of a RBE3 element through a zero length CBUSH to avoid excessive stiffening of the component. The independent nodes of the RBE3 are on the polygon connection surface.
- Force applied to one tooth of the gear, connected to the tooth surface with a RBE3 element. The value of this force represents the mating of the first stage planet with the sun gear at maximum torque.

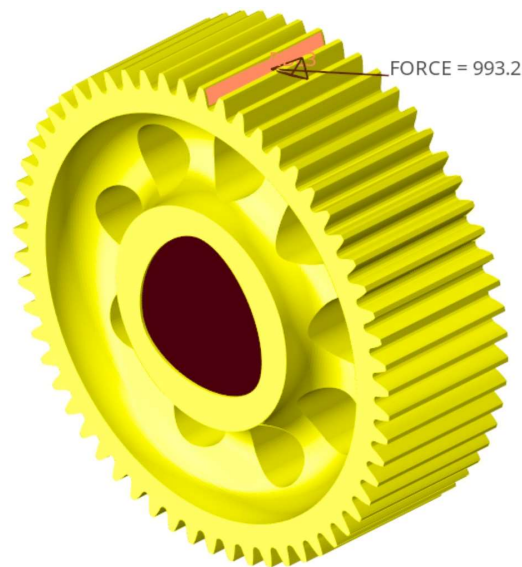


Figure 79. First stage planet gear FEM model

The maximum stressed reached is 198 MPa, meaning that the design is verified with a safety factor of 7,83. The maximum displacement is 8 μm , which is an acceptable value.

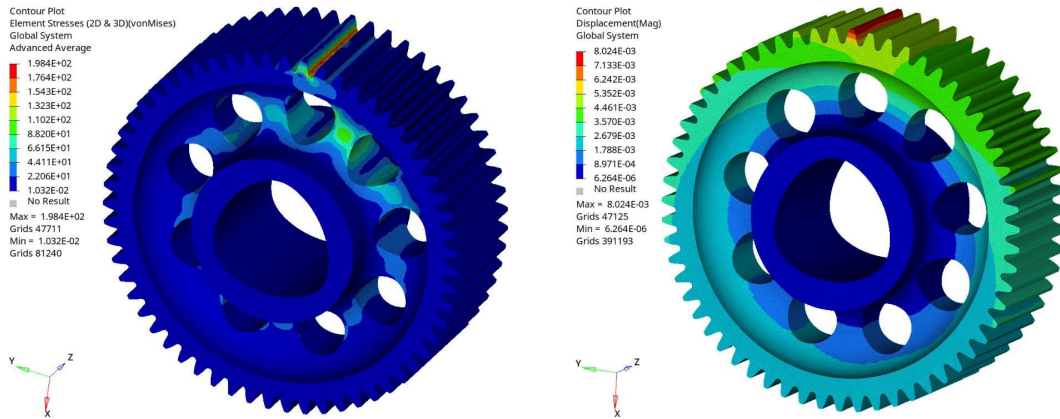


Figure 80. First stage planet gear Von Mises stress (left) and displacement (right)

Also the design of the second stage planet gear is verified with a FEM analysis. The mesh size of the component was set to 0,2 mm and the boundary conditions have been applied as follows:

- Constraint locking all the degrees of freedom except for the rotation of the gear applied in the hole for the pin shaft. The SPC is connected to the hole internal surface through a RBE3 element and a zero length CBUSH element.
- Constraint locking the gear rotation applied to the surface of the male polygonal connection surface. Again the SPC is connected to the surface via a RBE3 element and a CBUSH element.
- Force applied to one tooth of the gear, connected to the tooth surface with a RBE3 element. The value of this force represents the mating of the second stage planet with the ring gear at maximum torque.

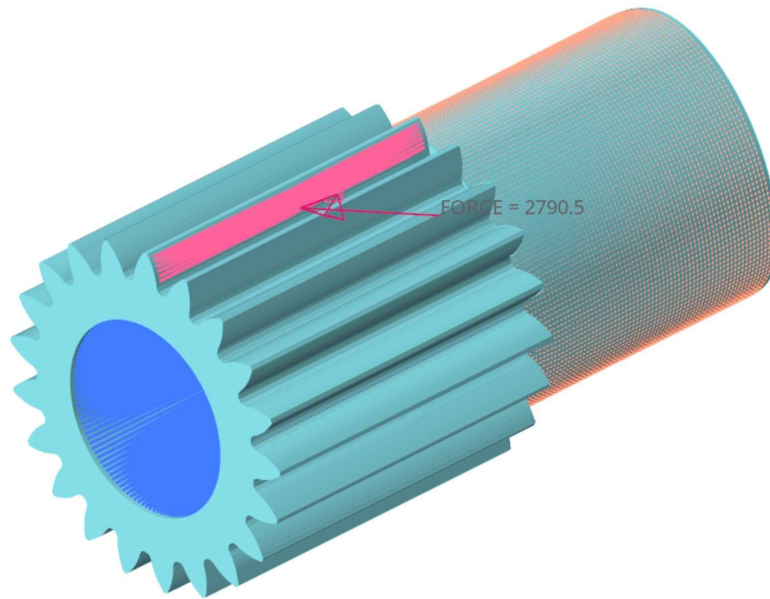


Figure 81. Second stage planet gear FEM model

The load applied on this second stage gear is much higher with respect to the first one. The maximum stress reached is 406 MPa, higher than in the first stage planet gear but still well below the material yield strength. The component is verified with a safety factor of 3,82 and the maximum displacement is 17,9 μm .

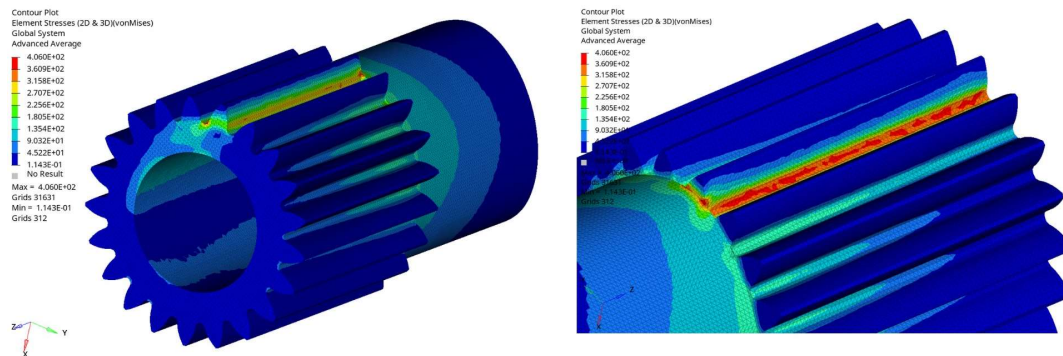


Figure 82. Second stage planet gear Von Mises stress

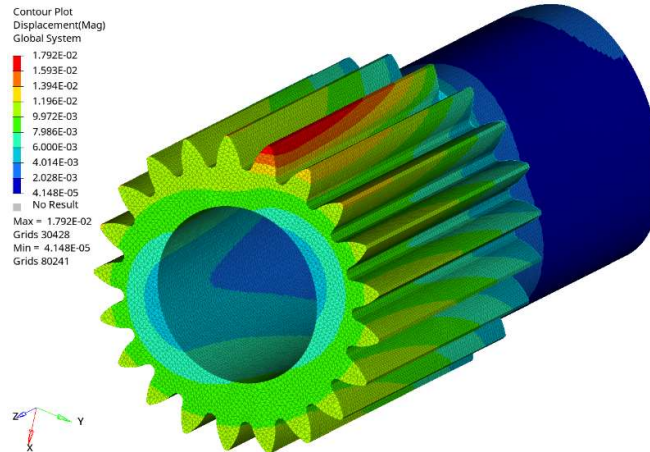


Figure 83. Second stage planet gear displacement

4.2.3. Pin shaft

The pin shaft acts as the support of the first and second stage planetary gears and as a connection between the planet carrier and the wheel hub. It is the element that transfer torque from the gears to the wheel hub.

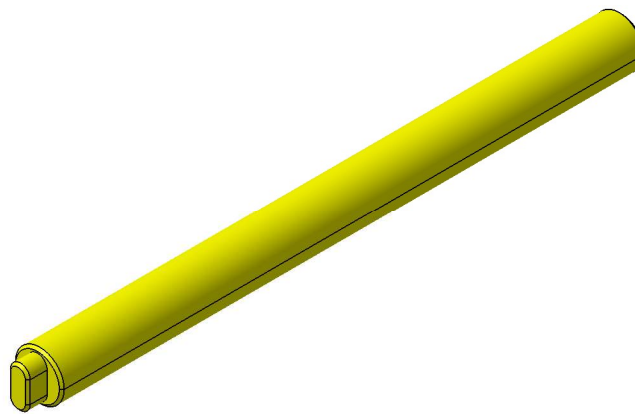


Figure 84. Pin shaft

The material chosen for the pin shaft is 18NiCrMo7 steel carburized. The component is subjected to high loads and contact stresses, for this reason the material adopted must have a good strength and surface hardness, while maintaining a ductile core to sustain the cyclical bending moment applied. The case hardening depth is set to 0,6 mm.

The pin shaft must be able to sustain the loads applied with minimum deformation, which would have a negative effect on gear meshing and bearings and components life, and at

the same time it should keep to a minimum the radial size, to reduce the geometrical constraints on gears, and thus gearbox, dimensions.

During the design phase two different configurations for the pin shaft have been considered, closely related to the lubricant choice discussed in section 5.2. The pin shaft for oil lubrication, having an axial hole and many radial holes to allow the passage of oil to lubricate the roller bearings, and the pin shaft for grease lubrication, a solid shaft.

In the end it was chosen to adopt the last version, that showed the following advantages:

- Lower stresses and stress concentrations, due to the absence of the holes for lubricant path;
- Higher stiffness and consequently lower deflection, due to the higher moment of inertia of the circular cross section with respect to the hollow one;
- Easier and cheaper manufacturing process.

To lock the rotation of the pin shaft around its axis, a small tooth was added to one end of the component. Mating with a correspondent groove in the planet carrier, it locks the rotation degrees of freedom to guarantee the optimal gearbox function.

As a first step for the verification, the calculations on the pin shaft have been carried out in KISSsoft. A coaxial shaft calculation module has been created, in which the two shafts are the pin shaft itself and the shaft of the two planet gears. The two shafts are connected through three connection roller bearings and the pin shaft is supported in correspondence of the contact with the planet carrier on one side and the wheel hub on the other one.

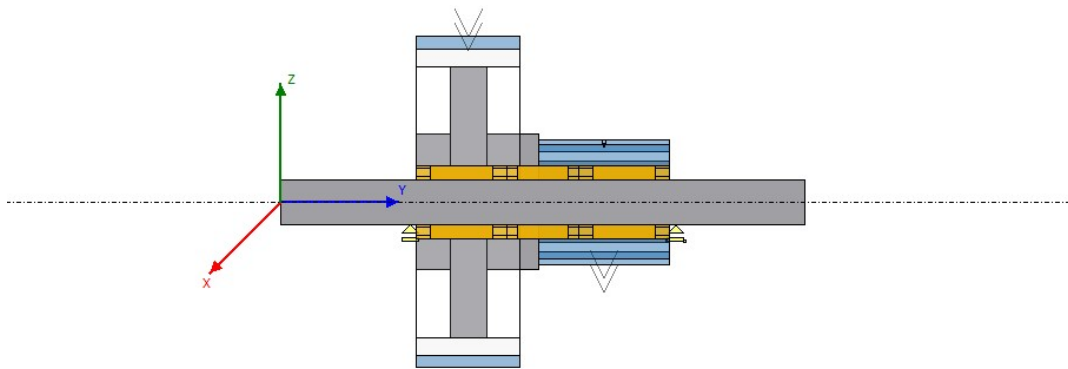


Figure 85. Planet_calc coaxial shaft calculation module

The calculation is performed at maximum nominal load and the results in terms of displacement and stress are shown below.

The peak deflection is obtained in the middle section of the shaft, with a value of around 0,03 mm, which is acceptable for the application. The peak stress reaches very high values, which are not realistic due to the impossibility of modelling the correct support condition for the shaft. Excluding the peaks owing to the punctual supports, the maximum stress reached is around 450 MPa, which is below the material yield strength.

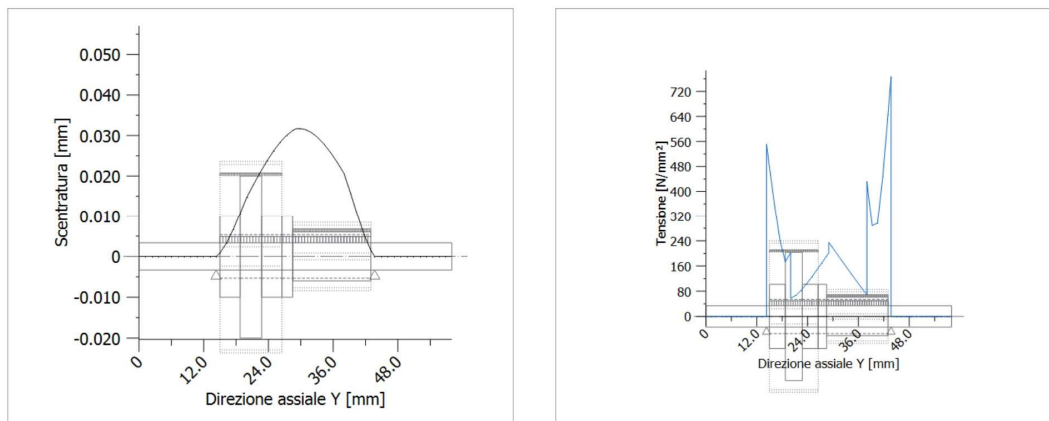


Figure 86. Pin shaft KISSsoft displacement (left) and stress (right)

The results obtained from the KISSsoft calculation have been compared with a FEM analysis. A simplified version of the component was meshed with an element size of 0,2 mm and the model has been set up as follows:

- Constraints locking all the degrees of freedom except for the axial rotation applied in correspondence of the contact with the planet carrier and wheel hub. Each of the constraint has been applied only on one half of the shaft, to better simulate the contact area. In both cases the SPC is connected to the pin shaft external surface through a RBE3 element and CBUSH.
- Constraint locking the rotation of the pin shaft applied on the tooth, where it is connected to planet carrier. Again the SPC is connected to the surface via a RBE3 element and a zero length CBUSH element.
- Forces representing the radial component of the force exchanged between gears in the two reduction stages. One force represents the load coming from the first stage and acts on one half of the surface, the other represents the load coming

from the second reduction stage and is applied on the other half of the shaft surface. The values consider the maximum applied torque.

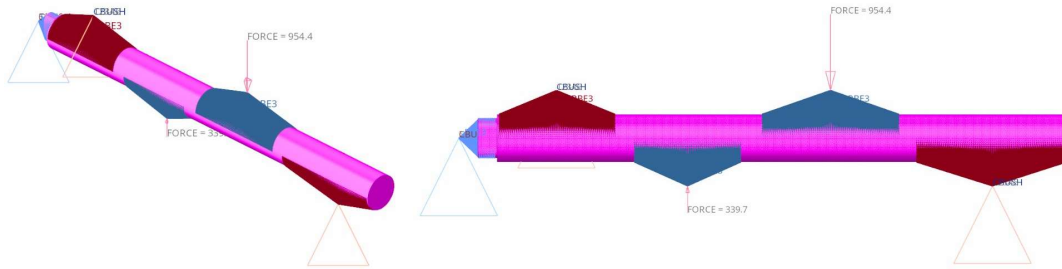


Figure 87. Pin shaft FEM model

The maximum stress reached is 206 MPa in the zone of the contact with the bearings and the gears. This value is lower with respect to the one calculated by KISSsoft, due to the more realistic model of the constraints and supports. The peak deflection is 0,033 mm. Both this value and the deformed shape are consistent with the results obtained in KISSsoft.

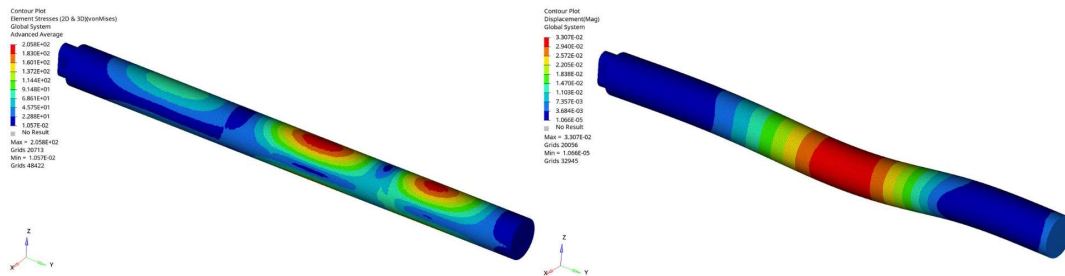


Figure 88. Pin shaft Von Mises stress (left) and displacement (right)

Both the stress and the displacement are acceptable, and the component is verified with a safety factor of 4,13.

4.2.4. Bearings

The rotation of the gears is decoupled from that of the pin shaft, which is locked, by the use of bearings. As far as the bearing choice is concerned, the geometric dimensions are constrained by the transmission layout itself.

One of the main objectives is to minimize the radial dimension of the bearings, to reduce the constraints on gear design. For this reason, the selected bearings are two SKF K 5x8x10 TN and one SKF K 5x8x8 TN needle roller bearings; both have the same

dimensions except for the axial length. The choice of using two different models is forced by the axial dimension of the planet gears assembly, which would not admit three bearings of the same dimension. The main dimensions and characteristics are shown below.

Model	SKF K 5x8x8 TN	SKF K 5x8x10 TN
Inner diameter - Fw	5 mm	5 mm
Outer diameter - Ew	8 mm	8 mm
Width - U	8 mm	10 mm
Dynamic load rating - C	2,29 kN	2,92 kN
Static load rating - C0	2 kN	2,7 kN
Limiting speed	40000 rpm	40000 rpm

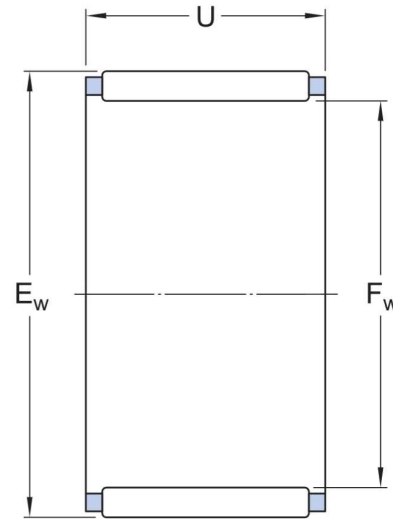


Figure 89. Needle roller bearings characteristics

Needle roller bearings represent the most compact solution in radial dimension and these models in particular don't have the outer and inner raceways, further reducing their diameter. Moreover, needle roller bearings present a high stiffness and can support relatively high loads. The downside of this solution is the need of high surface hardness components to sustain the stresses coming from the needles contact; in this application it is not an issue, since the components in contact are made from carburized steel and can act as bearing raceways.

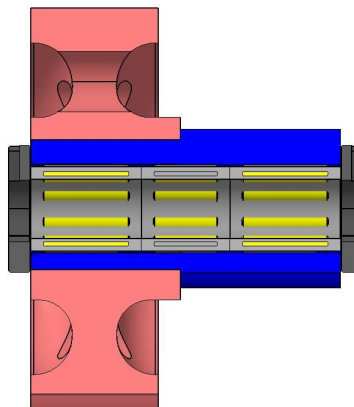


Figure 90. Needle roller bearings positioning

Bearings calculation is performed in KISSsoft using the coaxial shaft calculation module already adopted for the pin shaft design. The load considered is the peak nominal one, with a torque of 21 Nm and a rotational speed of 20000 rpm. The main results in terms of static safety factor and service life are summarized in the table below. The numbering of the bearings starts from the first stage planet gear.

	Bearing 1	Bearing 2	Bearing 3
Model	SKF K 5x8x10 TN	SKF K 5x8x8 TN	SKF K 5x8x10 TN
Safety factor	2,34	4,18	1,67
Service life	55 h	576 h	41 h

Table 10. Needle roller bearings life

It can be noticed that the overall load is mainly distributed between the first and the third bearing, whereas the one in the middle is way less stressed. Even though the latter seems to be a redundant element, the final decision was to keep all the bearings instead of keeping only the two side ones, substituting the middle bearing with a spacer. The reason is that a spacer would negatively affect the lubricant flow and, more importantly, not provide support in the region of maximum deformation of the shaft.

Since the second bearing is the least stressed one, the smaller SKF K 8x10x8 TN is used in this position. The third bearing is the most stressed one due to the higher forces coming from the second stage meshing and it consequently displays the shortest service life.

The first and the second bearings are verified for the required vehicle life, while the third one can't quite reach the target. However, considering that the analysis was performed in the worst-case condition for the entire transmission service life, which ultimately is a non-realistic event, and the possibility to perform predictive maintenance on the component, knowing that it is a critical one, the result is anyway considered satisfying for the application.

4.3. Ring gear

The ring gear meshes with the three second stage planetary gears and is then fixed to the upright to let the assembly work as a reducer with the output on the planet carrier and wheel hub.

The material chosen for the ring gear is Ferrum C61 with carburization treatment. The case hardening depth is set to 0,15 mm. This value is lower with respect to the one adopted for the other gears, since keeping the hardened layer to a minimum it is possible to reduce the treatment time and thus the distortion of the component when subjected to the high temperature environment. This aspect is critical for the ring gear, since it can't be grinded after the carburization treatment. For this reason, no extra material is included into the design.



Figure 91. Ring gear

The gear external diameter is set to 69,5 mm in order to comply with the required rim thickness factor Y_B defined in ISO 6336. For internal gears the minimum rim thickness to avoid increased bending stress at tooth root should be:

$$s_R = 3,5 * m_n = 3,5 * 0,6 \text{ mm} = 2,1 \text{ mm}$$

Where:

- s_R is the rim thickness
- m_n is the normal modulus

4.3.1. Upright interface

To avoid the rotation of the ring gear, the solution adopted is to machine external teeth on the gear outer surface. They will mate with the corresponding internal teeth machined on the upright inner surface. The number of these teeth is six, equally spaced on the circumference, and this value has been chosen as a compromise between the stress distribution and the manufacturing complexity.

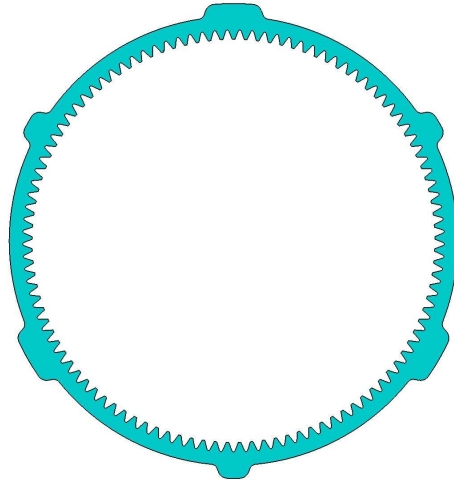


Figure 92. Ring gear fixing teeth

The ring gear external diameter mates with clearance with the upright, to facilitate the mounting operation. The axial movement is constrained by means of three custom calibrated screws, mounted radially on three of the teeth, spaced of 120° one from the other.

4.3.2. FEM analysis

The designed component is verified with a FEM analysis in Hypermesh, to analyse the behaviour of the teeth and the mounting under load. A simplified version of the ring gear is meshed with a size of 0,2 mm and the model has been set up as follows:

- Constraint locking all the degrees of freedom except for the axial movement applied to the faces of the external teeth, where there is the contact with the upright. Only one flank of each tooth is considered. The SPC is connected to the surfaces with a RBE3 element and a CBUSH element.

- Constraint locking the axial translation of the gear applied inside the holes where the three radial screws are mounted. Again the SPC is connected to the surfaces via a RBE3 element and a zero length CBUSH element.
- Three forces applied, each on one of three teeth equally spaced of 120° with each other. The forces considered represent the condition in which the three second stage planet gears mesh with the ring gear at maximum input torque from the motor. The forces are connected to the teeth surfaces with three RBE3 elements.

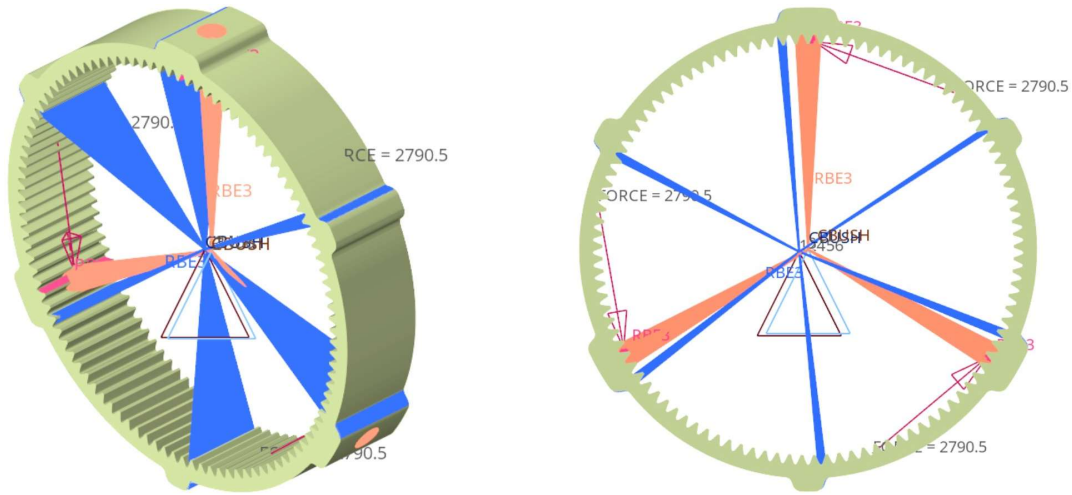


Figure 93. Ring gear FEM model

The maximum stress reached is 892 MPa in the area of the teeth under load and near the contact surfaces with the upright. The values are quite high, but the component is anyway verified with a sufficient safety factor of 1,74.

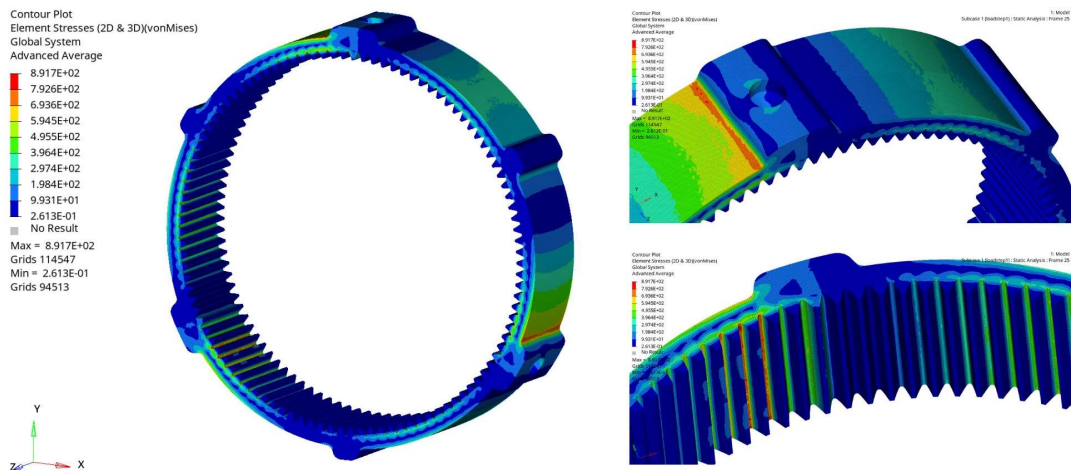


Figure 94. Ring gear Von Mises stress

The maximum deformation is 0,3 mm.

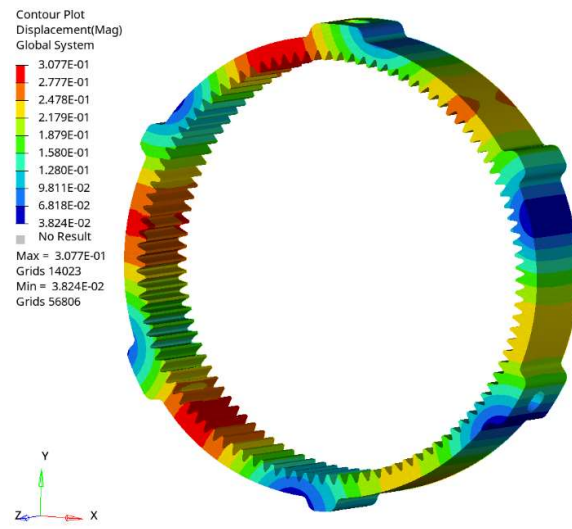


Figure 95. Ring gear displacement

5. WHEEL BEARINGS AND LUBRICATION

5.1. Wheel bearings

As already seen before, the planet carrier and the wheel hub together represent the output of the transmission. For this reason, they can rotate with respect to the fixed upright thanks to the presence of bearings. Since the rim is directly connected to the hub, the bearings connecting the carrier and hub to the upright are actually the wheel bearings of the vehicle.

5.1.1. Layout selection

In this application, wheel bearings allow the relative rotation with low friction between components and transfer the forces between them.

The loads coming from the transmission are internally balanced due to the presence of three planet groups equally spaced, so that the sum of the radial forces generated in the gear meshing is equal to zero. If these were the only forces applied, the bearings would be almost useless.

However, the bearings are also loaded by the loads coming from the wheels during normal operations, which must be transferred to the upright and then the suspension system passing through the wheel bearings. Thus, the bearings must be able to sustain both radial loads, resulting from the vertical load F_z at the wheel contact patch, and axial ones, resulting from the lateral force F_y at the wheel contact patch; the longitudinal force F_x is generally not sustained by the bearings when the contact patch is aligned with the wheel centre in axial direction, since they are free to rotate around the y -axis. Moreover, due to the axial offset between the point of application of the forces and the position of the wheel bearings, the assembly is subjected also to an overturning moment.

The layout adopted to sustain the applied loads is with two angular contact ball bearings mounted in “O” configuration, a very common solution for wheel bearings also in production vehicles.

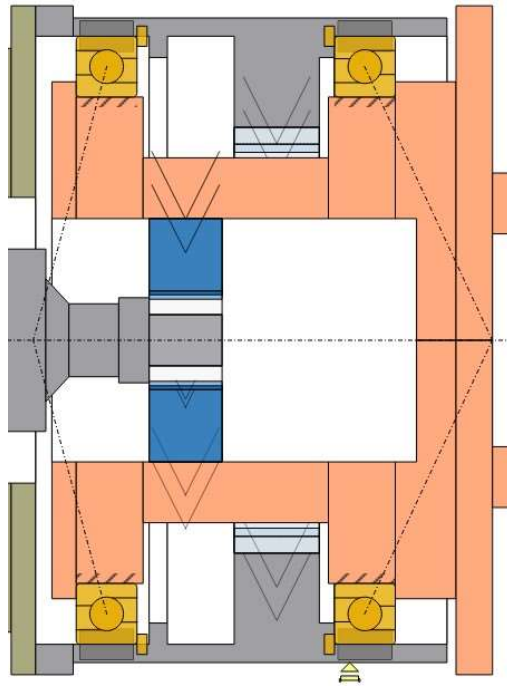


Figure 96. Wheel bearings layout "O" configuration

Angular contact ball bearings are suitable for the application since they can sustain both radial and axial loads in a compact package. However, a single angular contact ball bearing can sustain axial force only in a single direction. Since in this application the axial forces change direction depending on the cornering condition of the vehicle, two bearings are needed.

The larger the distance between the two bearings, the lower will be the radial force acting on them to counteract the overturning moment. For this reason, the bearings position has been chosen at the extremities of the assembly, leaving the maximum space available between them.

The two angular bearings have been designed with an "O" mounting, also called back-to-back, in which the tips of the cones formed by the pressure lines point outwards, forming an "O". This configuration guarantees the highest resistance to tilting moments, since the reaction points on the wheel axis are more spaced than with an "X" mounting, resulting in a greater arm for the reaction forces. This mounting also provides the highest stiffness, optimal for gears operation and for a consistent wheel contact with ground. The bearings

will have the designed seats with abutments to constrain their motion machined on the planet carrier, the wheel hub and the upright.

5.1.2. Model selection

Being the targets for the transmission design to reduce weight and volume of the assembly, the choice of the bearings has a great impact.

The chosen bearings have been two SKF 71816 ACD HC/P4 angular contact ball bearings, from the super precision catalogue of Squadra Corse's longtime partner SKF. These bearings were the smallest ones able to deliver the desired performances.

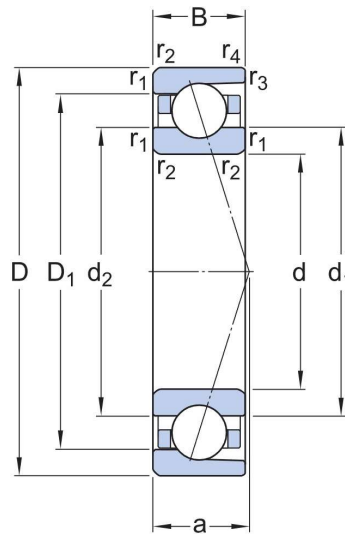


Figure 97. ACD bearings dimensions

They have a contact angle of 25° to sustain both radial and axial loads and can sustain relatively high loads considering the limited dimensions. The use of ceramic spheres allows to reach higher rotational speeds and to reduce the weight with respect to the equivalent bearing with steel spheres.

Bore diameter - d	80 mm
Outside diameter - D	100 mm
Width - B	10 mm
Basic dynamic load rating - C	13,8 kN

Basic static load rating – C_0	17 kN
Attainable speed for oil-air lubrication	20000 rpm
Contact angle - α	25 °
Mass	0,14 kg

Table 11. SKF 71816 ACD HC/P4 main dimensions

5.1.3. Life calculation

Bearings life calculation has been performed in KISSsoft, thanks to the *GB_calc* coaxial shaft calculation module, containing all the main components of the transmission and the two wheel bearings.

As said before, when no external loads are applied the bearings are unloaded and have infinite life. To simulate the effect of the contact patch forces on wheel bearings' life, a eccentric load has been added to the calculation module, representing a force acting with a radial offset with respect to the wheel axis. The loading condition considered is with the vehicle travelling on a curve at constant speed with a lateral acceleration of 2,5 g. This represents the most critical loading scenario for wheel bearings, since all the ground forces must be counteracted by them.

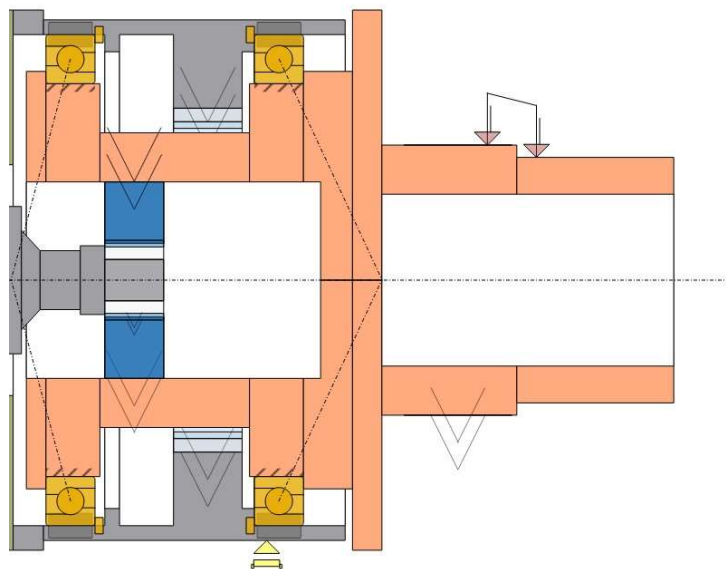


Figure 98. Mainline calculation module with eccentric force

The forces applied are from the most loaded wheel and have components:

- $F_y = 2989 \text{ N}$
- $F_z = 1856 \text{ N}$

The longitudinal component has not been considered and the point of application of the loads has been set in correspondence of the wheel contact patch. This is a very conservative approach, since it considers only the worst loading condition for the whole life of the transmission, which is clearly far from real applications.

The main results in terms of static safety factor and service life are summarized in the table below.

	Bearing Planet Carrier	Bearing Wheel Hub side
Model	SKF 71816 ACD HC/P4	SKF 71816 ACD HC/P4
Safety factor	2,24	2,83
Service life	59 h	71 h

Table 12. Wheel bearings life

The obtained results indicate that both wheel bearings can sustain this load over an extended duration. Being a conservative calculation, this result is further valuable regarding the bearings duration in real operating conditions. As expected, the planet carrier side bearing experiences a higher load compared to the wheel hub side bearing, which is inherent to this particular application and the specific loading scenario.

The calculations demonstrate that both bearings meet the system requirements in terms of service life and, looking at the graphs below, the force and pressure are well distributed across the bearing spheres in contact.

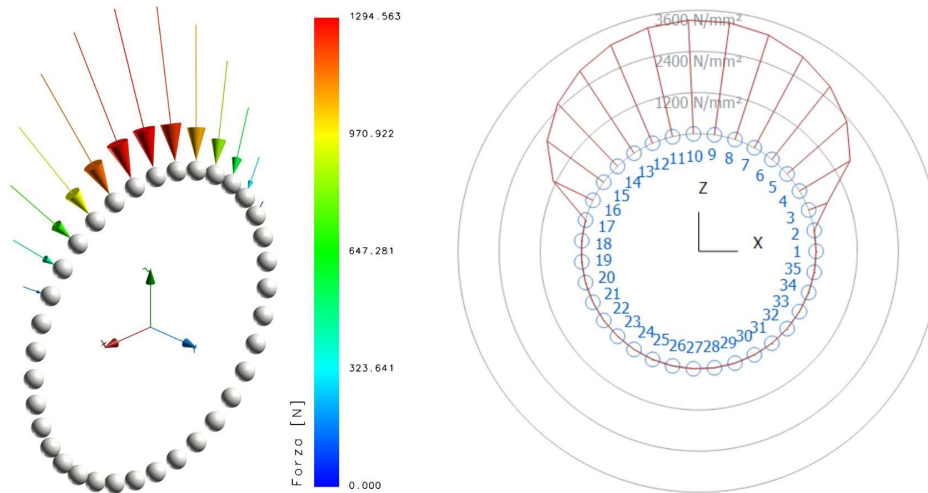


Figure 99. Force and pressure distribution, wheel bearing carrier side

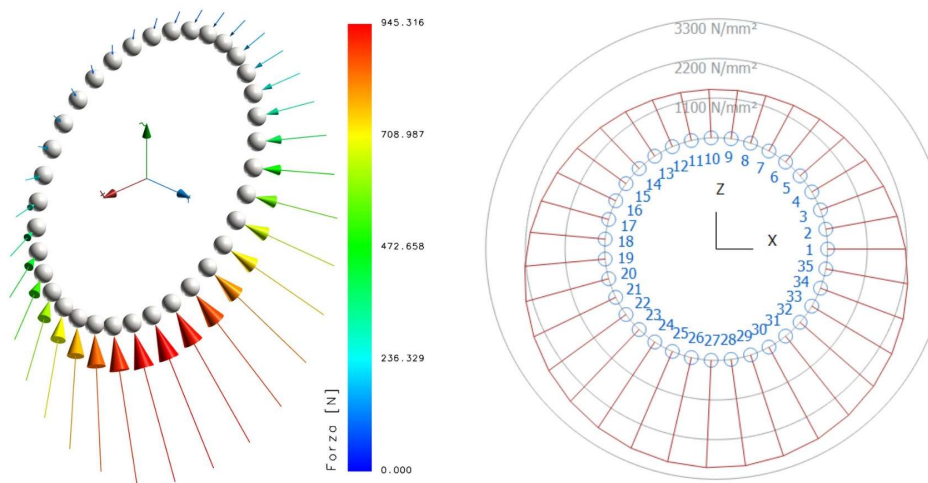


Figure 100. Force and pressure distribution, wheel bearing hub side

5.1.4. Preload

To further improve the bearings life, a proper preload should be applied.

To control the preload effectively, one of the most commonly employed methods is adjusting the axial displacement between the inner and outer rings of the two bearings.

Consequently, in this specific application, the axial preload is regulated by modifying the thickness of a precisely calibrated spacer (circled in red in the figure below), positioned between the outer raceway of the carrier side bearing and the corresponding abutment on the upright.

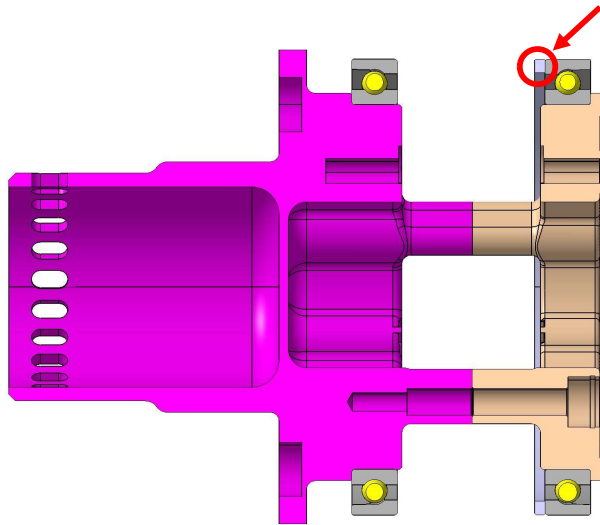


Figure 101. Preload adjustment ring

The designed preload value has been set to 15 μm to maximize the bearings life. To precisely reach this value, the calibrated spacer must be manufactured during the assembly operation to guarantee the correct preload when the screws connecting the planet carrier to the wheel hub are tightened.

This solution offers a very precise adjustment of the preload using a very compact and lightweight component.

5.2. Lubrication

Gearbox lubrication is a critical aspect for ensuring the efficient and reliable operation of gears and other mechanical components involved in the transmission. The primary purpose of gearbox lubrication is to reduce friction and wear between the gear teeth and other moving components. The two main possibilities regarding lubrication are the use of oil and/or grease; in this specific application both will be used together.

Oil is used to lubricate the whole gearbox, including gears and wheel bearings by splash lubrication. Splash lubrication is a simple and effective method for lubricating the transmission. Oil is located at the bottom of the upright inner bore and, as the moving parts rotate, they dip into the oil bath. The motion of the components agitates the oil, causing it to splash inside the upright, allowing it to reach all the components.

Grease is used specifically to lubricate the needle roller bearing inside the planets assembly. This choice has been done since it allows for a simpler and stronger design for the planet pin shaft, as described in section 4.2.3. The downside is the lower cooling effect of grease with respect to oil, but this is not critical since oil is still present inside the transmission and can help dissipate heat also in the area of the roller bearings. Moreover, temperature is not a big concern due to the short duration of Formula Student races.

5.2.1. Lubricant oil

In this gearbox application, the oil is entitled with the following tasks:

- Gears lubrication
- Bearings lubrication
- Protection of metal parts from corrosion
- Removal of dirt
- Heat dissipation

It is clear that an optimal oil choice is crucial for the transmission efficiency and performance: in particular oil viscosity plays an important role in the film thickness, which should always be greater than the average roughness of the tooth flank. As a matter of fact, the higher the oil viscosity, the more a decent film thickness is provided, especially at low rotational speeds, and the less scuffing and pitting phenomena can occur. On the other hand, a too high viscosity can cause an increase in friction losses and therefore a reduction in the overall transmission efficiency. A good balance between the two features should therefore be achieved. Moreover, the oil must be compatible with the selected grease in order to avoid foamy residues that would negatively affect the lubricants' properties.

The lubricant oil choice is a compromise between the needs of gears lubrication and bearings one, which may vary a lot in terms of required viscosity. For gear lubrication a suggestion for the oil viscosity is given in the following table developed by AGMA, as function of the gears type, dimensions and ambient temperature.

Type of Unit ^c and Low-Speed Center Distance	Ambient Temperature ^{d,e}	
	-10°C to + 10°C (15°F to 50°F)	10°C to 50°C (50°F to 125°F)
<i>Parallel Shaft (Single Reduction)</i>		
Up to 200 mm (to 8 in.)	2-3	3-4
Over 200 mm to 500 mm (8 to 20 in.)	2-3	4-5
Over 500 mm (over 20 in.)	3-4	4-5
<i>Parallel Shaft (Double Reduction)</i>		
Up to 200 mm (to 8 in.)	2-3	3-4
Over 200 mm (over 8 in.)	3-4	4-5
<i>Parallel Shaft (Triple Reduction)</i>		
Up to 200 mm (to 8 in.)	2-3	3-4
Over 200 mm to 500 mm (8 to 20 in.)	3-4	4-5
Over 500 mm (over 20 in.)	4-5	5-6
<i>Planetary-Gear Units (Housing Diameter)</i>		
Up to 400 mm (to 16 in.) O.D.	2-3	3-4
Over 400 mm (over 16 in.) O.D.	3-4	4-5
<i>Straight or Spiral-Bevel-Gear Units</i>		
Cone distance to 300 mm (to 12 in.)	2-3	4-5
Cone distance over 300 mm (over 12 in.)	3-4	5-6
Gear motors and shaft-mounted units	2-3	4-5
High-speed units ^f	1	2

Figure 102. AGMA oil selection table

Considering either a planetary gear reduction or a parallel shaft one, which are the most similar to the designed transmission, with a dimension of up to 200 mm and considering a temperature of around 60°C, the table suggests a AGMA lubricant number of 3 - 4. This value corresponds to an ISO 100 viscosity grade, with an average kinematic viscosity of 100 mm²/s.

This proposed oil viscosity for gear lubrication is not suitable for bearings. The calculation of the oil viscosity for bearings lubrication has been done following the procedure indicated by SKF, the supplier of the bearings employed in the transmission. The analytical process starts with the calculation of the mean diameter, d_m , of the SKF Super Precision angular contact wheel bearing SKF 71816 ACD HC/P4. Then the number of revolutions per minute is taken into consideration, analysing the conditions with the maximum achievable speed. The average diameter is equal to 90 mm, while the rotational speed can be evaluated as

$$n_{out} = \frac{n_{in}}{i} = \frac{20000 \text{ rpm}}{12,8} = 1562,5 \text{ rpm}$$

Where

- n_{out} is the rotational speed of the output shaft, and so of the wheel bearings
- n_{in} is the rotational speed of the motor
- i is the transmission ratio of the gearbox

Inserting these values in the diagram below the rated viscosity v_1 for optimal lubrication turns out to be around $10 \text{ mm}^2/\text{s}$.

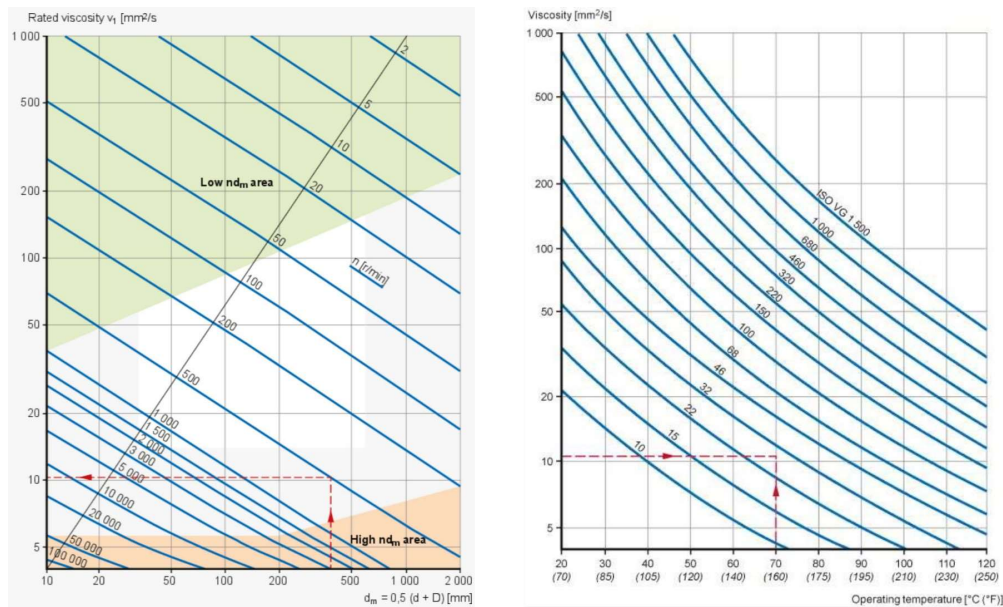


Figure 103. Oil viscosity for bearings lubrication

With the rated viscosity found and again considering an operational temperature of around 60°C , it is possible to obtain the corresponding ISO viscosity grade from the following diagram, which in this case is ISO 22.

The values found for optimal gears and bearings lubrication are quite different, thus it is needed to find a compromise in terms of oil viscosity. With the help of KISSsoft, using an iterative approach changing the oil adopted at each iteration, it has been possible to find the ISO viscosity grade yielding the best trade off in terms of bearings and gears service life and transmission efficiency. The oil viscosity delivering the best performances is ISO 46 grade, with an average viscosity of $46 \text{ mm}^2/\text{s}$.

The oil chosen has been TITAN SINTOFLUID FE SAE 75W, supplied by Squadra Corse's partner FUCHS. This synthetic lubricant has a kinematic viscosity of $40,8 \text{ mm}^2/\text{s}$

at the reference temperature of 40°C and offers good performances with temperature, guaranteeing good lubrication for gears and bearings in every operational condition. It is also compatible with different lubricant greases and with many elastomeric and sealant materials.

The lubricant level inside the gearbox casing is a critical parameter to ensure correct lubrication of mechanical components. An excessive quantity of lubricant can lead to elevated temperatures and hinder overall performances. This surplus oil can result in increased work exerted by the rotating gears as they splash through the excess lubricant, meeting more resistance to motion and impacting the gearbox's overall efficiency.

An often-practiced rule of thumb for planetary gearboxes, particularly those utilizing splash lubrication, suggests maintaining the oil level slightly above the lowermost position of the planet pin shaft. This oil level placement serves the dual purpose of facilitating efficient lubrication within the gearbox while ensuring that a substantial number of the bearing spheres cyclically immerse in the oil bath during operation. This approach helps minimize friction, reduce wear and tear, and manage operating temperatures within the planetary gearbox, ultimately contributing to its overall performance and longevity. This empirical rule is consistent with the oil level suggested by KISSsoft software. The resulting oil amount is around 80 ml, a quantity in line with what has been used in the past seasons, providing satisfactory performances.



Figure 104. Gearbox oil level

To keep the oil clean and to ensure proper gears and bearings lubrication, the oil should be changed often during the vehicle testing and racing season, especially at the beginning of transmission life, when it is more likely the generation of metallic dust in gears run-in period. A way to mitigate this issue is using a magnetic drain screw, which will collect the metallic particles floating inside the gearbox oil, preventing damages to gears surface.

5.2.2. Lubricant grease

Grease is used for needle roller bearings lubrication inside the planet assembly. The main difficulty faced during the grease selection has been the grease compatibility with the gearbox oil, which essentially lubricates both gears and wheel bearings.

The grease chosen has been RENOLIT PU-MA 2, again supplied and suggested by FUCHS for the specific application. It is a fully synthetic high temperature grease based on a polyurea thickener and a polyalphaolefin base oil, very common in automotive lubricants. The use of a PAO base oil grease guarantees optimal temperature stability, good resistance to corrosion and excellent lubrication. As far as the compatibility between the adopted oil and grease is concerned, a general guideline is reported in the following table. The matching between the grease base oil and the oil of interest must be fulfilled.

TABELLA DI COMPATIBILITÀ DELL'OLIO DI BASE

	Minerale/PAO	Estere	Poliglicole	Silicone: Metile	Silicone: Fenile	Polifenilettere	PFPE
Minerale/PAO	+	+	-	-	+	•	-
Estere	+	+	+	-	+	•	-
Poliglicole	-	+	+	-	-	-	-
Silicone: Metile	-	-	-	+	+	-	-
Silicone: Fenile	+	+	-	+	+	+	-
Polifenilettere	•	•	-	-	+	+	-
PFPE	-	-	-	-	-	-	+

+ = Compatibile

• = Test richiesto

- = Incompatibile

Figure 105. Grease-Oil compatibility table

In this situation, having both synthetic based grease and oil, the compatibility is guaranteed.

5.3. Seals

The oil for transmission lubrication must be contained inside the casing, which in this design is the upright, and must be retained inside of it by the use of proper seals. The compliance to this requirement, which is expressly required by Formula Student rulebook in T 7.2.4, is verified before any competition during the tilt test. This procedure, part of the technical inspections, is described in section IN 7 of FSAE rules and consists in tilting the vehicle up to an angle of 60°, to verify the presence of leaks and the rollover stability. Sealing is also important to protect mechanical components from dirt and debris during vehicle running.

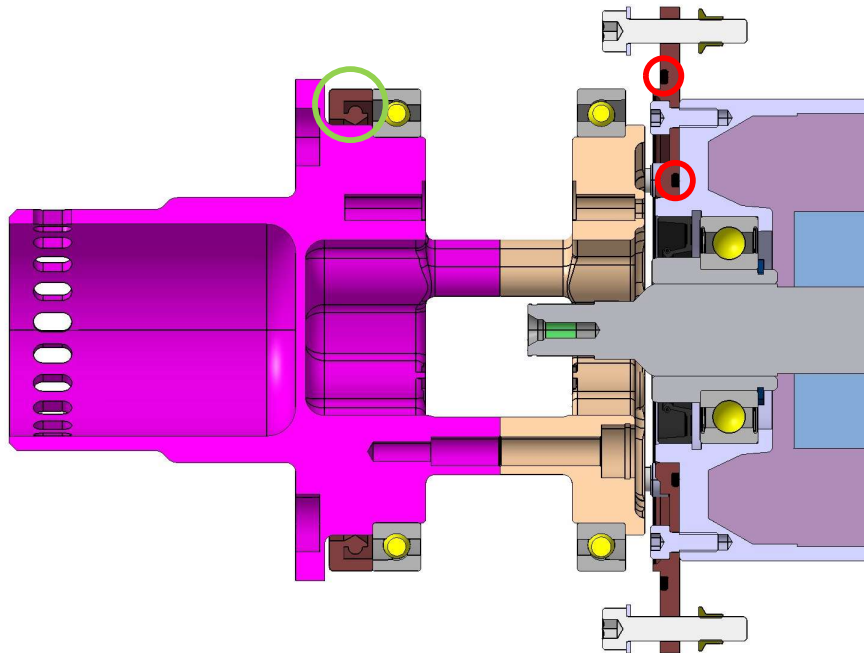


Figure 106. Seals

The sealing action is guaranteed by a radial shaft seal (highlighted in green in the figure above) on the wheel side and by two o-rings (highlighted in red in the figure above) on the motor side.

5.3.1. Radial shaft seal

On the wheel side, the seal must work between a stationary part, the upright, and a rotating one, the wheel hub. For this reason, the choice has been to use a radial shaft seal. Since

the seal must be able to retain oil, spring-loaded radial shaft seals are recommended in order to achieve the necessary radial load and resistance to dynamic runout for a satisfactory sealing performance.

It was decided to adopt a seal of type HMS5, whose section can be seen in the figure below.



Figure 107. HMS5 seal cross section

The rubber outside diameter provides optimized sealing ability on the upright surface, also in presence of misalignments or not optimal surface roughness. The spring-loaded sealing lip is able to guarantee an excellent sealing when no difference in pressure exists between the inside and the outside, as is in this application, while minimizing the sliding friction losses. The seal is mounted with the lip pointing inwards, since the main function is avoiding the oil exit from the upright.

Due to the constraints imposed by the geometrical dimensions of the components, the radial shaft seal chosen has been a HMS5 85x100x9 RG, supplied by SKF. The main dimensions of this component are summarized in the following table and can be seen in the figure.

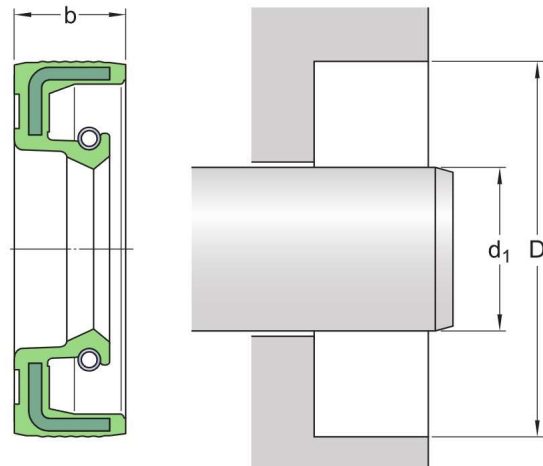


Figure 108. Radial shaft seal dimensions

Shaft diameter - d_1	85 mm
Hole diameter - D	100 mm
Width - b	9 mm

Table 13. HMS5 85x100x9 RG main dimensions

The letters HMS5 in the name indicate the seal lip design, while RG indicate the seal's lip material. In this case the used material is acrylonitrile-butadiene rubber, also known as nitrile rubber or NBR, which is a very common sealing material. The choice of the material has been verified following the graph shown below, in which it is possible to see if the selected material is suitable for the working conditions.

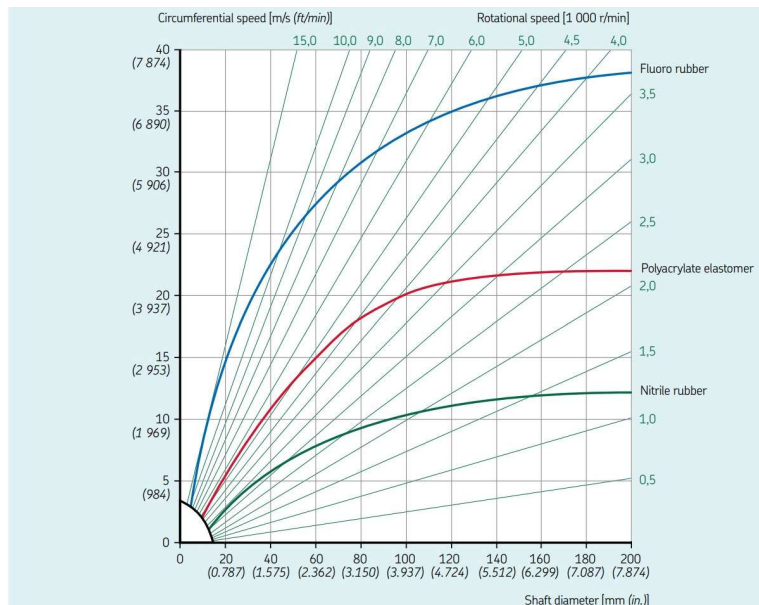


Figure 109. Radial shaft seal material selection

Since the seal works between the upright and the wheel hub, in this application the working conditions are:

- Rotational speed of 1560 rpm
- Circumferential speed of 6,9 m/s
- Shaft diameter of 85 mm

Looking at the graph it is possible to see that the material is able to withstand the applied working conditions. Moreover, the temperature range for NBR radial shaft seals is from -40°C to 100°C , suitable for the working temperature of 60°C . Also the rotational and circumferential speeds fall inside the permissible ones for HMS5 85x100x9 RG radial shaft seal.

5.3.2. O-rings

On the motor side, the seals work between two stationary elements: one between the motor plate and the upright and one between the motor and the motor plate. Due to the working conditions of these sealing elements, it is possible to use o-rings, which are very compact and lightweight and can work in static conditions.

The chosen material is NBR, the same of the radial shaft seal seen above, which is very common and is compatible with the lubricant used in the transmission. Also temperature

resistance, assuming a working temperature of around 60°C, in terms of service life is satisfactory for the application, as can be seen in the graph below.

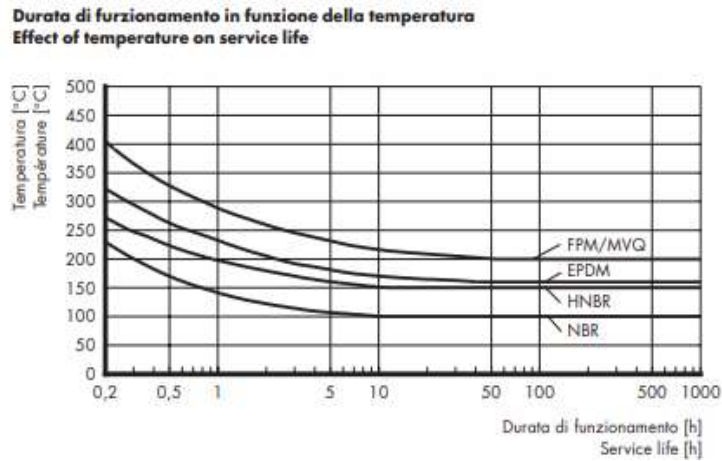


Figure 110. O-rings service life

In order to properly work, the o-rings must be compressed of 10 - 20%, depending on the nominal size of the component. In this configuration, both the o-rings are actively axially compressed during the assembly operation by tightening the screws that connect the motor plate to the motor and the motor plate to the upright.

Trapezoidal housings, which would keep the o-rings in place without slipping out have been examined but were discarded due to more complex manufacturing with no particular advantage to the assembly procedure. A rectangular housing was therefore selected for both the o-rings.

Due to the geometrical constraints on the components, the o-ring between the motor and the motor plate has been chosen with an internal diameter of 61 mm and a cross section diameter of 2 mm, while the one between the motor plate and the upright with an internal diameter of 104 mm and a cross section diameter of again 2 mm.

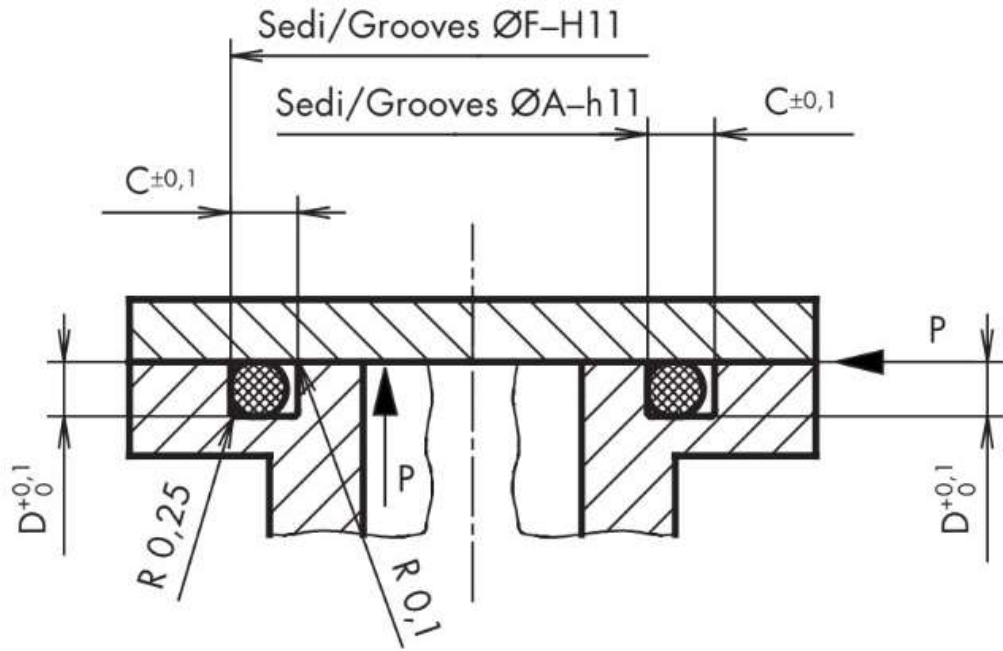


Figure 111. O-rings groove dimensions

The dimensions of the grooves can be extrapolated from tabulated values and, according to the figure above, are summarized below.

	O-ring 1	O-ring 2
Internal diameter	61 mm	104 mm
F	65 mm	108 mm
C	2,6 mm	2,8 mm
D	1,6 mm	1,6 mm

Table 14. O-rings and grooves dimensions

6. PLANETARY CARRIER AND WHEEL HUB

Once the geometry and design of the mechanical components, discussed in chapter 4, and of the wheel bearings and seals, analysed in chapter 5, have been defined, it is possible to proceed with the design of the planetary carrier and wheel hub assembly.

6.1. Mechanical design

As seen before, the planetary carrier and wheel hub represent the output of the transmission, which receive the torque from the pin shafts and transmit it to the wheel rim, to which they are directly connected. These two components must rotate together at the same speed and could therefore be designed as a unique component, but they have been designed as two separate parts for assembly reasons.

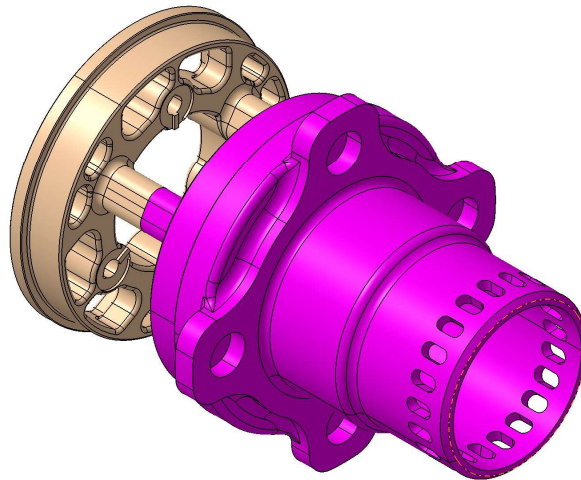


Figure 112. Planetary carrier and wheel hub assembly

The planet carrier and the wheel hub have interfaces with many different components of the transmission and wheel assembly, which impose some boundary conditions and geometrical constraints to the design of these components.

The wheel hub must be connected to the magnesium alloy wheel rim, so the final part of this component must fit inside the central hole on the rim and has to be threaded, to allow the use of the wheel nut to retain the rim to the hub. Moreover, a flange is needed to have a contact surface between the rim, the brake disc, the spacer and the hub itself. Finally,

on this flange some holes have been added to host the pins useful for the correct positioning of the wheel and as a safety feature in case of wheel nut loosening.

Both the hub and the carrier should have the space and the correct abutments to mate and constraint the wheel bearings. Furthermore, on the wheel hub it is also needed to have the space for the shaft seal installation.

The wheel hub and the carrier receive torque from the pin shafts, which are connected to both these elements. The components thus must have the seats to host the pin shafts and the related components, such as the shims. On the planetary carrier, the pin shaft seats also include the shaped holes to constraint the pin shaft rotation.

The carrier and the hub are assembled together by the use of three shoulder screws compliant to UNI ISO 7379 norm. These screws and the tightening torque have been designed to work relying on the friction generated during tightening between the two components, thus the calibrated part seems unnecessary. However, these calibrated screws are useful to guarantee the correct alignment between the two components during the assembly, thus avoiding problems in gears and bearings alignment. The tightening of the screws also generates the preload on the wheel bearings, as explained in section 5.1.4.

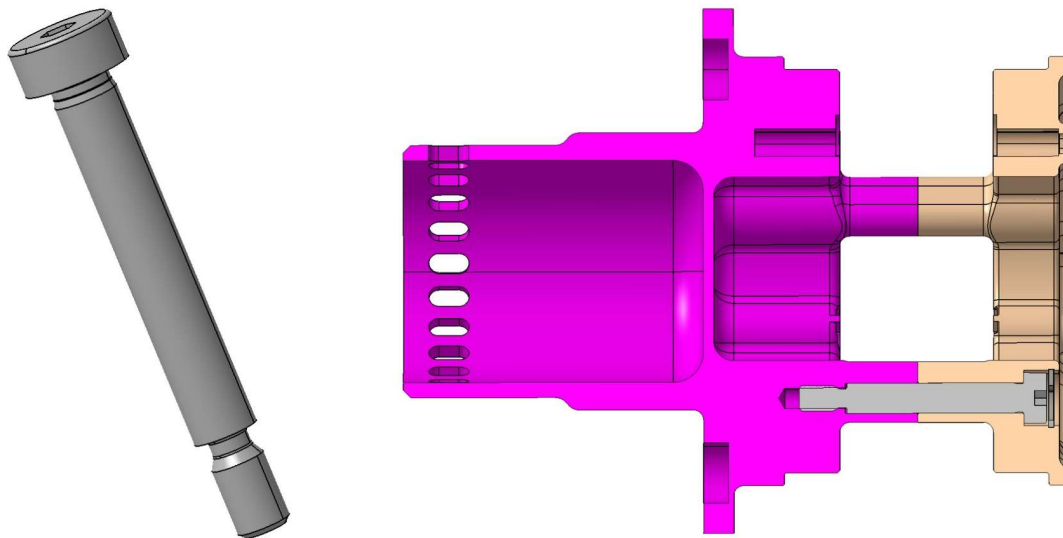


Figure 113. Shoulder screw

Besides the geometrical and assembly constraints, the planet carrier and wheel hub assembly should also comply with the performance requirements. The main targets for this assembly are:

- Weight reduction, since these components are part of the unsprung masses of the vehicle and are also rotating components. For these reasons their mass and overall inertia has a great impact on the vehicle performances. Moreover, carrier and hub are the biggest and heavier components of the whole transmission, which means that there is a good potential for weight reduction of the assembly as a percentage.
- Minimize displacement, since all deformations of this assembly will result in a movement of the tire contact patch and of the wheel characteristic angles, with a detrimental and unpredictable effect on vehicle dynamics.
- Static and fatigue strength, since the components are highly loaded and are subjected to varying and cyclical loading conditions.

6.2. Material selection

Given that weight reduction is a primary design objective, the selection of material plays a pivotal role. The choice therefore has been to use aluminium alloys, which are sufficiently strong and stiff to meet the targets, but at the same time lightweight and easy to machine.

As a first step, the material chosen was Al 2024-T6, an aluminium alloy with a good strength which is often used in aerospace applications. However, after the fatigue analysis was performed, this material was discarded due to the fatigue resistance which was not sufficient to meet the required service life.

To be able to sustain the applied loads, the material chosen both for the planetary carrier and the upright has been Al 7075-T6, commercially known as Ergal, a high-strength aluminium alloy with excellent mechanical properties. Ergal is very well known in the automotive and aerospace industry due to its high specific strength, which makes it suitable for building lightweight mechanical components. The yield strength of the material is around 500 MPa, which is higher than most other aluminium alloys. Also the

fatigue resistance of Al 7075-T6 is very good, higher than most other alloys, and makes it suitable to build components subjected to cyclic loading conditions.

Al 7075-T6	
Density	2,81 g/cm ³
Elastic modulus	71,7 GPa
Yield strength	500 MPa
Ultimate tensile strength	570 MPa
Hardness	150 HB

Table 15. Al 7075-T6 material characteristics

The name of this alloy indicates that it is subjected to the T6 heat treatment, that consists of solution heat treatment followed by quenching and subsequently by artificial aging. This treatment is applied to the raw material to enhance its mechanical properties.

After the manufacturing of the components, it is possible to perform a surface treatment on the aluminium alloy. The most common surface treatment is anodizing, which creates an oxide layer on the surface of the aluminium component, providing an increased wear and corrosion resistance. It has been decided to apply aesthetic anodizing to the planetary carrier, which is less subjected to wear, and hard anodizing to the wheel hub, which has to withstand the mounting and dismounting of the wheel nut hundreds of times during a racing season. Hard anodizing creates a thicker oxide layer with respect to aesthetic one and this aspect has to be taken into account when defining the tolerances for the components.

6.3. Loading conditions

To correctly design and analyse any mechanical component, it is important to understand the loading condition to which it will be subjected during its service life. This aspect is particularly critical for components such as the carrier and the wheel hub, which are directly loaded from the wheels, so the values of forces applied are closely related to the performance of the whole vehicle.

The calculations of the loads at the contact patch are performed every year by the vehicle dynamics division, that takes data from the track testing activities and estimations about the vehicle performances to calculate the loads at wheels in different conditions. The main load cases considered for components design are five, plus three extreme load cases which are only used as a further analysis to see how far the components can resist in extreme conditions.

The load cases are summarized in the following table in terms of vehicle acceleration and speed. Starting from these values it is then possible to extrapolate the forces acting on each wheel in every condition.

LOAD CASE	a_x [g]	a_y [g]	v [m/s]
Pure acceleration	1,6	\	10
Pure braking	-3	\	27,8
Pure lateral	\	-2,5	22,22
Acceleration in turn	1	-1,5	16,7
Braking in turn	-1	-1,5	16,7

Table 16. Design load cases - accelerations

The forces at the tire contact patch are independent from the rim size, thus the values calculated for the design of SC22 EVO have been considered in this analysis.

Depending on the specific load case, the values of the ground forces will change and also the most stressed wheel will be different. Namely rear wheels are most stressed during accelerations manoeuvres, while front ones are most loaded in braking. In any cornering condition the out of the bend curve wheel experiences the higher forces. The contact patch forces in every component are described below, together with the indication of the wheel on which are acting.

LOAD CASE	F_x [N]	F_y [N]	F_z [N]	Wheel
Pure acceleration	1483,3	0	1207,9	RL/RR
Pure braking	-2781,1	0	1884,9	FL/FR
Pure lateral	0	-2989	1856	RL
Acceleration in turn	1252	-1878	1641	RL
Braking in turn	-1147,6	-1721,4	1504,2	FL

Table 17. Design load cases - forces

Looking at these values it is possible to see that the two most demanding conditions are pure lateral and pure braking, with a resultant force applied at the tire contact patch of around 3500 N.

Apart from the ground forces, other loads are applied to the planet carrier and wheel hub assembly and should be considered on top of these. These forces are:

- Axial force due to wheel nut tightening, with a magnitude of 32000 N needed to transfer the torque by friction between the rim and the wheel hub;
- Axial forces due to shoulder screws tightening, with a magnitude of 3560 N needed to transfer forces by friction between the planetary carrier and the wheel hub;
- Pressure of 0,85 MPa caused by the wheel bearings preload.

6.4. Topology optimization

After having defined the geometrical constraints and the loading conditions, the next step in the design process of the planetary carrier and the wheel hub assembly is topology optimization of the components.

Topology optimization is a computational design approach crucial in the development of high-performance components, such as those employed in Formula Student prototypes. This method involves optimizing the distribution of material within a designated design space to meet specific performance objectives. The primary aim of topology optimization

is to determine the best material layout within a structure, taking into account factors like strength, stiffness and weight, identifying the most efficient and lightweight design while adhering to given constraints. By assessing the applied loads and boundary conditions, the algorithm reshapes the material distribution to minimize stress concentrations, enhance structural integrity and reduce excess material.

The optimization process commences with an initial design space, representing the volume or area where the optimized structure will be situated. This design space is then discretized into finite elements, creating the mesh. Throughout the optimization process, the algorithm systematically eliminates material from the design space, redistributes it, and assesses the resulting structural performance. Material removal is typically accomplished using mathematical or computational techniques, often employing density-based methods.

The optimization algorithm assesses the structure's performance based on predefined objectives and constraints. These objectives might encompass minimizing weight, maximizing stiffness, minimizing stress or deformation under specific loads, or a combination of these criteria.

Across multiple optimization iterations, the algorithm gradually enhances the material layout by removing less critical or redundant material. This iterative procedure continues until a convergence criterion is met or until the desired performance objectives are realized. The outcome of topology optimization is a material distribution or density map that illustrates the optimal layout within the design space.

The preliminary step was to come up with a simplified and raw geometry that still complied with the main constraints, but certainly would allow the optimizer to properly work on material reduction. In order to better simulate the behaviour of the real components, both topological optimization and FEM analysis were performed on the whole assembly. The imported CAD geometry has been cleaned up eliminating blends, chamfers and all those small non-structural changes in geometry that would negatively affect the model size and the computational time.

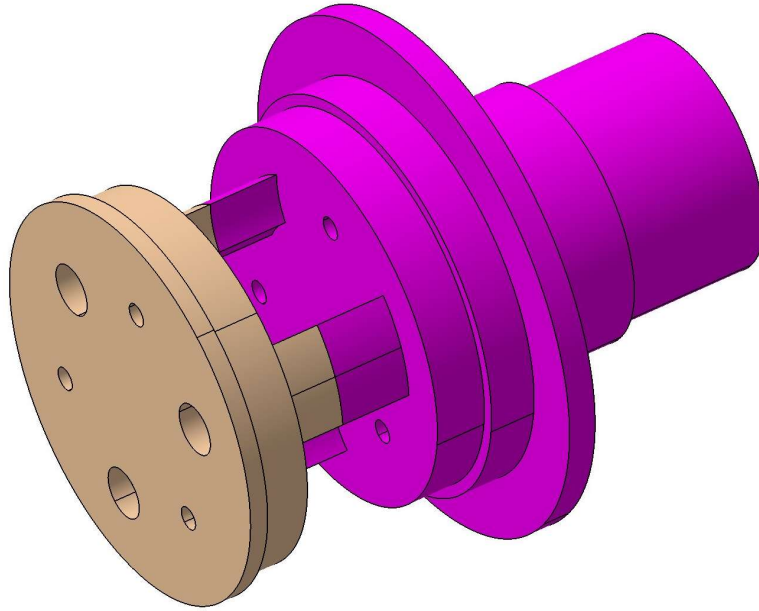


Figure 114. Planetary carrier and wheel hub assembly raw geometry

The optimization was initially set up on Inspire software, making partitions of the geometry to define the “design space” (brown in the figure below), the one where material will be removed and “non-design space” (grey in the figure below), the one that will remain unchanged after the optimization. As “non-design space” were defined the geometrical features mating with other components, such as the holes for the shoulder screws and for the housing of the pin shafts, the blind holes for the locating pins, the surfaces that go in contact with the wheel bearings and the shaft seal and the external surface of the hub which goes in contact with the rim of the wheel and the wheel nut. As a rule of thumb, the minimum thickness of the partitions was set at 2 mm.

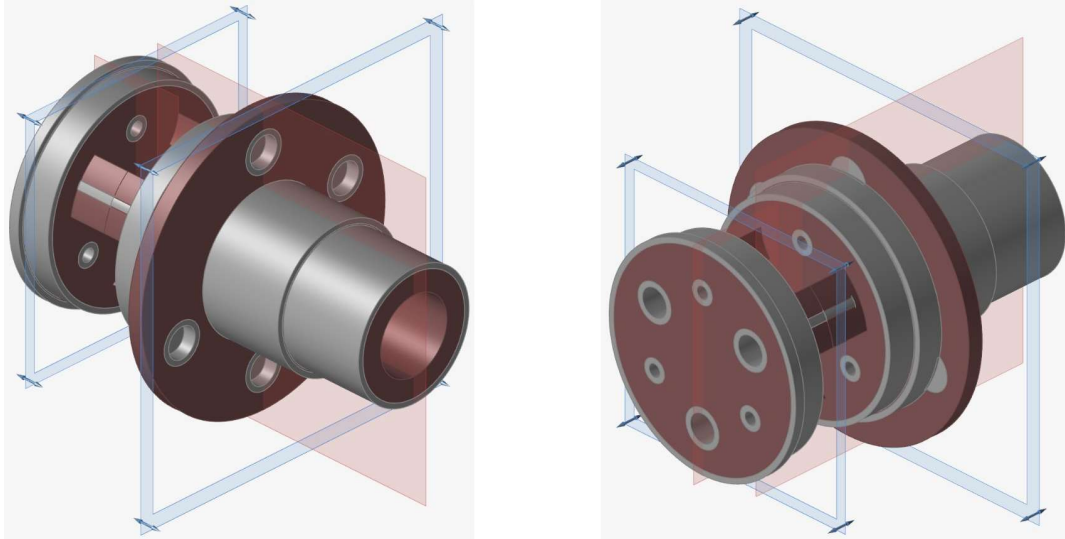


Figure 115. Optimization Inspire model

As the symmetry plane it was chosen the one parallel to the assembly axial direction, passing for the centre of a shoulder screw hole, the centre of a pin shaft housing and the centre of one of the blind holes on the hub. The use of symmetry planes, which can be seen in red in the model figure, helps to reduce the optimization complexity for components that are actually symmetric regarding geometry, constraints and loads.

As manufacturing constraint, a split draw has been applied, which indicates that, for parts manufactured by machining, the main direction of material removal is the one perpendicular to the defined drawing plane. In this case, for both the planetary carrier and the wheel hub, the drawing planes, which are in blue in the figure, have been defined perpendicular to the assembly rotation axis. This is helpful to avoid optimized shapes that are not manufacturable by conventional methods.

The mesh size was set for all the components at 1 mm of mean value and 0,5 mm as minimum value. This has been done as a compromise between accuracy and computational time and the use of a variable mesh dimension helps to better follow geometry in complex areas while reducing unnecessary fine mesh in simple areas.

The target of the optimization was set to “maximize stiffness”, with a target volume of the optimized component 35% of the original one. The stress constraint was set at 250 MPa, half of the material yield strength.

After all the pre-processing performed in Inspire, the model has been moved to Hypermesh, where loads and constraints were set as in the FEM model that is described in detail in the following paragraph. The only difference is that loads and constraints were applied only to “non-design space”, to avoid errors in the software. All the five load cases presented before have been applied, always considering the worst wheel to have conservative results.

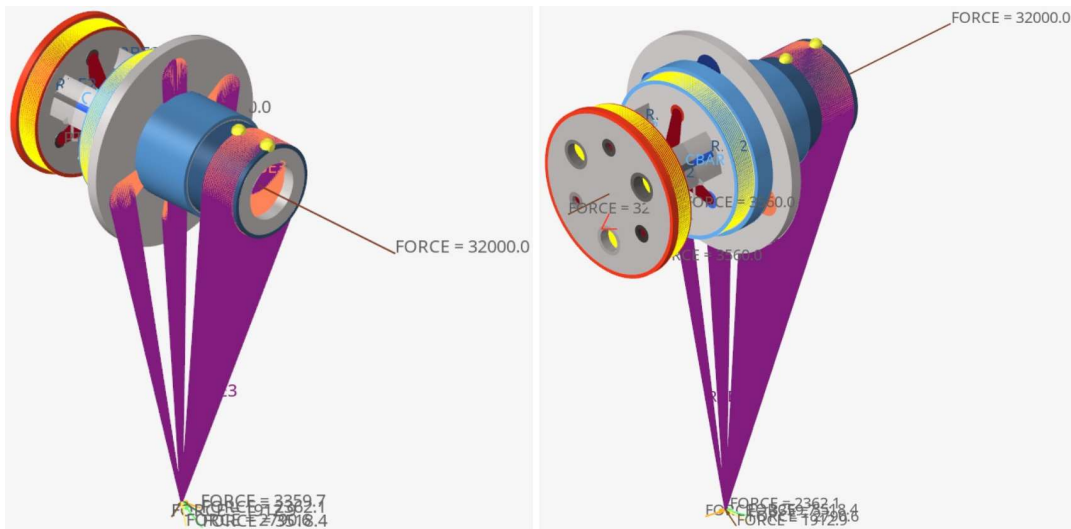


Figure 116. Optimization Hypermesh model

The optimization results were useful to sort out where to remove material and gain an advantage in terms of weight without removing material in critical areas. The results are reported in the following images.

Once the percentage of material removal has been selected at around 60% of the initial volume, from the results it is possible to highlight how the carrier has been considerably reduced, and the same stands for the internal section of the hub, which even presents a pass-through hole, which is however not possible to implement in the real part, since that wall is needed to avoid oil leakages.

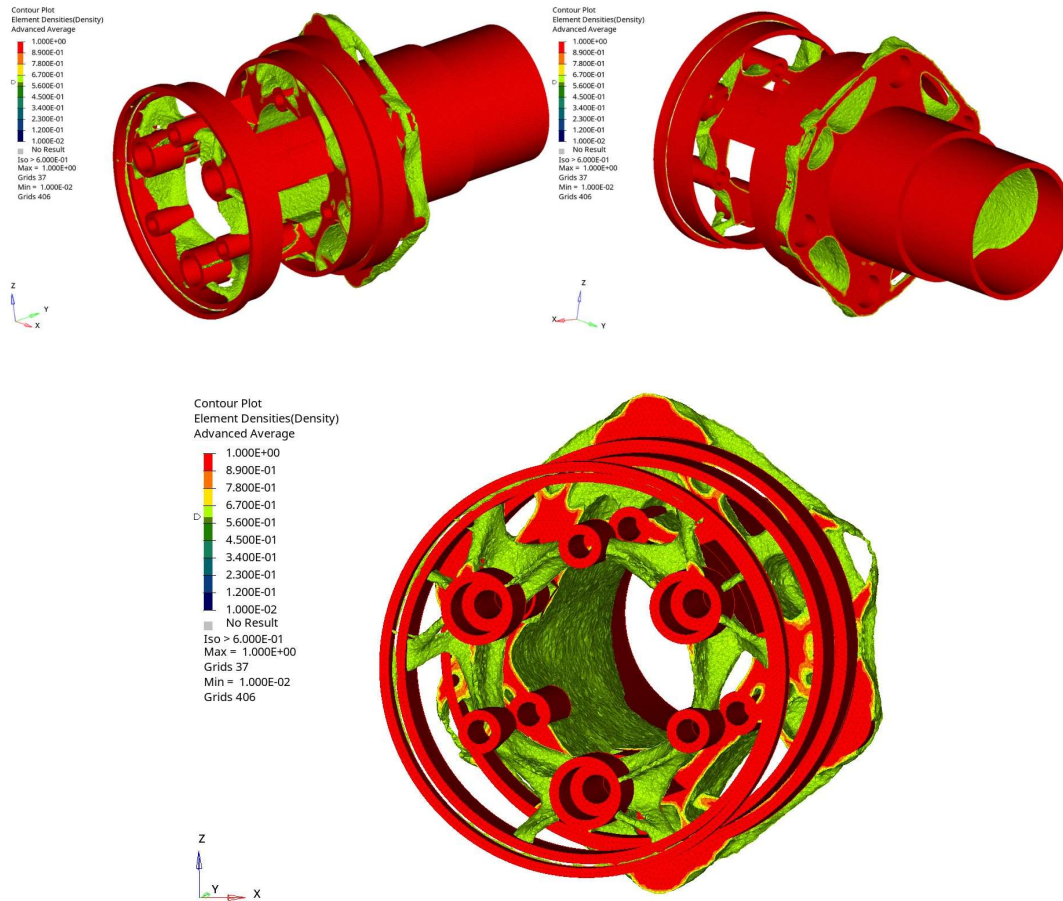


Figure 117. Different views of optimization results

The optimised model was very rough and complex, so it needed some reconstruction to arrive to the actual design of the components. The result has been imported into CAD environment, to be superimposed to the original parts and to proceed with the definition of the final geometry removing material where possible. In this phase it is important to follow the indications coming from topology optimization results, but always keeping in mind the geometrical and manufacturing constraints in the real components. The defined geometry has then to be validated with the FEM analysis.

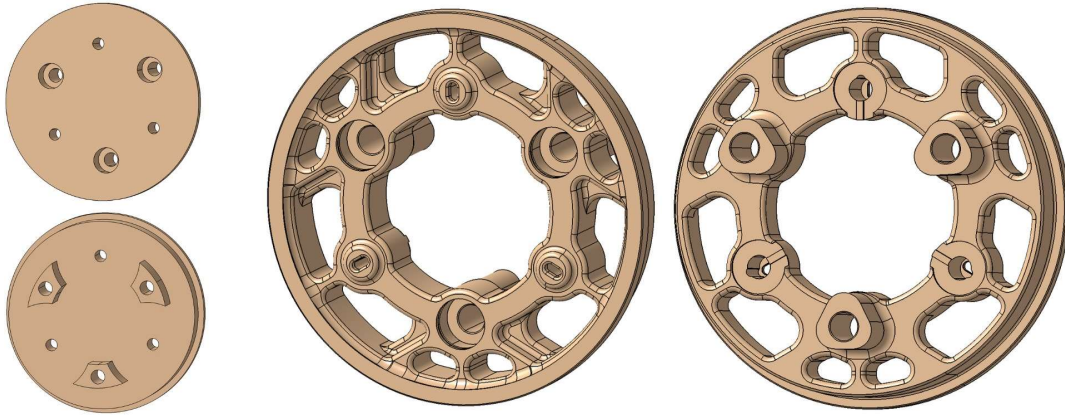


Figure 118. Planetary carrier before (left) and after (right) optimization

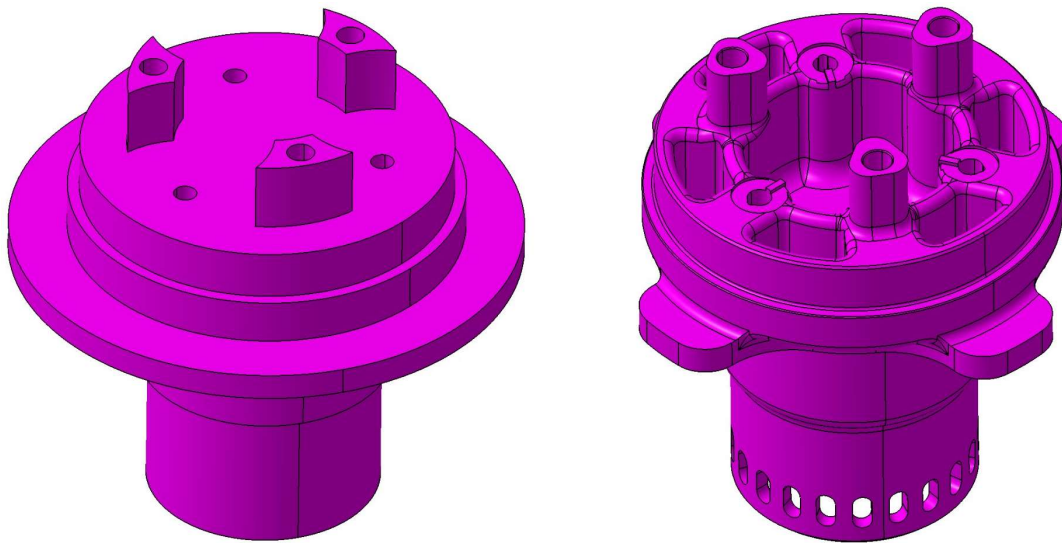


Figure 119. Wheel hub before (left) and after (right) optimization

After the optimization process the weight of the parts is:

- 98 g for the planetary carrier, 54% less than the starting geometry
- 352 g for the wheel hub, 49% less than the initial component

6.5. FEM analysis

The reconstructed geometry built from the optimization results must be validated with a FEM analysis. This is needed since the topology optimization is often very aggressive and the obtained geometry could result to be not able to sustain the design loads.

The planetary carrier and the wheel hub are analysed together, to have a better representation of the real conditions. The first step is the generation of a good 2D mesh for each component, able to follow closely the geometry. The 3D tetrahedral mesh is then generated from the 2D one. The element size has been set to 0,4 mm.

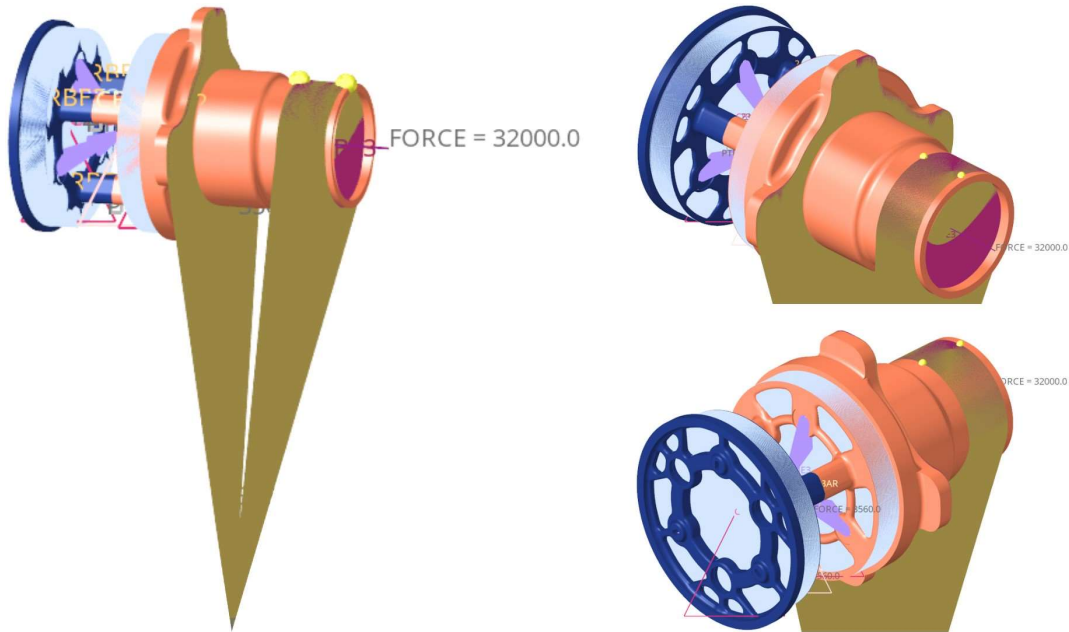


Figure 120. Planetary carrier and wheel hub FEM model

The two components are connected by means of contacts, generated automatically by Hypermesh and then refined manually. The surfaces involved are the ones where the two components are in contact when the calibrated screws are tightened. The contact is defined as "stick" type, which means that any relative sliding or slipping between mating surfaces is entirely prevented. This assumption implies that the threaded connection between the hub and the carrier is fully functional under design conditions, and all loads are transferred solely through friction.

After having prepared the geometry, it is possible to proceed with the application of constraints and loads as follows.

The upright constrains the motion of the planetary carrier and wheel hub assembly through the wheel bearings. The wheel bearings constraints were imposed by putting two RBE3 elements and two zero length CBUSH elements on the surfaces of contact between the components and the bearings inner raceways. The dependent node was chosen as the geometric centre of the respective RBE3, corresponding to the bearings geometrical

centre. The constraint was imposed locking all the DOFs except for the rotation around the wheel axis, which is indeed allowed by the wheel bearings, with an SPC on the dependent node.

The carrier and the hub are connected by contacts, as seen before, and by the effect of the shoulder screws tightening. These screws and their effect on the strength of the whole assembly have been modelled with 1D CBAR elements, assigning them the corresponding cross section and material. At the ends of the CBARs, two RBE2 elements are present, having as independent nodes the ends of the CBAR and as dependent ones the threaded part of the screw hole and the nodes where there is contact between the head of the screw and the carrier respectively. The CBAR elements and the RBE2 rigid elements are connected via two zero length CBUSH.

The reaction of the planet gears avoids the hub to rotate around its axis when ground forces are applied. This effect has been modelled with an SPC on the dependent node of an RBE3 element, locking only the rotation around the axis. The independent nodes of the RBE3 were chosen as the ones of the pin shafts housings on both the carrier and the wheel hub. The RBE3 and the SPC are connected via a zero length CBUSH.

The load deriving from the tightening of the wheel nut is applied as two opposite forces of 32 kN, each applied on a different RBE3 element. First RBE3 has as independent nodes the ones belonging to the threaded part of the hub, for a width corresponding to the width of the wheel nut; the force applied to this element is a tractive force. Second RBE3 has as independent nodes the ones belonging to the wheel hub flange; in this case the force applied is a compressive one. This is a conservative approach, since considers that the total force is sustained by the hub, while in reality it is shared with other components, such as the wheel rim, the spacer, and the brake disc carrier.

The load coming from the ground forces at the tire contact patch has been evaluated considering the five different load cases previously described, always considering the most critical wheel. These five different forces have been applied as different load collectors, each one acting on the dependent node of the same RBE3 element. This RBE3 has the independent nodes corresponding to the independent nodes of the RBE3s used for the forces of the wheel nut tightening and a dependent node in the position of the tire contact patch.

The preload of the wheel bearings is taken into account applying a pressure of 0.85 MPa on the nodes belonging to the surface of the abutments that are in contact with the bearings.

The load generated from the tightening of the shoulder screws is considered applying a pretension force of 3560 N to each CBAR element.

The analysis has been performed with five different loadsteps, one for each of the load cases, always considering all the other constraints and loads together. The results can be seen in the following images, showing the Von Mises stress and the displacement of the components for the most demanding and most critical conditions, which are pure braking and pure lateral.

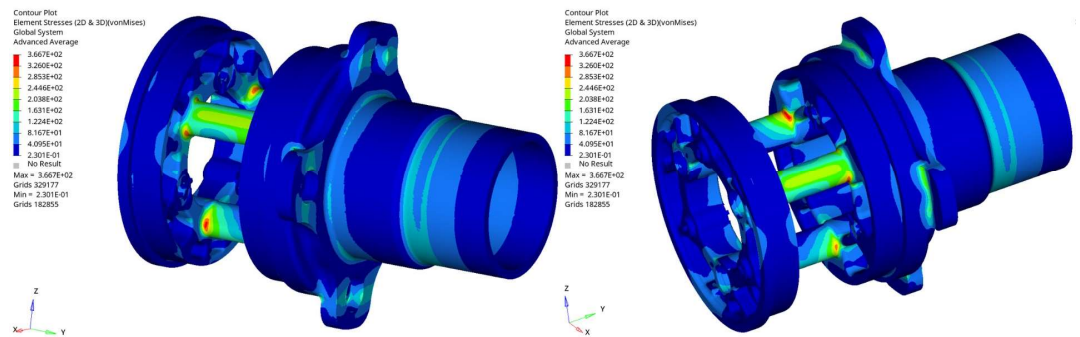


Figure 121. Planetary carrier and wheel hub Von Mises stress in pure braking

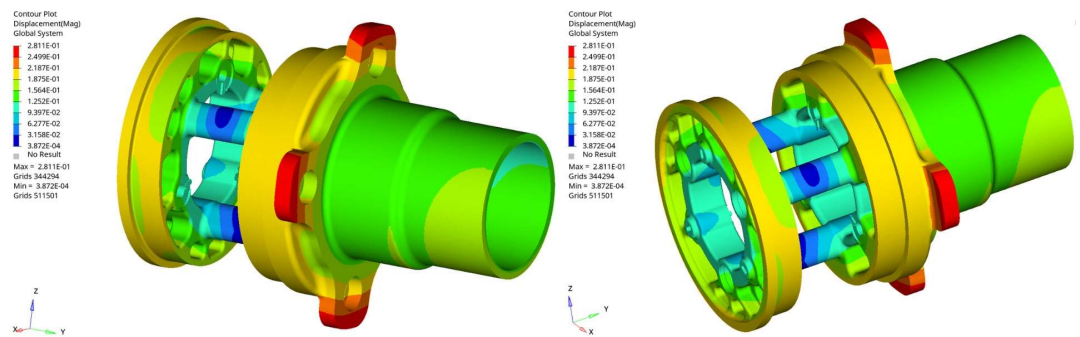


Figure 122. Planetary carrier and wheel hub displacement in pure braking

In pure braking the most stressed zone is localized in the towers where the shoulder screws are located, and the planetary carrier is in general more loaded with respect to the wheel hub. The peak stress reached is 367 MPa, which means that the components are verified with a safety factor of 1,4. The maximum displacement is around 0,28 mm, in the area of the wheel hub flange.

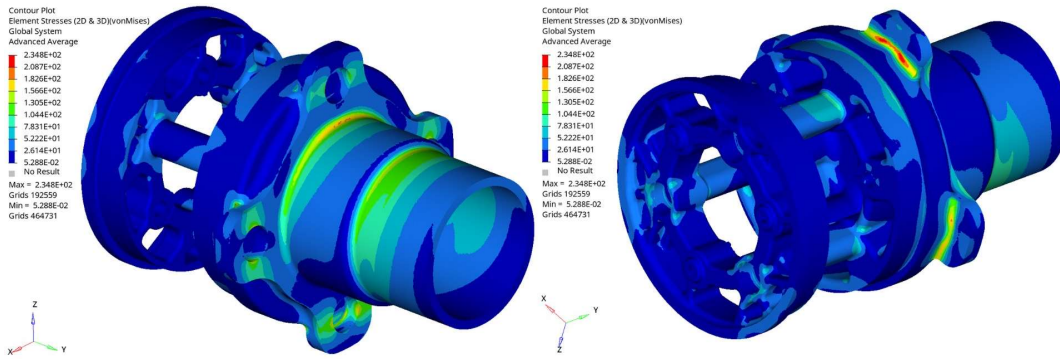


Figure 123. Planetary carrier and wheel hub Von Mises stress in pure lateral

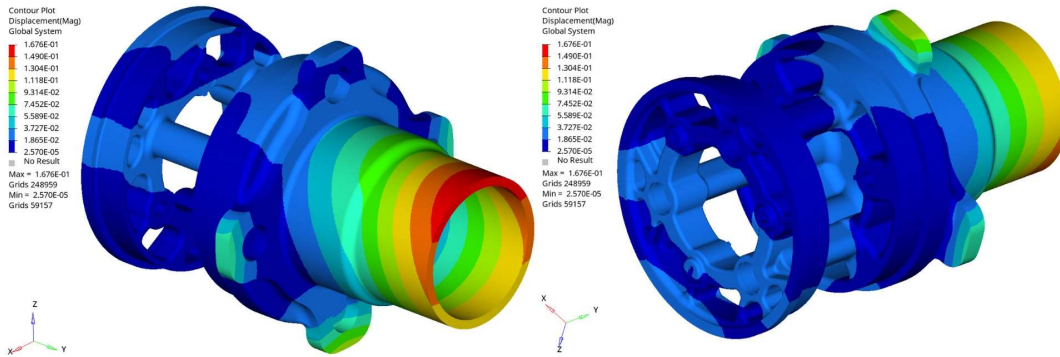


Figure 124. Planetary carrier and wheel hub displacement in pure lateral

In pure lateral the stresses experienced by the components are lower and are mainly distributed on the wheel hub, especially on the flange. This difference is due to the higher lateral force which acts on the flange with respect to pure braking load case. The peak stress reached is 235 MPa, resulting in a safety factor of 2,1. The maximum displacement is towards the end of the wheel hub, with a value of around 0,17 mm.

6.6. Fatigue analysis

Once the static design phase was concluded, a fatigue analysis was carried out on the whole assembly: the aim of this study was to evaluate if the actual configuration was safe enough against fatigue failure concerning the expected service life, which has been set at 50 h for the whole transmission.

Fatigue analysis is a process that revolves around the comprehension and prediction of components behaviour in the context of cyclic loading conditions. Fatigue failure manifests when a material or structure is subjected to repetitive loading and unloading

cycles, resulting in the initiation and propagation of cracks, ultimately leading to catastrophic failure. The principal objective of fatigue analysis is two-fold: to estimate the fatigue life, quantified in terms of the number of loading cycles a component can endure before failure, and to pinpoint critical locations susceptible to fatigue-induced damage. This analytical approach serves to uphold the reliability, safety, and durability of mechanical systems, mitigating the risk of unexpected failures. The most common fatigue analysis method, also the one used in this work, is the stress-life or S-N method, where S stands for the applied stress and N for the number of cycles to failure.

The definition of the load spectrum used for the fatigue analysis is a crucial step in this process. The loading condition chosen has been an autocross event performed by SC22 during the 2022 racing season. This event is the most demanding one in terms of vehicle performances and thus applied loads; for these reasons it has been selected for this analysis, to be conservative and cover the worst possible scenario. The wheel considered is the rear left one, which analysing the data resulted to be the most loaded one during the period taken into consideration. Before passing the load spectrum to the software, it is needed to rescale the values as a fraction of the maximum static forces used in the static analysis. The forces coming from the contact patch change during the autocross event, while the other applied loads remain constant ideally during the whole vehicle life.

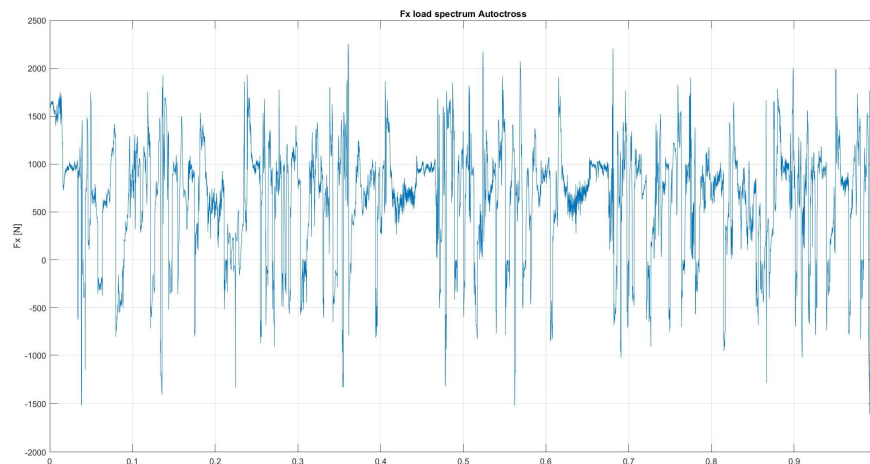


Figure 125. Fx load spectrum during autocross

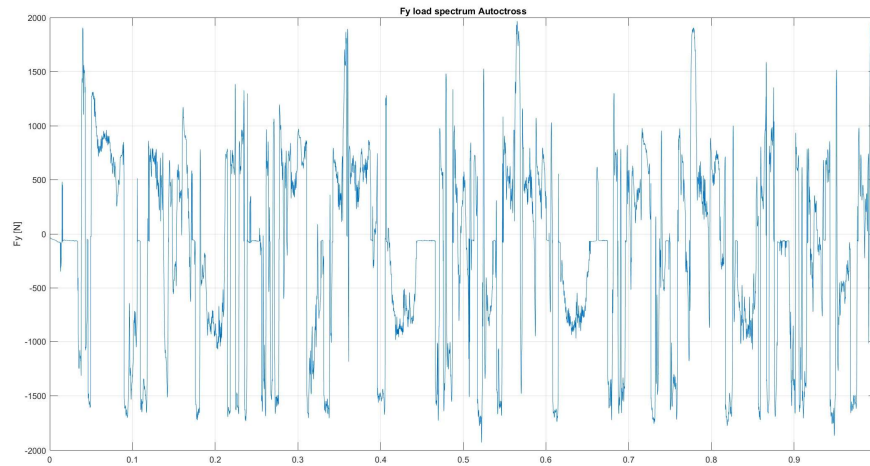


Figure 126. *Fy load spectrum during autocross*

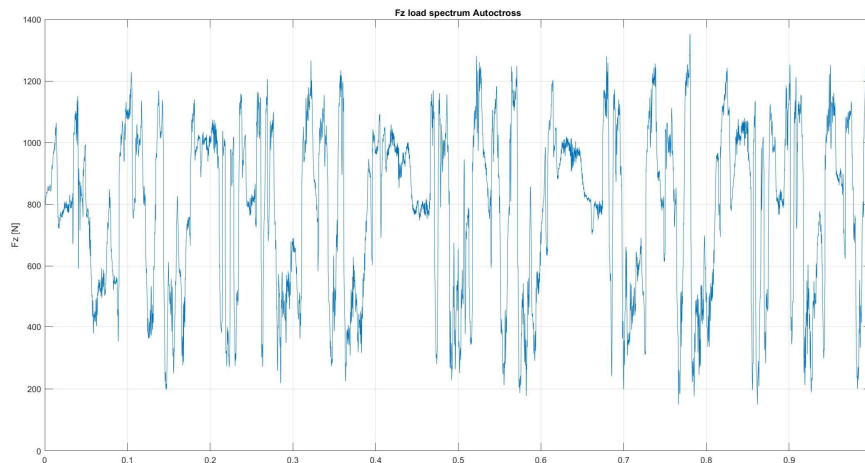


Figure 127. *Fz load spectrum during autocross*

The fatigue analysis is performed in Hyperlife software, a computational tool designed by Altair and specifically developed for fatigue and durability analysis and optimizations. The process starts from the static FEM analysis done before, that will be used by the software to simulate the cyclic application of the loads.

Particular attention has to be paid when defining the material and its fatigue properties. As seen above, the material chosen is Al 7075-T6, whose properties and S-N curve are already present in Hyperlife materials library. It has also been possible to define the surface treatment, anodization in this case, which has a great impact on fatigue life.

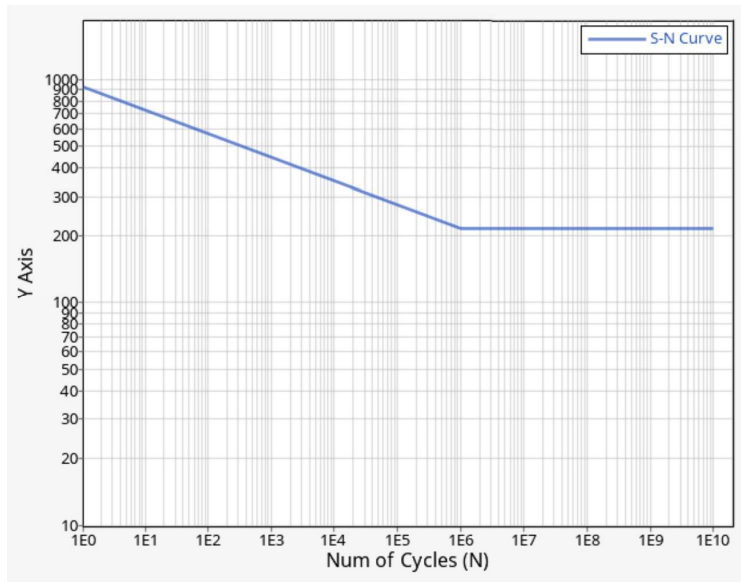
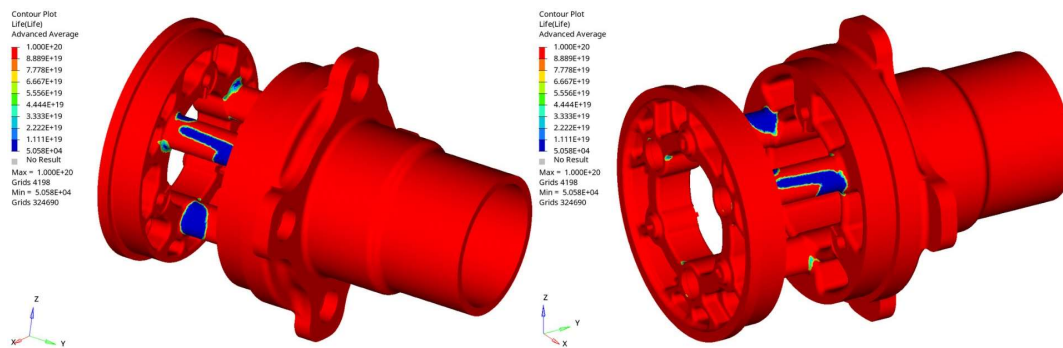


Figure 128. Ergal S-N curve

After having defined all the boundary conditions, the loading scenario, the material characteristics and other data regarding the calculation method that should be used by the software, it was possible to run the analysis. The results in terms of components life in number of cycles and damage are shown below.



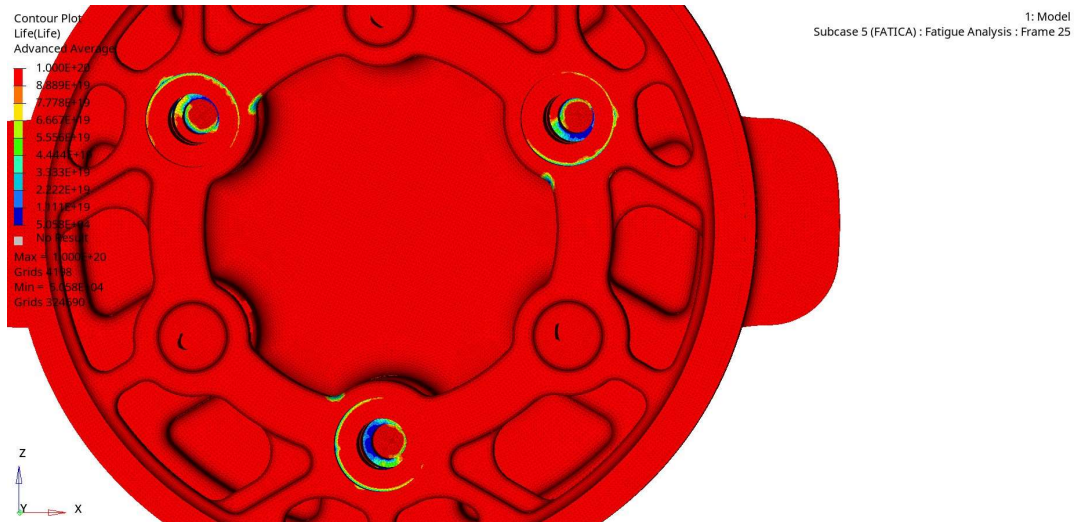


Figure 129. Different views of planetary carrier and wheel hub fatigue life

The results show that infinite life is not reached in the towers where the shoulders screws are tightened, both outside and inside the holes. These areas coincide with the most stressed ones of the static analysis. Looking at the values of the minimum life, which is around 50000 cycles, they are anyway more than enough for the application. Considering an average track length of 1 km for the autocross event, the components life is around 50000 km, which is much more than the desired service life, despite considering the worst case loading condition. The components can thus be considered verified against fatigue.

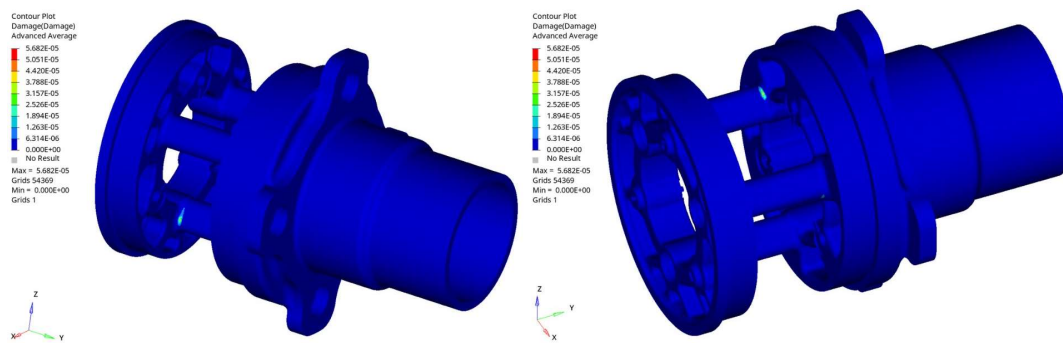


Figure 130. Fatigue analysis damage

Looking at the figure above, components show little damage in the areas corresponding to the most stressed ones while no damage at all throughout most of the components.

6.7. Wheel nut

The wheel rim is retained to the wheel hub by a single nut. The design of this component has an important impact on the design of the wheel hub, since the axial force generated by tightening is one of the major loads applied to the wheel hub.

The shape of the wheel nut is constrained by the wheel hub on the inner side, where there is the threaded part, and by the wheel rim on the outer side. The shape of the contact area between the nut and the rim is conical, which is beneficial both for maximizing the contact surface and because it provides for correct centring of the rim on the hub. The dimensions of these parts have been designed following the guidelines provided by OZ Racing, the rim manufacturer.

The final part of the nut has a hexagonal shape, to allow the use of wrenches and tools to tighten and untighten it. Finally, the slots are used to host a retaining spring, used to provide positive locking as requested by Formula Student rulebook.

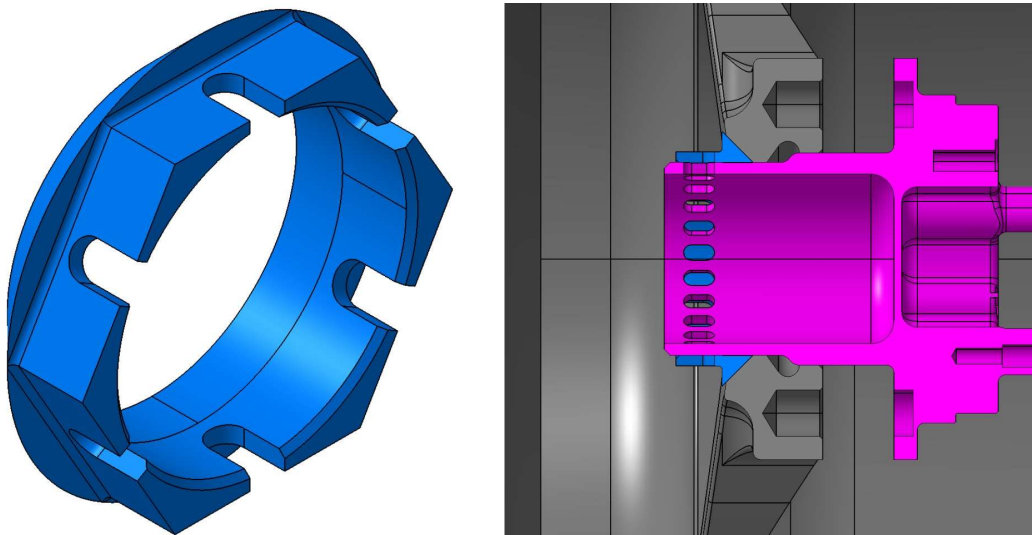


Figure 131. Wheel nut and wheel nut mounting

The material chosen for the wheel nut is Ergal, which is able to provide a sufficient strength in a lightweight component. The surface treatment to be applied is hard anodizing, which is fundamental to prevent excessive wear, both of the threaded section and of the hexagonal section where the wrench acts. The use of this surface treatment is also prescribed by the rules for aluminium wheel nuts.

The tightening torque has been carefully designed to have the torque transmission happening only relying on friction between surfaces. The resulting tightening torque is around 190 Nm.

The torque to transfer originates from the longitudinal forces applied at the tire contact patch. The maximum value originates from braking forces on front wheels and from tractive forces on rear wheels. To have the maximum longitudinal force contribution working to tighten the nut rather than untightening it, two wheel nuts have been designed with a right-hand thread, while the other two with a left-hand one. In particular right-hand thread is used for front right and rear left wheels and left-hand for front left and rear right ones.

7. CONCLUSIONS AND FUTURE PERSPECTIVES

To conclude this thesis work it is interesting to take a look at the final results obtained comparing them with the targets set at the beginning of the analysis and at same future perspectives.

7.1. Results obtained

In the following figure it is possible to see the final gears assembly.

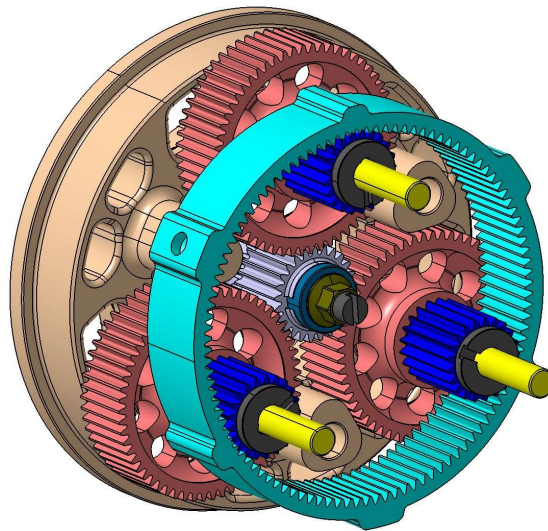


Figure 132. Gears assembly

In the figure below it is possible to see the complete transmission assembly, also including the wheel hub, the wheel bearings and the shaft seal.

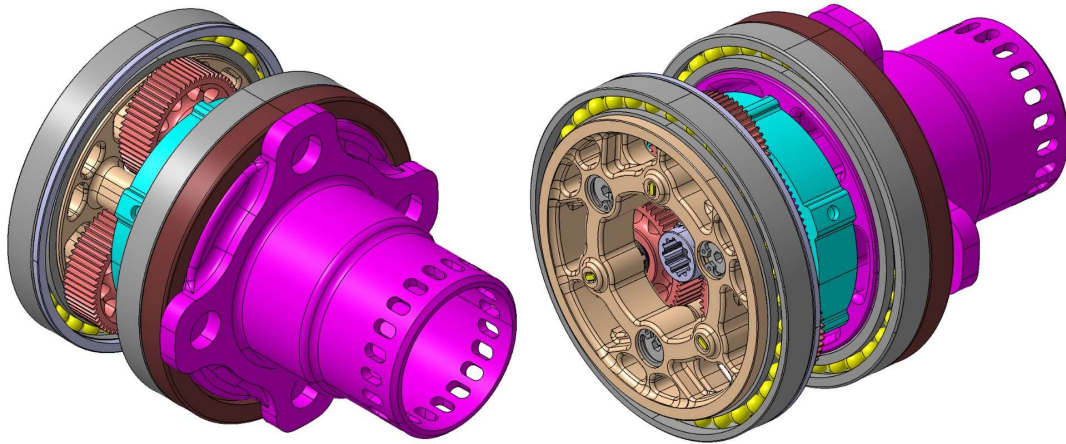


Figure 133. Transmission assembly

The next figure displays the transmission assembly and the motor assembled together, between which it is possible to see the presence of the motor plate, in brown in the image, and the screws that should fix the motor to the upright.

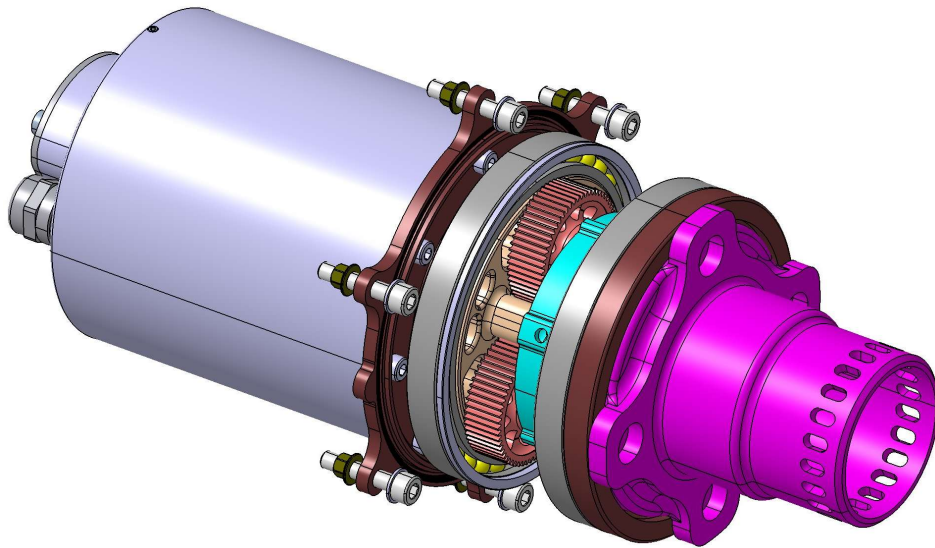


Figure 134. Transmission and motor assembly

Finally, it is possible to see the integration of the transmission and motor inside the wheel assembly. Being this a research project for future applications, the other components of the assembly, such as the upright and brakes, are not present, since they would need to be redesigned with respect to the ones already employed in the past to fit inside smaller wheel rims. From this figure it is noticeable the impact of the transmission on the wheel assembly packaging and how reducing as much as possible its volume would be beneficial to allow design freedom for other components and especially for suspension arms.

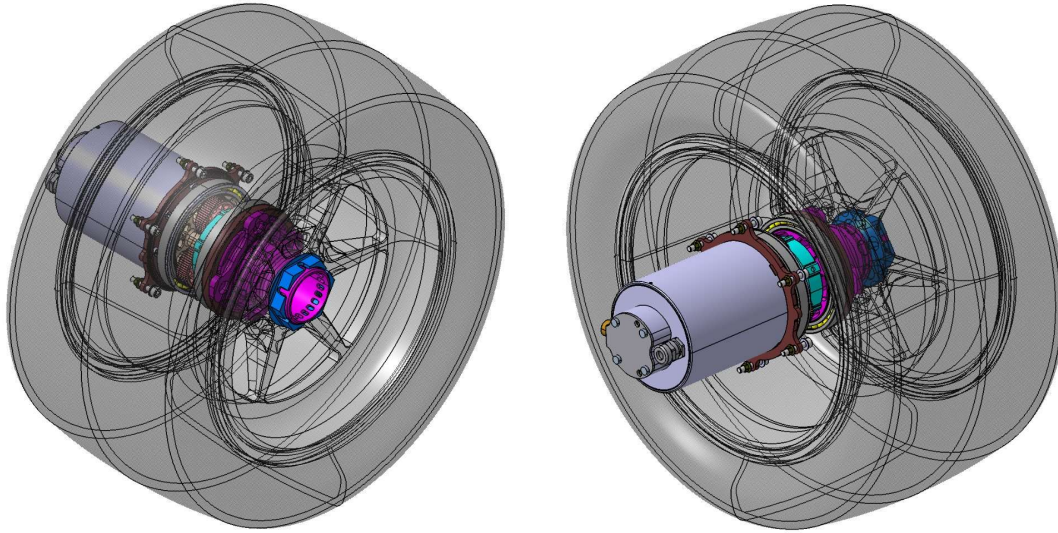


Figure 135. Wheel assembly

7.1.1. Weight reduction

The weight reduction can be appreciated looking at the table below, in which are compared the mass of the components mounted on SC22 EVO with the mass of the components designed in this work.

Component	Quantity	Weight SC22 EVO	Weight
Sun gear assembly	1	32 g	20 g
Planet gears assembly	3	92 g	76 g
Ring gear assembly	1	134 g	83 g
Planetary carrier	1	103 g	98 g
Wheel hub	1	423 g	352 g
Wheel bearings	2	140 g	140 g
Screws	3	13 g	11 g
Miscellaneous	1	51 g	51 g
Oil	1	87 g	69 g
Total	-	1,425 kg	1,214 kg

Table 18. Transmission components weight

The total weight reduction on the transmission assembly is of 211 g, which correspond to a reduction of 15%. This result is already quite satisfactory, considering that the transmission used in SC22 EVO was already well optimized, and would lead to a reduction of more than 800 g on the whole vehicle, even more valuable since it is unsprung mass reduction. A further weight reduction could be obtained by decreasing the size of wheel bearings, an option discarded in this analysis since it would have caused an increased axial length of the assembly.

7.1.2. Volume reduction

One of the targets imposed at the beginning of this work was also volume reduction, and a comparison between the designed transmission and the one adopted in SC22 EVO in terms of dimensions is shown in the following table.

Dimension	Size SC22 EVO	Size
Total length	82,45 mm	69,75 mm
Bearings outer diameter	100 mm	100 mm
Gears maximum diameter	97,6 mm	87,4 mm

Table 19. Transmission main dimensions

Looking at the values it is possible to appreciate that the overall length of the assembly, measured from the motor plate face to the wheel hub flange (thus the portion of the assembly that is contained in the upright), has been reduced by 12,7 mm, corresponding to a reduction of 15%. This result is very important in terms of wheel assembly packaging, especially regarding the design freedom of the suspensions. The overall length of the wheel hub has then been reduced by 8,5 mm in length due to the different offset of the 10" rim vs to the 13" one, further increasing the improvement in axial size. Summing these two results, the motor results to be over 20 mm deeper inside the wheel rim, with benefit for suspension movement and for aerodynamics.

The maximum diameter is limited by the outer size of the wheel bearings, which have been maintained the same as in the SC22 EVO. The maximum envelope of the gears has

been largely reduced and this aspect could be exploited to reduce the overall diameter of the transmission with a different packaging choice.

7.1.3. General improvements

Regarding the components' life, both the required service life and the demand of the load cases have been increased, but at the same time the safety factors for all the components were not reduced, but actually increased for most of them. This result is fundamental to achieve a high reliability of the transmission, which is one of the most expensive mechanical assemblies of the whole vehicle. Increased safety factors and components life could result in the same components being used for more than one season, with great advantages both from an economical and production time point of view.

Also, the assembly procedure complexity and duration should be reduced with respect to SC22 EVO, since the number of components has been decreased. The dowels, the components used in the past to lock the rotation of the planet pin shafts, and the corresponding retaining system are no more necessary thanks to the slots directly machined inside the planetary carrier. Dowels were really small, and their installation required lots of time and effort. Easy and fast assembly operations are beneficial to recover delays coming from production, allowing the car to hit the track earlier. Moreover, a simple assembly speeds up maintenance operations and the substitution of damaged parts. Reducing the number of components is also beneficial in terms of lead and production times of suppliers.

7.2. Future perspectives

In this work has been shown that even gears with very small normal module can withstand the stresses involved in a Formula Student competition with a satisfactory safety factor. Since it is quite unlikely that even smaller gears can be produced, the focus to further reduce the transmission weight and its size should move to different paths.

One of the possibilities to reduce the overall size of the transmission would be to completely redesign the gearbox structure, changing the packaging for example by moving the output from the planetary carrier to the ring gear or by reversing the order of

the two reduction stages. These choices would increase the compactness of the wheel assembly, but are difficult to be implemented using commercially available rims. To take full advantage of the small size gears, custom designed rims would be needed, allowing for lots of design freedom and the possibility to better integrate the motor, the upright and the transmission together.

Regarding weight reduction, a study could be carried out to find the most suitable material and heat treatment for this application. Moreover, also the possibility the use hybrid gears made of two different materials, a stronger one for the gears teeth which are most stressed and a lighter one for the central part, should be investigated. This would lead to strong and light gears, reducing cost of raw materials at the cost of an increased assembly complexity.

Finally, it would be very interesting and effective for future transmissions design to be able to test the gearbox on a test bench, to validate the KISSsoft model and the results about the components' life and efficiency. This test would also be useful to analyse the oil level and its motion inside the casing, eventually comparing the experimental results to fluid dynamics simulations.

7.3. Conclusions

In this thesis has been presented the design of the transmission for a electric Formula Student race car equipped with 10" wheel rims. The choice of this topic was motivated by one of the current trends in Formula Student competitions, that is the transition from 13" to 10" rims, which will be followed in the next seasons also by Squadra Corse. This transition offers many advantages, such as weight and inertia reduction, but requires the complete redesign of the wheel assembly, including the transmission.

This work covers many aspects of the design, starting from the description of the framework of the competition and of the competitors to arrive to the final design of all the main components of the transmission, passing for the analysis of many different layouts of powertrain and transmission.

The selected layout has been to use four independent out board electric motors directly connected to the wheels through a double stage epicyclic geartrain. This configuration

allows to maximize the vehicle performances while keeping the components weight and size to a minimum.

Analysing the results of all the analysis and the final mechanical design of the components and comparing them to the transmission mounted on SC22 EVO, the last and most advanced prototype of Squadra Corse, it is possible to appreciate a weight reduction of 15% and a reduction of 15% of the axial size of the assembly. These satisfactory outcomes have been obtained while at the same time increasing the required service life of the components and without sacrificing the safety factors, which have increased with respect to previous cars.

APPENDICES

Appendix A. AMK motor datasheet



Motor-Datenblatt motor data sheet

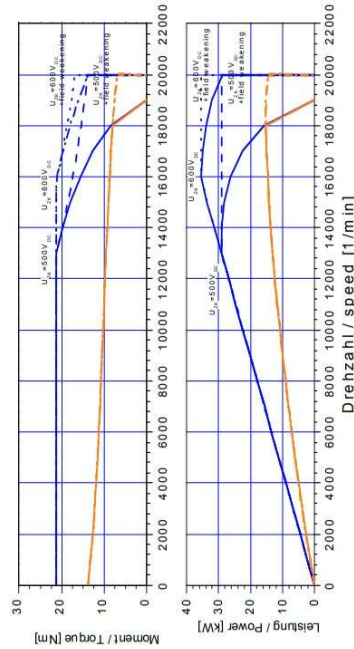
Bezeichnung/name **DD5-14-10-POW** - 18600-B5 Datum/date: 27.11.2018
 Teile-Nr./part number **A2370DD** Zeichn.-Nr./drawing no.: 12703-01260
 - Formula Student

Motorbeschreibung motor description:

Motorprinzip/motor principle: synchron
 Kühlart/cooling type: Flüssigkeit 4l/min
 Bauform/mounting type: IMB5
 Schutzart/degree of protection: IP 65
 Isolierklasse/insulation class: F

Leistungsdaten performance data:
 Betriebsart/duty type: S1 dT=100K
 Dauerstillstandsmoment/continuous Stall Torque "Mo": 13,8 Nm
 Maximales Moment/maximum torque "Mmax": 21 Nm
 Bemessungsmoment/rated torque "Mn" (ID32771): 9,8 Nm
 Bemessungsleistung/rated power "Pn": 12,3 kW
 Bemessungsdrehzahl/rated speed "Nn" (ID32772): 12000 rpm
 Theo. Leerlaufdrehzahl/theor. no-load-speed "No": 18617 rpm

Motorkennlinien performance - characteristics:



Kennlinie kann die maximal zulässige Drehzahl übersteigen! / Characteristic may exceed mechanical speed limit of motor

Elektrische Daten electrical data:

Nennspannung/rated voltage "Un" (ID32768): 350 V
 Nennstrom/rated current "In" (ID111): 41 Arms
 Dauerstillstandsstrom/cont. stall current "Io" (ID34096): 53,1 Arms
 Maximalstrom/maximum current "Imax" (ID109): 105 Arms
 Maximale Dauer für/duration for "Imax" (ID34168): 1,24 s
 Drehmomentkonstante/torque constant "kt": 0,26 Nm/Arms
 Spannungskonstante/voltage constant "ke" (ID 34234): 18,8 V/kU/min
 Schaltung/connection type: D
 Polzahl/number of poles "2p" (ID32775): 10 Pole
 Klemmenwiderstand/terminal resistance "Rt" (ID34164): 0,135 Ohm
 Klemmeninduktivität/terminal inductance "Lt" (ID34167): 0 mH
 Querschseninduktivität/quadrature axis inductance "Lq" (ID34046): 0,12 mH
 Hauptachseninduktivität/direct axis inductance "Ld" (ID34045): 0,24 mH
 Magn.-Strom/magn. current "Im" (ID32769): 35 Arms
 Magn.-Strom/magn. current "Im1" (ID32770): 0 Arms
 Rotorzeitkonstante/rotor time constant "Tr" (ID32774): 0,01 s

Reglereinstellungen controller settings:

Stromregler current controller:

Verstärkung q-Achse/gain q-axis "Kpq" (ID34151): 0,64 V/A
 Verstärkung d-Achse/gain d-axis "Kpd" (ID34152): 0,58 V/A
 Nachstellzeitkonstante/time constant "Tnq" (ID34050): 1,2 ms
 Nachstellzeitkonstante/time constant "Tnd" (ID34052): 1,2 ms
 Adaption Verstärkung/adaption gain "Kpq2" (ID 34179): 20 %
 Adaption Nachstellzeit/adaption time constant "Tnq2" (ID 34180): 400 %
 Untere Anpaßschwelle/lower adaption limit "Iua" (ID34177): 19 %
 Obere Anpaßschwelle/upper adaption limit "Ioa" (ID34178): 68 %

Drehzahlregler speed controller (default for plain motor):

Verstärkung/gain "Kp_n" (ID100): 40
 Nachstellzeitkonstante/time constant "Tn_n" (ID101): 20 ms

Spannungsregler voltage controller:

Spannungsregler/voltage controller "Kp" (ID34148): 0,08 AV
 Spannungsregler/voltage controller "Tn" (ID34149): 6 ms
 Spannungsüberhöhung "dU" (ID34235): 116 %
 Systemwiderstand "Rs" (ID34233): 0 Ohm

Für dieses Dokument und die darin enthaltenen Angaben behalten wir uns alle Rechte und technische Änderungen vor.
 All rights reserved for this document and all information included. Technical modifications reserved
 (c) AMK Antriebs- und Steuerungstechnik GmbH Co. KG

Motor-Datenblatt motor data sheet

Bezeichnung/name **DD5-14-10-POW** - 18600-B5
 Teil-Nr./part numbe **A2370DD**

- Formula Student Datum/date: 27.11.2018
 Zeichn.-Nr./drawing no.: 12703-01260

Mechanische Daten mechanical data:

Gesamtmasse/motor mass "m": 3,55 kg
 Motorträgheitsmoment/inertia "J": 2,74 kgcm²
 Mech. zul. Drehzahl/mech. speed limit "Nmax": 20000 rpm
 Rundlauf/run out (DIN 42955): N
 Wuchtgüte/balancing quality: G2,5
 Passfeder/shaft key: -

Lagerbelastung bearing load:

A/B - Lager/A/B - side bearing:
 Lagertyp/bearing type : 6005 / 6003
 Fettsorte/type of grease: GE2 / GE2
 theo. Fettgebrauchsdauer/grease life time: 13000 / 18000 h
 bei Nenn Drehzahl und 70°C Lageraußenringtemp./at rated speed and 158°F at outer bearing ring
 erforderliche Fettmenge/necessary grease quantity : 0 / g
 Maximale Axialkraft bei Montage/max. axial force for assembly: 3275 N
A - Lager/A - side bearing:



Bremsendaten brake data:

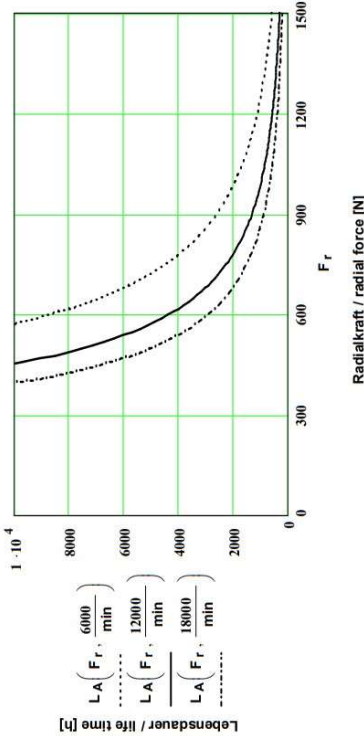
Typ/type: -
 Bremsmoment/brake torque: Nm
 Bremsstrom/brake current: A
 Bremsenspannung/brake voltage: V
 Spannungsart/voltage type: -
 Einfallzeit/engage time "Te": ms
 max. Bremsenergie/max. braking energy: J
 einmalig/single engagement: J
 Lebenslang/lifetime: -

Lüfterdaten fan data:

AMK-TNr./AMK part number:
 Lüfterspannung/fan voltage: V
 Strom/current: A
 Frequenz/frequency: Hz

Wicklungsschutz thermistor:

Typ/type: KTY84
 Ansprechtemp./operation temp: - °C
 Widerstand/resistance (25°C) <= : 629 Ω
 Impulszahl/number of pulses: 262144



Geberdaten position encoder data: Bemerkungen remarks:

AMK-TNr./AMK part number: 108072
 Typ/type: P
 Impulszahl/number of pulses: 262144
 automatisch erstellt, Geber 18 Bit,
 Sonderparameter FSE
 Daten nur gültig mit entsprechender Wasserkühlung

* Typenschildbezeichnung unterstrichen; bitte bei Rückfragen immer angeben /Nameplate data underlined; please state with every inquiry

Ersteller/created by: SMM Änderung/revision: 0.00 Änderungsdatum/motor revision motor date: 26.10.2016
 Für dieses Dokument und die darin enthaltenen Angaben behalten wir uns alle Rechte und technische Änderungen vor
 All rights reserved for this document and all information included. Technical modifications reserved
 (c) AMK Antriebs- und Steuerungstechnik GmbH Co. KG

Figure 136. AMK motor datasheet

Appendix B. Ferrium C61 datasheet

Ferrium® C61™ Product Data Sheet



Revision: SHP/C61/10/2016

...where performance matters

Offering a superior alternative

Ferrium® 61 is a case-hardened Gear Steel with ultra-high-strength core

Advances in racing engine designs and increased engine power has caused an increase in the failure of dog rings, gears, camshafts, input shafts, racks and pinions.

The design objective for Ferrium® C61 was to develop a high-performance secondary-hardening gear and bearing steel with similar surface properties to conventional gear steels such as AISI 9310 and EN36C, however, with the added benefits of an ultra-high-strength core and excellent fracture toughness.

Ferrium® C61 is a member of a new class of martensitic secondary-hardening gear and bearing steels that utilize an efficient M2C precipitate strengthening dispersion. Because of the efficiency of this strengthening dispersion, a superior combination of properties is possible for a given application. Ferrium® C61 was designed to provide carburized surface properties (60-62 HRC) similar to conventional gear steels such as AISI 9310 and EN36C with the added benefit of an ultra-high-strength core along with excellent fracture toughness.

Ferrium® C61™ Chemical Composition (nominal wt. %)						
Fe	C	Co	Cr	Ni	Mo	V
Bal	0.15	18	3.5	9.5	1.1	0.08

Overview of Ferrium® C61 Properties (typical)					
YS	UTS	EI	Core Hardness	CVN	K _{IC}
(ksi)	(ksi)	(%)	(HRC)	(ft-lb)	(ksi√in)
225	240	15	48-50	50	130

About Smiths High Performance

Smiths High Performance is a leading stockholder and supplier of high-performance engineering materials to the global motorsport sector. We are supply partners in a range of specialist motorsport markets including Formula 1, Formula E, NASCAR, MOTO GP, WEC & WRC.

Further technical data available on the reverse of this Datasheet



Advantages

Ferrium® C61 is targeted as a superior alternative to conventional gear products such as AISI 9310 and EN36C for new smaller, lighter, high-temperature resistant component designs, or to upgrade the material in an existing component where a re-design is not feasible.

Ferrium® C61 has surface-wear properties similar to those found in popular commercial alloys but provides an ultra-high-strength, high-toughness, high-temperature-resistant core. Other features include superior axial and STBF fatigue resistance.

Ferrium® C61 is particularly advantageous to reduce the size and weight of integrally geared driveshafts.

www.smithshp.com

info@smithshp.com

Processing

Ferrium® C61 is a high-temperature carburizing product. Solution heat treatment and carburizing treatment are combined. The alloy is quenched directly from the carburizing temperature. After quenching to room temperature Ferrium® C61 is subjected to liquid nitrogen immersion to assure a complete martensitic transformation. It is typically tempered at 900°F (482°C) and has excellent thermal resistance approaching this temperature. If desired, replacing carburizing with nitriding will result in improved surface hardness. Using both nitriding and case carburizing may result in a brittle surface, resulting in sub-surface spalling initiation and significantly lower fatigue life; users should complete internal trials before considering this combination.

Case carburizing produces a gradient in the volume fraction of the M2C carbides and results in an increase in hardness and surface residual compressive stress. The efficiency of the M2C strengthening response allows this class of steels to achieve very high surface hardness with reduced carbon content. Thus, this class of steels meets very high surface hardness without the formation of detrimental primary carbides. For superior fatigue performance, we recommend final shot peening.

Fatigue

Ferrium® C61 alloy has the best fatigue life of several materials evaluated and shows 15% enhancement over EN36C in a notch bending fatigue test. The sample is a Ford Research Lab design, incorporating 4-point loading and an approximately 0.050-inch notch root radius. All samples were finished ground and shot-peened after heat treatment.

Mean Coefficient of Thermal Expansion			
Temperature Range		Heat Treated Condition	
°C	°F	10 ⁻⁸ /°C	10 ⁻⁸ /°F
20-100	68-212	9.54	5.30
20-200	68-392	9.59	5.33
20-300	68-572	10.76	5.98
20-400	68-752	11.09	6.16
20-500	68-932	11.28	6.27
Alloy		Cycles to Failure	
Ferrium		4.61 x 10 ⁴	
EN36C		4.00 x 10 ⁴	

Product Forms

Manufactured in typical ingot, bar and billet forms.

Patent

US Patent Number 6,176,946 B1.

...where performance matters...

When you purchase high-performance materials from **Smiths High Performance**, you will be joining some of the biggest and best global engineering companies. We are a Tier 1 supply chain partner to the world's leading motorsport companies. Our unique business structure and ethos allows us to offer services which are otherwise unavailable in this market sector.

www.smithshp.com info@smithshp.com



Unit 3, Juno Place
Stratton Business Park, Biggleswade,
Bedfordshire SG18 8XP
Tel: +44 (0)1767 604 708



All information in our data sheet is based on approximate testing and is stated to the best of our knowledge and belief. It is presented apart from contractual obligations and does not constitute any guarantee of properties or of processing or application possibilities in individual cases. Our warranties and liabilities are stated exclusively in our terms of trading.

© Smiths High Performance 2021

Figure 138. Ferrium C61 datasheet

Appendix C. Lubricant datasheet

PRODUCT INFORMATION



TITAN SINTOFLUID FE SAE 75W

Synthetic, fuel-economy manual transmission fluid offering increased gearbox efficiency in passenger cars due to low viscosity level. Reduces fuel consumption and offers best properties at low temperature. Suitable as fill for life fluid according to manufacturer.

Description

TITAN SINTOFLUID FE SAE 75W is being produced based on a modern, OEM-proven additive technology with multiple synchromesh compatibility embedded in a high-quality base oil matrix with synthetic components. The unique formulation is focused on maximum fuel economy.

Application

TITAN SINTOFLUID FE SAE 75W is miscible and compatible with conventional branded gear oils. However, mixing with other gear oils should be avoided in order to fully utilize the product's benefits. A complete oil change is recommended when converting to TITAN SINTOFLUID FE SAE 75W. For information on product safety and proper disposal please refer to the latest Material Safety Data Sheet.

Advantages/Benefits

- Offers the possibility of fuel economy to the customers aware on fuel consumption
- Rationalization of product diversity to one FE-MTF-product with several application opportunities.
- TITAN SINTOFLUID FE SAE 75W offers reliable operation under high loads in manual transmissions during the whole oil operation time (Fill-for-life).
- Prevents reliably from wear, sludge formation, agglomeration and corrosion.
- TITAN SINTOFLUID FE SAE 75W offers an outstanding viscosity temperature behaviour lying above the performance of many normal service gearbox lubricants, thus ensuring lubrication at very low as well as very high operation temperatures.
- Prevents from bearing wear
- TITAN SINTOFLUID FE SAE 75W is thermally highly stable and does not foam even under highest stress.
- TITAN SINTOFLUID FE SAE 75W is compatible with many elastomers and other sealant materials.

Specifications

- API GL-4

Approvals

- -

FUCHS Recommendations

- VW TL 521 71 (G 052 171 A1/A2)
- VW TL 521 78 (G 052 178 A2)
- VW TL 525 12 (G 052 512 A2)
- VW TL 726 (G 052 726 A2/G 055 726 A2/G 060 726 A2/G 070 726 A2)

PI60383e, PMA, 08.02.2011, Page 1

FUCHS EUROPE SCHMIERSTOFFE GMBH
Friesenheimer Straße 19
68169 Mannheim/Germany

Telefon: +49 621 3701-0
Telefax: +49 621 3701-570
E-Mail: zentrale@fuchs-europe.de

PRODUCT INFORMATION



CHARACTERISTICS

Density at 15 °C	DIN 51757	0.873 g/ml
Flash Point, CoC	DIN ISO 2592	221 °C
Pour Point	DIN ISO 3016	-44 °C
Foaming Tendency Seq. I/II	ASTM D 892	20/0 ; 30/0 ml
Dynamic Viscosity at - 40°C	DIN 51398	75,000 mPas
Kinematic Viscosity at 40°C	DIN 51562-1	40.8 mm ² /s
Kinematic Viscosity at 100°C	DIN 51562-1	6.7 mm ² /s
Viscosity Index	DIN ISO 2909	119

PI60383e, PMA, 08.02.2011, Page 2

FUCHS EUROPE SCHMIERSTOFFE GMBH
Friesenheimer Straße 19
68169 Mannheim/Germany

Telefon: +49 621 3701-0
Telefax: +49 621 3701-570
E-Mail: zentrale@fuchs-europe.de

Figure 139. FUCHS TITAN SINTOFLUID FE SAE 75W lubricant oil datasheet

RENOLIT PU-MA 2

Descrizione

RENOLIT PU-MA 2 è un grasso per alte temperature totalmente sintetico, a base di un ispessente organico e con lubrificanti solidi. RENOLIT PU-MA 2 ha un'elevata stabilità termica, garantisce una duratura protezione contro la corrosione, dimostra ottima resistenza all'acqua e una lubricità ottimale su di un ampio intervallo di temperature.

Applicazioni

RENOLIT PU-MA 2 è impiegato per la lubrificazione a lungo termine di cuscinetti operanti su di un ampio intervallo di temperatura.

RENOLIT PU-MA 2 è adatto per la lubrificazione di motori elettrici, ventilatori d'aria calda, cuscinetti veloci, forni, miscelatori, cilindri essiccatori di macchine da carta, cuscinetti di calandre, ecc.

Si sconsiglia la miscelazione di grassi di diversa tipologia che possono manifestare incompatibilità reciproca e differente comportamento reologico.

Vantaggi

- **Eccellente stabilità termica**
- **Buona stabilità meccanica**
- **Elevato potere EP**
- **Ottima protezione contro la corrosione**
- **Resistente all'acqua**
- **Buon comportamento anche alle basse temperature**

Modalità di stoccaggio e smaltimento

Conservare il prodotto in imballi originali chiusi, in un ambiente secco, a temperature comprese tra 0°C e 40°C. Il prodotto così conservato mantiene le sue caratteristiche inalterate per un periodo di almeno tre anni.

Per lo smaltimento, conferire il prodotto al Consorzio Obbligatorio degli Oli Usati in ottemperanza alle norme vigenti.

2020 – PM3 SP – pag. 1/2

FUCHS LUBRIFICANTI SPA
Via Riva, 16
14021 – Buttigliera d'Asti (AT)
Italia

Tel. 011.99.22.811
Fax 011.99.22.857
dacindustria@fuchslubrificanti.it

Le informazioni contenute nella presente Scheda Tecnica non costituiscono specifica; nessuna garanzia è espressa o sottintesa riguardo l'accuratezza di questi dati o i risultati che si ottengono dal loro uso. Questi possono subire variazioni senza preavviso. Il venditore non sarà responsabile di eventuali guasti, danni o inconvenienti risultanti dall'uso improprio del prodotto nei processi industriali dell'acquirente o in combinazione con altre sostanze.

RENOLIT PU-MA 2

Caratteristiche Medie Indicative

Proprietà	Unità	Valore	Metodo
Classificazione	---	KPFHC 2 R-40	DIN 51502
		ISO-L-X-DFEB	ISO 6743-9
Colore	---	Beige	---
Addensante	---	Poliurea	---
Punto di goccia	°C	≥240	IP 396
Penetrazione lavorata (Pw 60)	0,1 mm	265+295	DIN ISO 2137
Gradazione NLGI	---	2	DIN 51818
Protezione corrosione (test Emcor)	° di corr.	0-0	DIN 51802
Corrosione rame a 120°C	° di corr.	1-100	DIN 51811
Resistenza all'acqua	stadio	1-90	DIN 51807-1
Test 4 sfere, carico saldatura	N	2600	DIN 51350-4
Viscosità olio base a 40 °C	mm ² /s	100	DIN 51562-1
Campo di temperatura	°C	da -40 a +180	DIN 51825

2020 – PM3 SP – pag. 2/2

FUCHS LUBRIFICANTI SPA
Via Riva, 16
14021 – Buttigliera d'Asti (AT)
Italia

Tel. 011.99.22.811
Fax 011.99.22.857
dacindustria@fuchslubrificanti.it

Le informazioni contenute nella presente Scheda Tecnica non costituiscono specifica; nessuna garanzia è espressa o sottintesa riguardo l'accuratezza di questi dati o i risultati che si ottengono dal loro uso. Questi possono subire variazioni senza preavviso. Il venditore non sarà responsabile di eventuali guasti, danni o inconvenienti risultanti dall'uso improprio del prodotto nei processi industriali dell'acquirente o in combinazione con altre sostanze.

Figure 140. FUCHS RENOLIT PU-MA 2 lubricant grease datasheet

REFERENCES

1. Formula Student Germany, *Formula Student rules 2023*
2. <https://squadracorsepolito.com/>
3. <https://matweb.com/>
4. S. Bakshi, P. Dhillon, T. Maruvada, *Design and Optimization of Planetary Gearbox for a Formula Student Vehicle*, SAE Int. J. Mater. Manf. 7(3):2014, 2014
5. G. White, G. Cunningham, D. Doyle, *Design of an Electric Drive Transmission for a Formula Student Race Car*, SAE Int. J. Advances & Curr. Prac. in Mobility 1(3):1345-1351, 2019
6. P. A. Aune, *a Four Wheel Drive System for a Formula Style Electric Racecar*, 2016
7. D.W. Dudley, J. Sprengers, D. Schröder, H. Yamashina, *Manuale del Motoriduttore - Bonfiglioli*, Springer, 1997
8. BS ISO 6336:2019, *Calculation of load capacity of spur and helical gears*, International Organization for Standardization, 2019
9. A. Dobler, M. Hergessel, T. Tobie, K. Stahl, *Increased Tooth Bending Strength and Pitting Load Capacity of Fine Module Gears*, Geartechnology (September/October 2016), 48-53, 2016.
10. T. Shen, T. Krantz, J. Sebastian, *Advanced Gear Alloys for Ultra High Strength Applications*, NASA/TM-2011-217121, 2011
11. Carpenter technology, *Ferrium C61 material datasheet*
12. Carpenter technology, *Ferrium C64 material datasheet*
13. Smiths High Performance, *Ferrium C61 material datasheet*
14. Smiths High Performance, *Ferrium C64 material datasheet*
15. Smiths, *BS S156 material datasheet*
16. Aubert&Duval, *NC310YW material datasheet*
17. B. Jeong, M. Kato, K. Inoue, N. Takatsu, *The Bending Strength of Carburized Fine Module Gear Teeth*, JSME International Journal (Vol. 35, No. 1, 1992), 136-141, 1992
18. E. Alexsson, E. Henrikson, C. Lund, C. Tsobanoglou, *Design of a Weight-Optimized Gearbox for a Formula Student Car*, 2021
19. S. P. Radzevich, *Dudley's Handbook of Practical Gear Design and Manufacture*, CRC Press, 2016
20. M. Turci, *Errore di trasmissione e modifiche di ingranaggi*, 2019

21. K. Michaelis, B.-R. Höhn, M. Hinterstoiber, *Influence factors on gearbox power loss*, Industrial Lubrication and Tribology, Vol. 63 Iss 1 pp. 46 – 55, 2011
22. J. Badal, *Analysis of different powertrain configurations for a formula style electric race car*, 2019
23. M. Cova, *Design of an epicycloidal geartrain for a four-wheel drive Formula Student electric vehicle*, 2020
24. KISSsoft AG, *Help manual*
25. SKF, *Super-precision bearings catalogue*, 2016
26. SKF, *Needle roller bearings catalogue*, 2015
27. SKF, *Industrial shaft seals catalogue*, 2021
28. AMK, *DD5-14-10 POW Motor datasheet*, 2018
29. FUCHS, *TITAN SINTOFLUID FE SAE 75W datasheet*
30. FUCHS, *RENOLIT PU-MA 2 datasheet*
31. Angst+Pfister, *Basic catalogue*
32. G. Belingardi, *Slides from the "Fundamentals of Machine Design" course*, Politecnico di Torino, 2020
33. E. Galvagno, *Slides from the "Powertrain Components Design" course*, Politecnico di Torino, 2022
34. Squadra Corse PoliTO, *Geartrain design presentation*, 2022
35. Squadra Corse PoliTO, *Geartrain design book*, 2022

LIST OF FIGURES

Figure 1. SC22 at Formula ATA	7
Figure 2. SC12e and its transmission	10
Figure 3. SCR and its transmission	11
Figure 4. SCXV and its transmission	11
Figure 5. SC22EVO and its wheel assembly.....	13
Figure 6. GreenTeam transmission.....	14
Figure 7. TuFast unsprung masses.....	14
Figure 8. Formula Student Team Delft wheel assembly	15
Figure 9. DHBW transmission	15
Figure 10. Single in-board motor scheme	17
Figure 11. Twin in-board motors scheme	18
Figure 12. Four in-board motors scheme	19
Figure 13. Two out-board motors scheme	20
Figure 14. Four out-board motors scheme	21
Figure 15. AMK motors characteristic curves.....	23
Figure 16. AMK motors efficiency table.....	23
Figure 17. Pareto diagram of SC22EVO unsprung masses.....	24
Figure 18. 10" vs 13" wheels comparison	26
Figure 19. Acceleration lap time vs transmission ratio	27
Figure 20. Autocross lap time and energy spent vs transmission ratio.....	28
Figure 21. Competition scoring with different transmission ratios	28
Figure 22. Traction model	29
Figure 23. Two gear pairs in series scheme	30
Figure 24. Simple planetary system in series to a gear pair scheme	31

Figure 25. Simple planetary system scheme	32
Figure 26. Two planetary systems in series scheme	33
Figure 27. Compound planetary system scheme	34
Figure 28. Rim thickness factor.....	36
Figure 29. Requested torque during autocross	40
Figure 30. Requested power during autocross	40
Figure 31. KISSsys transmission model 3D view	43
Figure 32. KISSsys transmission model tree.....	45
Figure 33. KISSsys model kinematic diagram	48
Figure 34. GB_calc coaxial shaft	49
Figure 35. Gear internal geometry.....	51
Figure 36. Gear reference profile	52
Figure 37. Carburizing process duration and temperature	59
Figure 38. Profile shift coefficient.....	63
Figure 39. First stage meshing gears	65
Figure 40. Second stage meshing gears.....	66
Figure 41. Tip and root relief modifications.....	67
Figure 42. Crowning modification	68
Figure 43. First stage normal load distribution after (left) and before (right) profile modifications	69
Figure 44. First stage normal force on tooth after (left) and before (right) profile modifications	69
Figure 45. First stage normal force on tooth after (left) and before (right) profile modifications 3D view	69
Figure 46. Second stage normal load distribution after (left) and before (right) profile modifications	70

Figure 47. Second stage normal force on tooth after (left) and before (right) profile modifications	70
Figure 48. Second stage normal force on tooth after (left) and before (right) profile modifications 3D view	71
Figure 49. Alternating bending factor.....	72
Figure 50. Type of pinion gear according to ISO 6336	73
Figure 51. First (left) and second (right) stage specific sliding.....	74
Figure 52. Root stresses for sun gear (left) and for first stage planet gear (right) at peak torque	74
Figure 53. Root stresses for second stage planet gear (left) and for ring gear (right) at peak torque	75
Figure 54. 3D stress distribution for sun gear (left) and for first stage planet gear (right) at peak torque.....	75
Figure 55. 3D stress distribution for second stage planet gear (left) and for ring gear (right) at peak torque.....	75
Figure 56. 3D contact pressure distribution for first (left) and second (right) stage at peak torque	76
Figure 57. Safety factors for first (left) and second (right) stage	76
Figure 58. First (left) and second (right) stage hardness curve recommendation	76
Figure 59. Root stresses for sun gear (left) and for first stage planet gear (right) with load spectrum	77
Figure 60. Root stresses for second stage planet gear (left) and for ring gear (right) with load spectrum.....	78
Figure 61. 3D stress distribution for sun gear (left) and for first stage planet gear (right) with load spectrum	78
Figure 62. 3D stress distribution for second stage planet gear (left) and for ring gear (right) with load spectrum	78
Figure 63. 3D contact pressure distribution for first (left) and second (right) stage with load spectrum.....	79

Figure 64. KISSsys transmission model 3D view for efficiency analysis.....	81
Figure 65. Sun gear.....	83
Figure 66. Motor output spline	84
Figure 67. Motor output spline section view	85
Figure 68. Sun gear mounting section view	86
Figure 69. Sun gear positive locking mechanism.....	86
Figure 70. Sun gear FEM model	88
Figure 71. Sun gear Von Mises stress.....	88
Figure 72. Sun gear displacement.....	89
Figure 73. Planet gears assembly	89
Figure 74. Planet shim.....	90
Figure 75. P3G profile.....	91
Figure 76. P3G vs P4C polygonal profile	92
Figure 77. Second stage planet gear	93
Figure 78. First stage planet gear.....	93
Figure 79. First stage planet gear FEM model	94
Figure 80. First stage planet gear Von Mises stress (left) and displacement (right).....	95
Figure 81. Second stage planet gear FEM model.....	96
Figure 82. Second stage planet gear Von Mises stress	96
Figure 83. Second stage planet gear displacement	97
Figure 84. Pin shaft.....	97
Figure 85. Planet_calc coaxial shaft calculation module	98
Figure 86. Pin shaft KISSsoft displacement (left) and stress (right).....	99
Figure 87. Pin shaft FEM model	100
Figure 88. Pin shaft Von Mises stress (left) and displacement (right).....	100
Figure 89. Needle roller bearings characteristics	101

Figure 90. Needle roller bearings positioning	101
Figure 91. Ring gear	103
Figure 92. Ring gear fixing teeth.....	104
Figure 93. Ring gear FEM model.....	105
Figure 94. Ring gear Von Mises stress	105
Figure 95. Ring gear displacement.....	106
Figure 96. Wheel bearings layout "O" configuration	108
Figure 97. ACD bearings dimensions.....	109
Figure 98. Mainline calculation module with eccentric force	110
Figure 99. Force and pressure distribution, wheel bearing carrier side.....	112
Figure 100. Force and pressure distribution, wheel bearing hub side	112
Figure 101. Preload adjustment ring	113
Figure 102. AGMA oil selection table.....	115
Figure 103. Oil viscosity for bearings lubrication	116
Figure 104. Gearbox oil level	117
Figure 105. Grease-Oil compatibility table	118
Figure 106. Seals	119
Figure 107. HMS5 seal cross section	120
Figure 108. Radial shaft seal dimensions	121
Figure 109. Radial shaft seal material selection.....	122
Figure 110. O-rings service life	123
Figure 111. O-rings groove dimensions	124
Figure 112. Planetary carrier and wheel hub assembly	125
Figure 113. Shoulder screw	126
Figure 114. Planetary carrier and wheel hub assembly raw geometry	132
Figure 115. Optimization Inspire model.....	133

Figure 116. Optimization Hypermesh model	134
Figure 117. Different views of optimization results	135
Figure 118. Planetary carrier before (left) and after (right) optimization.....	136
Figure 119. Wheel hub before (left) and after (right) optimization.....	136
Figure 120. Planetary carrier and wheel hub FEM model.....	137
Figure 121. Planetary carrier and wheel hub Von Mises stress in pure braking.....	139
Figure 122. Planetary carrier and wheel hub displacement in pure braking	139
Figure 123. Planetary carrier and wheel hub Von Mises stress in pure lateral.....	140
Figure 124. Planetary carrier and wheel hub displacement in pure lateral.....	140
Figure 125. Fx load spectrum during autocross	141
Figure 126. Fy load spectrum during autocross	142
Figure 127. Fz load spectrum during autocross.....	142
Figure 128. Ergal S-N curve.....	143
Figure 129. Different views of planetary carrier and wheel hub fatigue life	144
Figure 130. Fatigue analysis damage	144
Figure 131. Wheel nut and wheel nut mounting	145
Figure 132. Gears assembly	147
Figure 133. Transmission assembly	148
Figure 134. Transmission and motor assembly	148
Figure 135. Wheel assembly	149
Figure 136. AMK motor datasheet	155
Figure 137. AMK motor technical drawing	156
Figure 138. Ferrium C61 datasheet	158
Figure 139. FUCHS TITAN SINTOFLUID FE SAE 75W lubricant oil datasheet	160
Figure 140. FUCHS RENOLIT PU-MA 2 lubricant grease datasheet.....	162

LIST OF TABLES

Table 1. Events scoring.....	9
Table 2. Steel 18NiCrMo7 characteristics	60
Table 3. Steel BS S156 characteristics	60
Table 4. Steel Ferrium C61 characteristics	61
Table 5. Steel NC310YW characteristics	62
Table 6. First reduction stage data	64
Table 7. Second reduction stage data.....	65
Table 8. Gears safety factors at peak load	73
Table 9. Gears safety factors with load spectrum.....	77
Table 10. Needle roller bearings life	102
Table 11. SKF 71816 ACD HC/P4 main dimensions.....	110
Table 12. Wheel bearings life	111
Table 13. HMS5 85x100x9 RG main dimensions.....	121
Table 14. O-rings and grooves dimensions	124
Table 15. Al 7075-T6 material characteristics.....	128
Table 16. Design load cases - accelerations	129
Table 17. Design load cases - forces.....	130
Table 18. Transmission components weight.....	150
Table 19. Transmission main dimensions.....	150